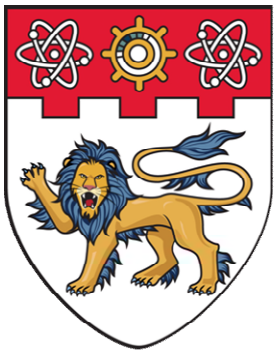

NANYANG TECHNOLOGICAL UNIVERSITY
SINGAPORE

SYNTHESIS, CHARACTERIZATION AND PERFORMANCE EVALUATION OF NANO-ENERGETIC COMPOSITE

TAN MENG LU

SCHOOL OF MATERIALS SCIENCE AND ENGINEERING

2019

SYNTHESIS, CHARACTERIZATION AND PERFORMANCE EVALUATION OF NANO-ENERGETIC COMPOSITE

TAN MENG LU

SCHOOL OF MATERIALS SCIENCE AND ENGINEERING

A thesis submitted to the Nanyang Technological University in partial fulfilment of the requirement for the degree of Masters of Engineering

2019

Statement of Originality

I hereby certify that the work embodied in this thesis is the result of original research and has not been submitted for a higher degree to any other University or Institution.

16/08/2018
Date

Tan Meng Lu

Supervisor Declaration Statement

I have reviewed the content and presentation style of this thesis and declare it is free of plagiarism and of sufficient grammatical clarity to be examined. To the best of my knowledge, the research and writing are those of the candidate except as acknowledged in the Author Attribution Statement. I confirm that the investigations were conducted in accord with the ethics policies and integrity standards of Nanyang Technological University and that the research data are presented honestly and without prejudice.

16/08/2018
Date

Prof. Hng Huey Hoon

Authorship Attribution Statement

This Masters of Engineering thesis includes content where I received support from my supervisor(s) and colleagues as follows:

- The initial project title and direction was discussed and designed together with Professor Hng Huey Hoon. She provided advice on the overall project direction throughout the course.
- I prepared the report drafts. Advices were also taken from Professor Hng Huey Hoon and Dr Sreekumar Pisharath.
- I co-designed the thermal kinetic studies, in consultation with Dr. Nimesh Sasidharan. Processing and analysis of results were performed with advice taken from both Dr. Nimesh Sasidharan and Dr. Serene Chan Hay Yee.

16/08/2018
.....
Date

.....
Tan Meng Lu

Abstract

Thermites belong to a class of energetic material comprising of a metal as a fuel and a metal oxide as the oxidizer. The research on nano-thermites has significantly emerged in the last two decades and novel ways to harness their energy with improved reactivity, reduced sensitivity and high stability remains highly desirable to date. In this work, Al/NiO nano-thermite system was studied due to their relatively gasless reaction. Gasless thermite reactions could offer potential in applications requiring little flow disturbances and vibrations. A novel self-assembly technique to promote better intermixing of the fuel-oxidizer system through surface functionalization with complimentary functional groups as well as the addition of an energetic polymer binder to reduce the sensitivity were studied.

The heat release characteristics and reaction mechanism of Al/NiO nano-thermites were studied. n-Al/n-NiO with different equivalence ratio (ER) were prepared and their heat of reactions measured using a bomb calorimeter. The heat of reaction increased from a fuel lean formulation to a slightly fuel rich formulation at ER 1.2, yielding an optimized heat of reaction of 3649 J/g. Their highly exothermic nature was studied using a Differential Scanning Calorimeter (DSC). The reaction products during the different stages of the decomposition were analyzed using a powder X-ray Diffraction (XRD) to understand the reaction mechanism of this alumino-thermic reaction.

Surface functionalization of n-Al and n-NiO using organosilanes with complimentary end groups (epoxide/ amino) to bring about the fuel-oxidizer self-assembly were performed. The self-assembled n-Al/n-NiO showed a better intermixing of the binary composite powder from their Scanning Electron Microscopy/Energy Dispersive X-ray (SEM/EDX) photographs. The self-assembled system displayed a larger heat release before aluminum melting as well as an increased heat release rate from their DSC profiles. The preference for reaction prior to aluminum melting (or solid-state reaction) is an indication of intimate interaction between the fuel and oxidizer. The self-assembly process was shown to increase the energy release rate of organosilane-functionalized nano-thermites in their pressure studies. The overall energy release rate of the functionalized n-Al/n-NiO was, however, not better than unfunctionalized n-Al/n-NiO. Self-assembled organosilane-

functionalized n-Al/n-NiO was found to have higher activation energy barrier (240 kJ/mol) as compared to physically mixed n-Al/n-NiO (203 kJ/mol). The increase is a result of increased diffusion barrier for Al and O, introduced by the additional organosilane surface graft. The surface functionalization could significantly reduce the electrostatic discharge (ESD) sensitivity of this material. The improved ESD minimum ignition energy is higher than what the human body is capable of discharging, making them safer to handle.

An energetic polymer, terpolymer of tetrafluoroethylene, hexafluoropropylene and vinylidene fluoride (THV), was added to the nano-thermite to function as a binding agent as well as improve the safety of handling the highly sensitive n-Al/n-NiO. THV fluoropolymer was added to n-Al/n-NiO in varying weight percentages (0 to 40). The effect of THV addition to n-Al/n-NiO on their reactivity and sensitivity were evaluated. A 30 wt% THV addition to n-Al/n-NiO (ER 1.2) could successfully preserve the reactivity of the nano-thermite as well as improve the safety of handling by decreasing their sensitivity to ESD and friction. Recommended future work includes surface functionalization and self-assembly using highly energetic linkers as well as application-based research for potential use as primer in detonators and in gasless door breaching or metal cutting.

Lay Summary

The work described in this report is on the research of a high heat releasing mixture composition. The reactive nano-powder mixture comprises of a metal and a metal oxide. The potential for high heat release at a very fast rate can be realized in such powder mixtures, rendering them useful in many military and civilian applications. Such high heat releasing and self-sustained reactions was previously unachievable when nano-sized metal and metal oxides powders were not available because the high reaction rate were attributed to the increase in the surface contact area of these reactants.

However, these reactive nano-sized materials are difficult to handle safely as they can be easily ignited and can potentially injure the user. In this work, we attempt to modify the surfaces of these nano-sized reactants to improve both their reactivity as well as safety in handling. We adopted two modification approaches. In the first approach, we chemically modify the surfaces of each reactant to improve the mixture homogeneity, which can potentially lead to improved reactant interaction. This surface treatment was found to successfully improve the homogeneity as well as improve the safety of handling by making them less sensitive to electrostatic discharge. However, this surface treatment also introduced dead weight to the reactive material and could not further improve the overall performance.

In the second approach, an attempt to make this hazardous material safer for handling was made by adding polymer to the reactive mixture. The use of a fluorine-containing polymer in the work described could successfully make them safer to handle as well as preserve their high reactivity. The polymer containing powder mixture had the capability to be easily transformed into 3-dimensional structures through further processing.

Acknowledgements

I would want to extend my sincere thanks and acknowledgement to those who have been supportive towards my M.Eng. journey and/or those whom have played a part in it. Without them, the completion of this report would not be possible.

First and foremost, I'd like to thank Professor Hng Huey Hoon for being my project supervisor. She has been ever so patient and gracious in guiding me during my endeavors and is always inspiring me to think out of the box.

I'd like to thank all the staffs in Energetics Research Institute who have helped me in one way or another. I would like to express special thanks to Dr. Sreekumar Pisharath and Dr. Nimesh Sasidharan, who have always been there to offer good technical advices. I also thank the institute for providing the financial support required for the completion of this M.Eng. program.

Last but not least, I thank my family who has been there to offer their moral and emotional support regardless of whatever problem I faced. My mum's selfless giving has encouraged me to overcome all obstacles.

Table of Contents

Table Captions

Figure Captions

Abbreviations

AAMCAB	(Acrylamidomethyl) cellulose acetate butyrate
APS	Average Particle Size
APTMS	3-Aminopropyl Trimethoxysilane
ARDEC	Army Research, Development and Engineering Centre
ASTM	American Society for Testing and Materials
BET	Brunauer, Emmett and Teller
CTPB	carboxy terminated polybutadiene
DSC	Differential Scanning Calorimeter
E_a	Activation energy
EDX	Energy Dispersive X-Ray
ER	Equivalence Ratio
ESD	Electro-Static Discharge
FTIR	Fourier Transform Infrared Spectroscopy
GAP	Glycidyl Azide Polymer
GPTMS	3-Glycidoxypropyl Trimethoxysilane
HFP	hexafluoropropylene
HTPB	hydroxyl terminated polybutadiene
HTPE	hydroxyl terminated polyether
ICDD	International Centre for Diffraction Data
n-Al	nanometer sized Aluminum
n-NiO	nanometer sized Nickel Oxide
PBX	Polymer-Bonded Explosive
PDF	Powder Diffraction File
PGN	poly(glycidyl nitrate)
PIR	Pre-Ignition Reaction
polyAMMO	Poly(3-azidomethyl 3-methyl oxetane)
polyBAMO	poly-3,3-bis(3-azidomethyl)oxetane
polyNIMMO	poly(3-nitratomethyl-3-methyloxetane)
SEM	Scanning Electron Microscopy
TFE	tetrafluoroethylene
TGA	Thermo-Gravimetric Analyzer

TG-DTA	thermogravimetry and differential thermal analysis
THV	Terpolymer (tetrafluoroethylene, hexafluoropropylene, vinylidene fluoride)
VDF	vinylidene fluoride
XRD	X-ray Diffraction

Chapter 1

Introduction

This chapter gives an introduction on nano-thermites and its use as an energetic material. The main challenges with respect to its use are highlighted, and these include their reaction rate, safety in handling as well as storage stability. The motivations behind this work as well as the significance of the possible accomplishments are explained. Al/NiO is a relatively less explored nano-thermite system offering low gas production. As high energy release rate as well as low sensitivity to external stimuli are desirable characteristics of thermites, it will be of high research significance to achieve improvement in these areas. It will also be of interest to investigate if the inclusion of polymeric binder, that could transform loose powders to a 3-Dimensional reactive matrix, could be used to tune the sensitivity while preserving the reactivity of n-Al/n-NiO. It is hypothesized that through the surface functionalization of the fuel and the oxidizer particles with complimentary surface modifiers, an improved composition homogeneity leading to increased energy release rate could be achieved. It is also hypothesized that the addition of an energetic binder could reduce the sensitivity of n-Al/n-NiO while preserving their reactivity. Finally, the research objectives are detailed in the last section of this chapter.

Thermites belong to a category of energetic material comprising of a metal as a fuel and a metal oxide as the oxidizer. The redox reaction between the metal and metal oxide is highly exothermic. A typical alumino-thermic reaction (aluminum as the fuel along with a metal oxide) has enthalpy of reaction higher than that of TNT (trinitrotoluene). The exothermicity of thermite reaction has long been advantageously used for civilian applications such as welding. However, their use for military and space applications has been limited due to their sluggish reaction rate. The development of nanotechnology has made the synthesis of nano-sized metallic and metal oxide particles possible, thereby creating a nano-thermite system. With significant reduction in the size of the reactants, nano-thermites have opened up new possibilities for enhancing the energy release of thermites by curtailing diffusion controlled chemical reactions. The research on nano-thermites has significantly emerged in the last two decades and novel ways to harness their energy with improved reaction rate remains highly desirable to date.

A unique characteristic of the nano-thermite system is that the energy release rate can be tailored to occur over a wide range of time scales. Highly reactive nano-thermite materials can provide high impulses since they release the chemical energy over a shorter time scale. The impulses usually exceed what is obtainable from a battery source. Over the years, nano-thermite materials have been used for a variety of practical applications depending on: a) nature of chemical species evolved (eg: produce gases with antibacterial properties); b) evolution of gaseous products to generate thrust; and c) provides heat energy that could be converted into other useful forms. Thus, nano-thermite materials occupy a remarkable position in the progressive research area on nanoenergetics. However, the far reaching applicability of nano-thermite materials has been fraught with challenges.

1.1 Challenges in Nano-thermites

The key technical challenges with respect to the application of nano-thermite materials are briefly summarized in this section. The reaction mechanism of nano-thermite has not been well understood owing to the inherent complexity associated with the solid state reactions of such binary composite systems. Although nano-thermites have high energy density in comparison to many monomolecular energetic molecules, their reaction rates

are never comparable to monomolecular energetic molecules owing to their heterogeneous behavior. Reaction rate between the metal and metal oxide is typically diffusion controlled and is thus dependent on factors including the contact surface area of the two reactants.

One major problem related to the practical applicability of nano-thermites is their relatively higher sensitivity towards external stimuli, including friction and ESD, causing unwanted ignition. Thus, an energetic material having high sensitivity to these stimuli renders it unsafe to handle as it is prone to accidental ignition. An energetic material with low sensitivity to external stimuli ensures the safe usage and handling of such materials and is a highly desirable characteristic.

The aging problem of nano-aluminum has been a long standing issue hindering the widespread practical usage of nano-thermites. Nano-aluminum; the fuel component of nano-thermite mixture loses reactivity on exposure to air in the ambient environment. Thus, they have limited shelf-life unless they are stored in highly inert environment. Currently, research efforts are directed towards achieving optimal energy release rate of the nano-thermite system by balancing the homogeneity and contact surface characteristics. The ability to achieve good reactivity with improved storage stability and safety in handling remains a huge challenge.

1.2 Research Motivation

Alumino-thermic systems will be studied in this work due to n-Al being the most popularly used nano-metallic fuel in thermite systems. Its popularity stem from its abundancy, low cost and good reactivity. While many different metal oxides have been studied in conjunction with aluminum as potential thermite systems. n-Al/n-CuO and n-Al/n-Fe_2O_3 remain to be two of the most widely studied systems. n-Al/n-CuO is known for its high combustion rate and high theoretical heat of reaction. However, it is accompanied with high sensitivity to friction and ESD, making it much more difficult to use safely. n-Al/n-Fe_2O_3 is the other more widely researched system due to the low cost and high availability of nano-size Fe_2O_3 as well as the relatively lower sensitivity to external stimuli responsible for unwanted ignition during handling. n-Al/n-NiO remains a relatively new thermite system that is not intensively researched and understood.

One unique characteristic of Al/NiO nano-thermite lies in the amount of gas produced from its reaction. The amount of gas produced by the Al/NiO reaction is one of the least among nano-thermites (0.0063 g of gas/g of thermite). This is only 0.7 percent of that produced by another gaseous thermite system like Al/Bi_2O_3. It can be a desirable property for applications requiring little gas evolution, flow disturbances and vibrations. Applications in confined spaces and material formation may find use for such materials. In spite of this, Al/NiO nano-thermite system has not been exhaustively investigated and no published data on their gas generation characteristics has been found. Neither can sensitivity data be found on Al/NiO nano-thermites.

Energy release rate is a critical performance parameter tunable with respect to the homogeneity and contact area of the components of the nano-thermite system. In order to understand the energy release rate, it is important to study the kinetics, identify the reaction intermediates and interpret the mechanistic pathways of the nano-thermite reaction. Therefore, the first step in this thesis will be to study the reaction kinetics of Al/NiO nano-thermites at different equivalence ratios (ER).

The binary nanoparticle self-assembly offers the potential to tune and tailor the energy release rate of nano-thermites by improving: a) the homogeneity of binary mixture; and b) the efficiency of interaction between the reactants. Even though self-assembly process has been successfully attempted on several other nano-thermite systems, it has not been reported for the Al/NiO system.

Gases that are generated from a thermite reaction comprises mainly of the oxygen released from the oxidizer, metallic vapors as well as any other gaseous reaction products that are formed at the very high reaction temperature. The amount produced from each reaction is dependant on the thermodynamics of the reaction and the physical properties of the products formed under that condition. Hence, if the reaction releases sufficient amount of heat to vaporize its intermediates and/or products, a larger amount of gas release can be expected.[1] Polymers are often added or coated on nano-thermite powder compositions to act as a binding agent with the aim of creating a 3-dimensional matrix. Al/NiO reaction inherently produces very little gas and it will be interesting to study the effect of introducing a polymeric binder to understand its effect on the gas generation

characteristic of this nano-thermite system. Such studies have not been conducted for Al/NiO nano-thermites.

1.3 Research Significance

Al/NiO nano-thermite is not an exhaustively studied nano-thermite system. To the best of the author's knowledge, there has never been any detailed reporting of the reaction mechanism, reactivity, pressure generation and sensitivity of the Al/NiO nano-thermite system. The first step of this research will provide a comprehensive understanding of all the above mentioned aspects. The findings of this part of the thesis will provide significant input to the nanoenergetics database as a whole for considering Al/NiO system for applications.

Surface modification of nano-aluminum has been reported as a means to improve its shelf life by delaying the ageing phenomenon[2] and this can largely enhance its applicability. Nano-aluminum surface passivation with the added function of improving its interaction with the nano-metal oxide in a nano-thermite composition is a novel idea. Through the choice of complimentary functional groups on both the nano-aluminum and nano-metal oxide, the homogeneity of mixing between the components is expected to improve. This, in turn, could possibly lead to a more complete reaction with an improved reaction rate. While some self-assembly work to improve intermixing has been reported for other nano-thermite systems (i.e. Al/CuO, Al/Fe_2O_3, Al/Bi_2O_3, Al/MoO_3), focus were on proving improved homogeneity rather than reaction performance. Reaction rate improvement has not been very clear and no known reports on their effect on sensitivity were found. Through this work, it is intended to perform a thorough study on how self-assembly affects reaction rate and sensitivity. All of which are determining factors for its performance and safety in handling, respectively.

Polymers are often added as binder in reactive mixtures such as nano-thermites to expand the practical usability of nano-thermite powder, offering a solution to transform the powder into a 3-dimensional reactive matrix. Nano-thermite powders that were coated with polymer binder could be easily pressed into 3-dimensional structures while film forming polymer could transform the energetic powder into reactive coatings or films. However, the addition of polymeric binders to nano-thermites decrease their reaction rate

drastically and would change the amount of gas generated from the system due to its organic nature. It would be important to understand the effect of adding polymeric binder on the pressure generation characteristic of the inherently gasless Al/NiO system.

1.4 Hypothesis/ Problem Statement

It is hypothesized that by introducing complementary functional groups on both the fuel and oxidizer particles, such surface modification can lead to better intermixing and the increased area of contact between them in a nano-thermite system can improve their energy release rate. The incorporation of energetic polymer will reduce their sensitivity to external stimuli and improve the safety of handling these materials while potentially preserving the combustion rate of n-Al/ n-NiO.

1.5 Objectives

The objectives of this thesis are to investigate Al/NiO nano-thermite system with respect to:

a) Kinetics of reaction between Al and NiO reactants
b) Effect of self-assembly through surface modification to improve the homogeneity and energy release rates
c) Effect of surface modification on pressure generation characteristics and sensitivity to ignition by external stimuli of nano-thermites
d) Effect of energetic polymer on the pressure generation characteristics and sensitivity to ignition by external stimuli of nano-thermites

Characterizations will focus on thermal reaction analysis, pressure generation and sensitivity to external stimuli. Spectroscopic and microscopy analysis including techniques such as FTIR, XRD, XPS, SEM/EDX, TEM/EDX will be used to study the nanoparticles before and after functionalization as well as the self-assembly. Sensitivity to external stimuli including ESD, friction and impact will give insights to the safety in handling these materials before and after surface modifications and fluoropolymer coating. The studies and characterization techniques to be adopted to meet each objective are summarized in Figure 1.1.

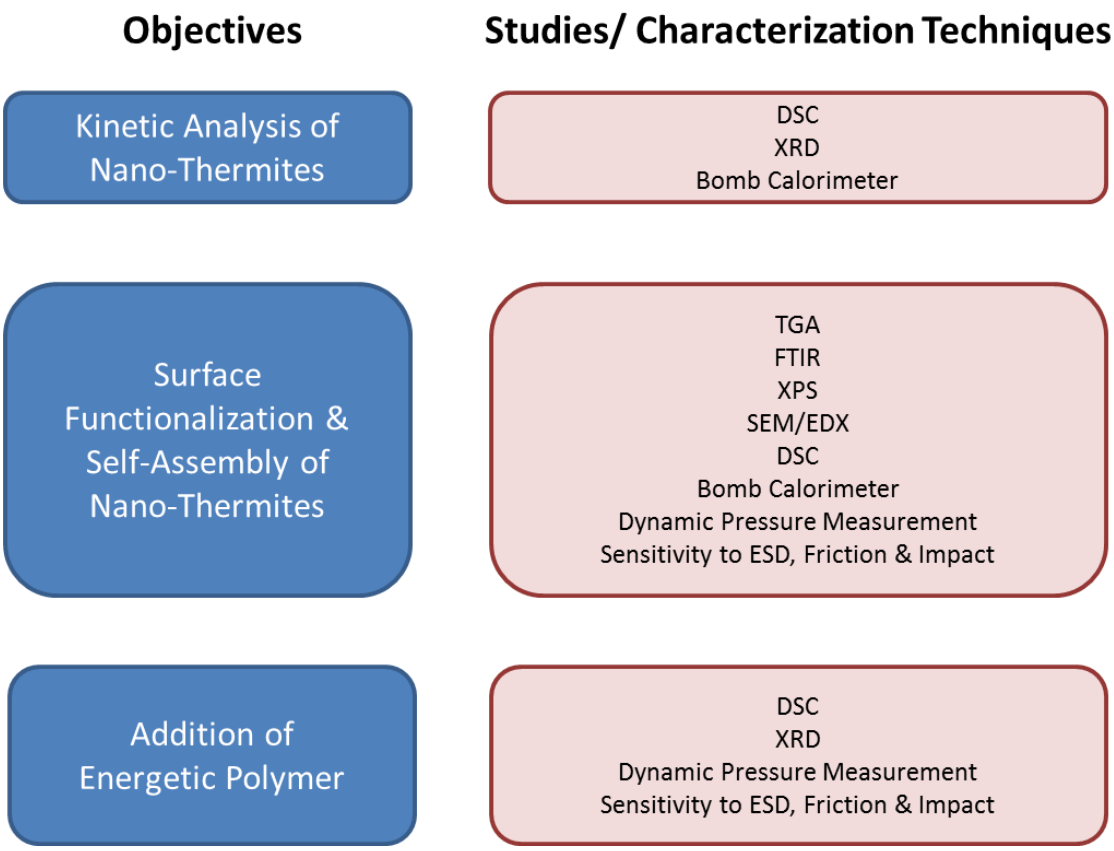

Figure 1.1: Studies and characterization techniques adopted to meet the three main objectives in this thesis.

References

1. Yu, C.; Zhang, W.; Shen, R.; Xu, X.; Cheng, J.; Ye, J.; Qin, Z.; Chao, Y., 3D ordered macroporous NiO/Al nanothermite film with significantly improved higher heat output, lower ignition temperature and less gas production. *Materials & Design* **2016,** *110*, 304-310.

2. Pisharath, S.; Zhang, F.; Ang, H. G., Influence of passivation on ageing of nano-aluminum: Heat flux calorimetry and microstructural studies. Thermochimica Acta 2016, 635, 59-69.

Chapter 2

Literature Review

Related works from the literature are presented here in a few sections. The reason why much research has focused on the use of nano-sized components in a thermite system is due to their increased reaction rate. The various thermite materials adopted for research, including Al/CuO, Al/Fe_2O_3, Al/Bi_2O_3, Al/MoO_3 and Al/NiO are discussed. Nano-thermites are highly sensitive to ESD and literature with supporting information on their ESD sensitivity values are highlighted. The storage stability of nano-thermites is related to the aging problem of their metallic component and some efforts on n-Al passivation are discussed. The various fabrication techniques of nano-thermites including solvent mixing, layered deposition, sol-gel, arrested reactive milling and self-assembly found from the literature are also discussed. Finally, some background on the use of energetic binders including fluoropolymer, nitrogen containing polymer and other gas-generating polymers are elaborated. The chapter ends with a summary and concluding remarks from what could be learned and gathered from the literature.

2.1 Nano-sized Reactants in Superthermites

Thermites, which consist of mixtures of metal as fuel and metal oxide as the oxidizer, have been widely utilized in applications requiring high heat production. A classical thermite formulation, such as Al/Fe_2O_3 prepared in its stoichiometric ratio, has a high volumetric heat of reaction of 16.53 kJ/cm^3. This value is far higher than what many typical monomolecular energetic molecules can offer. Martirosyan et al compared the energy densities for various thermites to those of common monomolecular energetic molecules such as 2,4,6-trinitrotoluene (TNT), pentaerythritoltetranitrate (PETN) and 1,3,5-trinitroperhydro-1,3,5-triazine (RDX),as shown in Figure 2.1). [1] However, while thermites offer high volumetric energy densities, their rate of energy release are typically limited by diffusion and mass transport barriers since it is a reaction between two separate reactants. With the ready availability of nano-sized reactants, the development of nano-thermites has displayed remarkably improved energy release rates in comparison to their micron-sized counterparts.[2-4] The utilization of nano-sized aluminum, with its higher specific surface area, promises a better heat transfer and more complete combustion, resulting in shorter initiation and burn time as well as a better specific impulse.[2] Thus, it is not surprising that recent research developments on thermites has all been focused on the use of nano-sized reactants and on ways to further improve their energy release rates. Thermites using nano-sized reactants are termed metastable intermolecular composites (MIC), nano-thermites or superthermites due to their highly improved reaction performance.

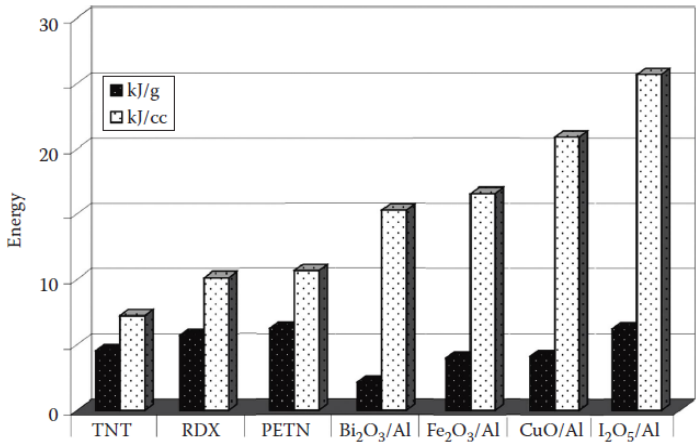

Figure 2.1: Comparisons of energy densities of some thermite compositions with some of the most common monomolecular explosives (TNT, PETN, and RDX).[1]

2.2 Various Nano-Thermites Material System

The possible combinations of metal and metal oxides for thermite reactions are very extensive and a long list of such combination is published by Fischer et al, containing information on their respective heat of reaction and adiabatic flame temperature.[5] Among the vast selection of metal fuels, aluminum remains the most popular in thermite reactions and has been studied more extensively than other metals. Its high popularity is a result of its low cost, wide availability, and relatively high volumetric heat of oxidation, low melting temperature (933 K) and ease of ignition. Kuo et al [6] compares the heat of oxidation of various metals (Figure 2.2) and discussed the underlying problems that some other metal fuel possessed. While Boron did receive some research effort due to it possessing the highest volumetric heat of oxidation among the lot (Figure 2.2), problems include the high melting temperature (2348 K) and accompanying long ignition delay cum incomplete combustion. [6] Other metal having high volumetric heat of oxidation like Beryllium, Titanium and Tungsten each harbors its own limitation including the toxicity of Beryllium oxide, high cost of Titanium and extremely high melting temperature of Tungsten (3695 K). [6]

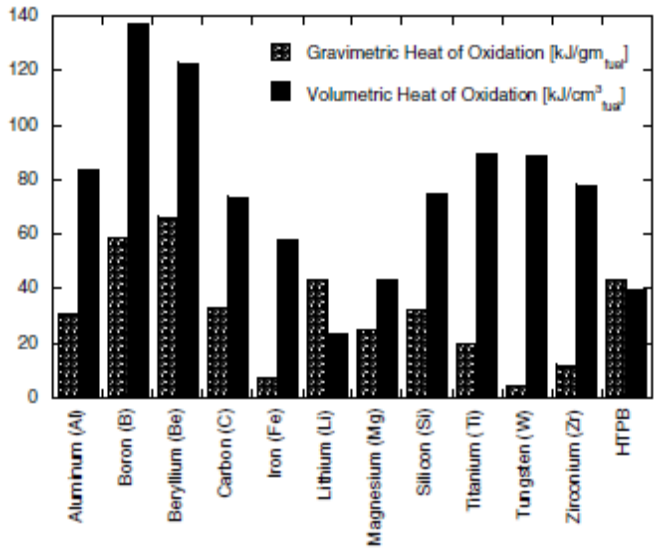

Figure 2.2: Heat of oxidation for various metals and Hydroxyl-Terminated Polybutadiene (HTPB) as a standard fuel binder in solid propellants. [6]

Metal oxides that have been commonly studied for thermite reactions with Al metal include Fe_2O_3, MoO_3, CuO, Bi_2O_3.[3] Al/Fe_2O_3 is the most classical example of thermites, and has been traditionally used in railroad welding application. It remains popular for studies[7-20], likely due to its low material cost. Al/CuO is the nano-thermite system receiving probably the most research attention in the past two decades[21-45] and acts almost like a benchmark with both its high heat of reaction and fast reaction rate. Al/Bi_2O_3 is also a popular system for research[32, 40, 46, 47], especially where gas and pressure generation is highly desirable due to the relatively larger amount of gas produced (0.8941 g of gas per g of thermite).[5] The system was reported as one producing the highest maximum pressure and fastest burn rate when compared to Al/CuO, Al/MoO_3 and Al/PTFE. [40] However, Al/Bi_2O_3 also displays the highest sensitivity to electrostatic discharge in comparison to many other nano-thermites (Table 2.3) with a reported tolerance of as low as 0.125 micro-Joules.[46] The low tolerance to ESD makes this system extremely difficult to handle safely. Al/MoO_3, which is also widely studied, [32, 40, 48-57] is the system displaying one of the highest gravimetric heat of reaction (1124 Cal/g)[5], although the burn rate is not as high as Al/Bi_2O_3 and Al/CuO.

Among the thermite systems, Al/NiO nano-thermite receives comparatively lesser attention. It is one thermite reaction that produced significantly less gas, which is theoretically only 0.7 percent of that produced by Al/Bi_2O_3 or 1.8 percent of that produced by Al/CuO. The potential of gasless thermites for applications as microinitiator, which require little component vibration and flow disturbance has been mentioned by various authors.[58-60] Zhang et al [61], fabricated a Al/NiO film on a silicon substrate using thermal evaporation technique. A Ni layer was deposited and oxidized before Al was deposited above the formed NiO. The NiO layer formed was reported to display a unique honeycomb structure with nano-sized features. The main advantage of this fabrication technique on a silicon substrate is the possibility of direct incorporation into a microelectronic system. Yan et al [62] reported the formation of Al/NiO multilayers through magnetron sputtering. Zhang et al [60] also reported on the formation of Al/NiO film on stainless steel substrates through electrophoretic deposition using a pre-mixed nano-thermite suspension and the author claims it to be a faster process in comparison to magnetron sputtering for film formation. While these three authors reported the development of Al/NiO films formed on substrates, Wen et al [59] focused on Al/NiO powder with the use of NiO nano-wires, not requiring the use of any substrates.

Commercially acquired n-Al and NiO nano-wires synthesized using hydrothermal synthesis were ultrasonicated in isopropanol to form the nano-thermite powder mixture.

In an attempt to find out if NiO doping could change the reaction rate of Al/NiO, Seshadri et al, synthesized n-doped and p-doped NiO and compared their effect on burn rates of Al/NiO/FC-2175 pellets. FC-2175 is a fluoroelastomer and a copolymer of vinylidene fluoride and hexafluoropropylene. It is commonly applied as either an oxidizer or a binder. In this case, the authors applied it as a binder, purely to provide mechanical integrity to their pressed pellet samples, ignoring its function as an oxidizer during their formulation process. While it has been previously postulated that p-doped NiO are better oxidizers than n-doped NiO [63], Seshadri et al did not manage to obtain an improved burn rate from p-doping NiO as there were many other factors that could affect their burn rate including particle agglomeration of the oxidizer and density of the pressed pellet samples. They reported a burn rate of approximately 40 mm/s for n-Al/n-NiO without any binder.[64]

Table 2.1: Reaction properties including Heat of reaction, adiabatic reaction temperature, state of reaction products and amount of gas produced for a few common thermite systems.[5]

Reactants		**Adiabatic reaction Temperature (K)**		**State of Products**		**g of gas per g**	**Heat of reaction**	
Constituents	**ρ_{TMD}, g/cm^3**	**w/o phase changes**	**w/ phase changes**	**State of oxide**	**State of metal**		**-Q, Cal/g**	**-Q, Cal/cm^3**
2Al + Bi_2O_3	7.188	3995	3253	l-g	gas	0.8941	506.1	3638
2Al + 3CuO	5.109	5718	2843	liquid	l-g	0.3431	974.1	4976
2Al + Fe_2O_3	4.175	4382	3135	liquid	l-g	0.0784	945.4	3947
2Al + MoO_3	3.808	5574	3253	l-g	liquid	0.2473	1124	4279
2Al + 3NiO	5.214	3968	3187	liquid	l-g	0.0063	822.3	4288

2.3 Sensitivity and Stability of Nano-Thermites

Although, nano-thermites has gained much attention in research due to their marked increased in reactivity as compared to their micron size counterparts, their widespread

usage in actual applications has been largely limited by both their stability as well as sensitivity to external stimulus. Nano-thermite mixtures are inherently sensitive to ignition by heat, friction, and electrostatic discharge. Their high sensitivity to electrostatic discharge is a prominent problem[65] and their ESD tolerance (micro-Joules to milli-Joules) are significantly lower in comparison to conventional explosives such as TNT, RDX and PETN, which are in the range of a few Joules. Their stability during storage is also an important issue as they are subjected to degradation through contact with water vapor. [66] The total energy content of nano-thermites was reported to decrease through aging. [16]

2.3.1 ESD Sensitivity

Nano-thermites are known to display rather high sensitivity to ESD, which could cause unwanted ignition during preparation or applications. Thus, a system which is reasonably safe to work with and use becomes desirable. The human body is capable of dissipating up to 8.33 mJ of energy in a simulated study on static electric energy output. [67]

Researchers from Los Alamos National Laboratory, USA, attempted to decrease the ESD sensitivity of Al/CuO nano-thermite via the addition of Viton A. Viton A is a copolymer of vinylidene fluoride and hexafluoropropylene marketed by DuPont, containing 66% of fluorine content. Viton A was pre-dissolved in acetone and coated onto the surfaces of n-Al and n-CuO particles. The ESD ignition threshold as well as performance (in terms of time to peak pressure and peak pressure) of n-Al/n-CuO coated with different percentages of Viton A (0, 3, 5 and 10 weight%) were measured. The incorporation of Viton A into the system was found to decrease their ESD sensitivity, but their time to peak pressure as well as peak pressure were also decreased from the increasing addition of Viton A. The results proved that Viton A polymeric coating could be used to decrease their ESD sensitivity (improved in safety), and the amount could be tuned to balance the sensitivity and performance depending on the needs. The author attributed the increase in ignition threshold to the increase in electrical resistivity from the polymeric coating. [68]

Table 2.2: ESD ignition threshold and performance (time to peak pressure, peak pressure) of n-Al/n-CuO coated with 0, 3, 5 and 10 weight% of Viton A. [68]

Percent Viton A by mass (%)	Time-to-peak pressure (μs)	Peak pressure, gauge (atm)	Ignition threshold (mJ)
0	170.82	5.00	< 0.14
3	574.42	2.42	0.80
5	825.72	2.19	2.11
10	5077.10	0.86	21.22

Chelsea et al correlated ESD sensitivities to both the electrical conductivity[69] of the thermite material as well as the aluminum particle size[70] used in the thermite system. In his report using micron-size thermites, Al/CuO was the only thermite system that got ignited due to its much higher electrical conductivity and the recorded minimum ignition energy (MIE) of Al/CuO having 50 weight% fuel is 4mJ.[69] There are also authors who separately conclude the dependence of ESD sensitivity on the particle size of both the aluminum and the oxidizer. Chelsea et al reported a high dependence of ignition energy on aluminum size in Al//MoO_3 nano-thermite, where MoO_3 with an average size of 44 nm was used. Measured MIE decreased from 4 mJ to 1 mJ and 0.25 mJ when Al size decreased from 2 μm to 100 nm and 50 nm, respectively.[70] Curtis et al reported dependence of ESD ignition threshold on oxidizer particle size in Al/Bi_2O_3 nano-thermite where the measured MIE decreased from 225 to 9 μJ when Bi_2O_3 size decreased from 320 to 50 nm (80 nm Al used throughout). [71]

Due to the dependence of a nano-thermite's ESD sensitivity to its electric conductivity, which could easily change from the mixtures' physical form, intimacy of contact, inherent conductivity, particle size and others, it is never clear cut from the literature to obtain a consistent ESD sensitivity value for any particular nano-thermite system. Comparison of data is more reliable if they were reported by the same research group using the same conditions. The ESD ignition threshold values for various nano-thermite investigated by different researchers is summarized in Table 2.3.

Table 2.3: Summary table of ignition threshold for various nano-thermites published by various authors

ESD ignition threshold	**Aluminum based nano-thermite**					**Phosphorus based nano-thermite**		
Author & year of published results	**Al-Bi_2O_3**	**Al-MoO_3**	**Al-Fe_2O_3**	**Al-CuO**	**Al-MnO_2**	**µm P / n-CuO**	**µm P / n-NiO**	**µm P / n-Fe_2O_3**
Puszynski, 2007[46]	0.125 µJ	50 µJ	1.25 mJ					
Carole Rossi, 2015 [72]	< 1 mJ		1 mJ	50 mJ				
David G. Kelly, 2016 [73]		6 mJ		>156 mJ				
Foley, 2007[68]				<0.14 mJ+				
Weir, 2013[70]		0.25 - 4 mJ ^						
Curtis Johnson, 2011[71]	9-225 µJ ^^							
Thiruvengadathan, 2015 [74]	0.16 mJ*							
Comet, 2008 [75]					1 mJ#			
Comet, 2010[76]						0.21 mJ	358.69 mJ	24.12 mJ

+ ignition energy increase if Viton A coating is applied

* ignition energy increase increases up to 1.2mJ if Graphene Oxide is added

ignition energy increase if MnO_2 is embedded within Carbon nanotube

^ ignition energy increase with Al particle size

^^ ignition energy increase with Bi_2O_3 size

2.3.2 Storage Stability of Nano-Thermites

While most research efforts focused on improving the performance of nano-thermites, the practical aspect of storage stability is often neglected. The oxidation of active metal content within the nano-thermite as well as the degradation through reaction with the atmospheric water vapor inhibits the retention of the high energy content of nano-thermites. Nano-aluminum particles are typically naturally passivated by an oxide outer layer of a few nm thick, which acts as a natural protection of the bulk Al within and prevents the high pyroforicity of nano-aluminum.

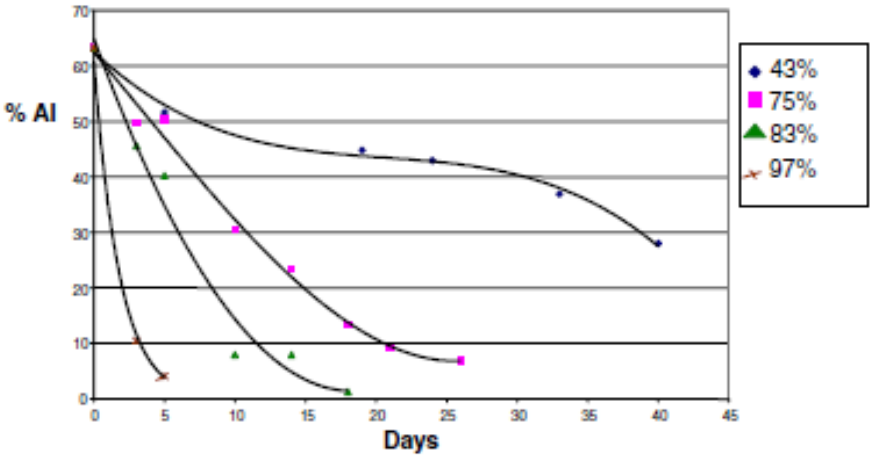

Figure 2.3: Decrease in active aluminum content with time from exposure to moisture at different humidity values.[77]

There have been quite a number of reports on n-Al passivation to improve their stability against oxidation through coating of the n-Al. Wang et al coated n-Al with PTFE to enhance their resistance against water and improve its reactivity.[78] n-Al coating using nitrocellulose was also attempted to passivate as well as improve the reactivity of n-Al, before its use in Al/CuO nano-thermite.[25] Pisharath et al [79] reported on improved resistance to ageing from surface modification of n-Al with three different organosilanes, including aminopropyltrimethoxysilane, azidopropyltrimethoxysilane and perfluorodecyltriethoxysilane. Other n-Al coatings using carbon[80], metallic Ni[81], perfluoro-organic carboxylates [82], and polymers (polyolefine and polyurethane[83]) have also been reported.

Studies on the stability of nano-thermites and efforts on passivation of nano-thermite as a system to improve their storage stability are fewer. Ke et al worked on developing a super-hydrophobic Al/Fe_2O_3 nano-thermite film in an attempt to increase their storage stability. In his work, he coated Al/Fe_2O_3 nano-thermite film prepared through electrophoretic deposition with 1H,1H,2H,2H-perfluorodecyltriethoxysilane to increase the resistance against water. The author reported a huge reduction in energy of unpassivated Al/Fe_2O_3 thermite from aging and a reduction on the loss of such energy was found through their passivation technique. [16]

2.4 Fabrication Techniques of Nano-Thermites

2.4.1 Solvent Mixing

The wide availability of nano-sized aluminum and metal oxides allowed the ease in preparation of their mixture through simple powder mixing. However, due to the low tolerance to electrostatic discharge, nano-thermite powders were never mixed in the dry form. Mixing of the nano-thermite powders were typically performed in a liquid medium, with hexane and isopropanol being the most popular medium.[4, 10, 84, 85] Liquid suspensions of the nanoparticles were mixed with the aid of ultrasonic actuators to break up the nanoparticle agglomerates. This is the most conventional and simplest way of mixing the metal/metal oxide nano-thermite powder and has been adopted in many studies.

2.4.2 Layered Deposition

Layered deposition technique is useful for producing ultrathin layers of nanoparticles. Alternating layers of aluminum and oxides can be deposited on different substrates. The technique allows stoichiometric amount of oxidizer to be deposited directly onto fuel particles. Barbee et al. fabricated Ni/Al energetic multilayer using through electron beam evaporation, onto which Al/Fe_2O_3 is coated by sol-gel technique. These nano-laminate composites can be used as igniters where they can undergo ignition upon suitable thermal, electrical or laser input.[86] Thin layer formations have been demonstrated using various techniques including thermal deposition, magnetron sputtering and electrophoretic depositions. Al/CuO nanofoils produced using magnetron sputtering has been researched rather extensively by research groups in US [87, 88] and France [33, 37]. The technique can be adopted to form alternating metal/metal oxide multi-layered structure (Figure 2.4).[37, 89] Zhang et al have also successfully formed Al/NiO and Al/CuO bilayered nanocomposites, adopting thermal evaporation and electroplating of metals as well as oxidation for in situ formation of oxides. [22, 61] Electrophoretic deposition has been adopted to deposit either a combined Al/CuO nano-thermite layer onto a conductive substrate [28, 90]or to deposit a layer of n-Al onto a Cu wire substrate with pre-formed CuO nano-wires (Figure 2.5).[23,41] The limitation of electrophoretic deposition is the need of a conductive substrate for deposition to take place, but it does offers faster processing in comparison to magnetron

sputtering which requires tedious interchange of sputtering material between each alternating layer. However, precise control of the ratio of fuel to oxidizer using the electrophoresis deposition is difficult to achieve.

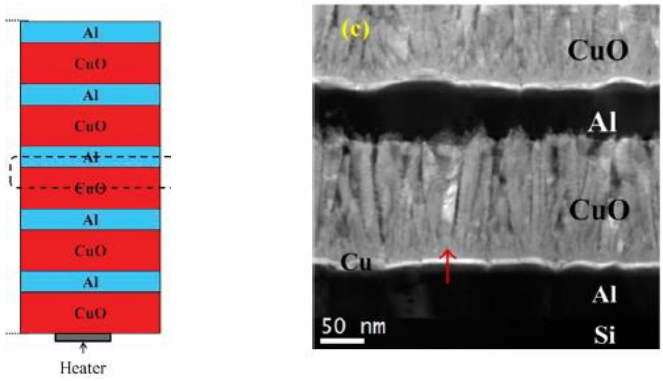

Figure 2.4: Al/CuO multi-layered nanolaminates produced through magnetron sputtering. [37, 89]

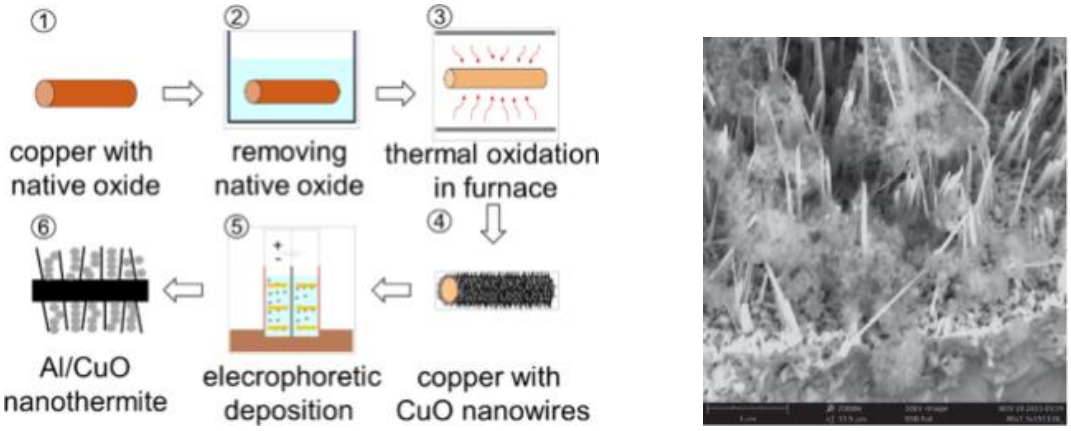

Figure 2.5: Electrophoretic deposition of n-Al to CuO nanowires. [41]

2.4.3 Sol-Gel

The sol-gel method has been known for many decades for the synthesis of many nano-sized oxides employing low temperatures. Nano structured energetic materials has been prepared using sol-gel chemistry by Gash et al.[91] In order to prepare nano-thermite composites, the metal is added just before the gelation of the oxide while stirring the solution constantly. The advantage of sol-gel processing is that it generates intimate

mixing of the fuel and oxidizer components and allows a uniform dispersion of fuel particles in an oxidizer network without involving any concentration gradient and settling effects. Both Al/Fe_2O_3 and Al/WO_3 have been reportedly produced by the same group of researchers. [10, 92-93] Some of the disadvantages include the difficulty in scaling up, limited metal precursors which can be gelled, impurities introduced from gelling chemicals and the high porosity of the matrix which is unsuitable for some applications.

2.4.4 Arrested Reactive Milling

Arrested reactive milling (ARM) has been used to prepare various nano-thermites including Al/Fe_2O_3, Al/CuO, Al/MoO_3 as well as some intermetallics such as Bi-Ti, Al-Ni. It is a versatile and economically viable technique. The ARM technique utilizes a 'top-down' approach where the nano-scaled structure is obtained by refining coarser starting materials. In ARM, the regular metal and/or metal oxide powders are employed as starting materials and are ball milled and the milling process is interrupted just before the self-sustained exothermic reaction is mechanically triggered. This technique results in the formation of fully dense, micron-sized composite particles with nanoscale structural features (Figure 2.6). This technique has been used extensively by the research group led by Dreizin.[29, 42,55, 94, 95]

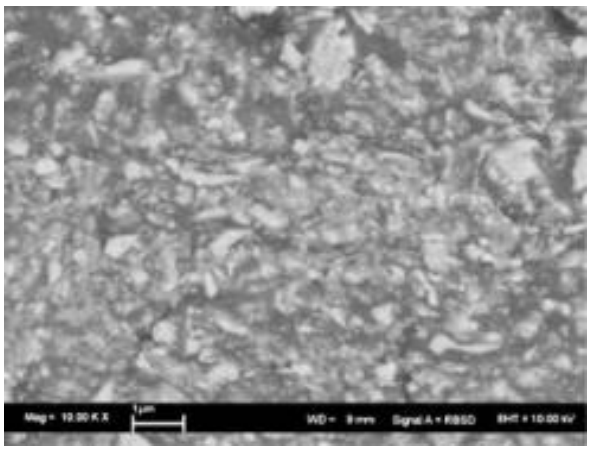

Figure 2.6: Al/CuO micron-size composite particles with nano-features produced using Arrestive Reactive Mixing.[95]

2.4.5 Self-Assembly

Supramolecular chemistry is defined by Prof. Jean-Marie Lehn in his Nobel lecture as "the chemistry of the intermolecular bond, covering the structures and functions of the entities formed by the association of two or more chemical species".[96] This field of studies brought about the focus on studying the chemistry beyond molecules and the intermolecular forces which could bring about organizations of these molecules and the subsequent creation of structures beyond. Molecular self-assembly is "the spontaneous association of molecules under equilibrium conditions into stable, structurally well-defined aggregates joined by non-covalent bonds" as described by Whitesides.[97]

While this concept of self-assembly may have originated from the organization of molecules, the range of scale that it could be applied to is endless. In the context of nanoscience and nanotechnology, self-assembly can begin from the molecular level such as the formation of self-assembled monolayers on nano-sized component surfaces to the ultimate arrangements of nano-sized components into larger ensembles.[98] Molecules with specific functionality can be chosen to form self-assembled monolayers on nano-particle surfaces to bring about surface functionalization that could lead to various material design possibilities. Surfaces with desired physical or chemical properties can be created. It can also lead to further induced interactions between the nano-particles leading to larger self-assembled entities displaying a desired function or property.

The commonly known head groups for attachment to metal and metal oxide surfaces to form self-assembled monolayers include thiols, silanes, carboxylic acids, phosphonic acids. However, thiols (-SH) groups are not known to bond to all metal/ metal oxide surfaces.[99] Metals and their oxides that has demonstrated good affinity for alkanethiols include gold, silver and copper.[100] Chemisorption was also proven successful on ZnO, but unsuccessful on TiO_2, Al_2O_3, and MgO.[101] No such specificity in attachment of silanes, carboxylic and phosphonic groups to particular metal/metal oxide substrates was reported. However, the affinity of ligands to the surface of their substrate does vary according to both the ligand head group as well as the substrate. While carboxylic groups display good flexibility in its attachment to a wide selection of metal/metal oxides, their attachments are generally weaker. Folkers et al [99] introduced the possibility of using hydroxamic acid groups as an alternative showing better binding constants to metal ions

in comparison to carboxylates. In his studies, he managed to rank the affinities of few ligands (hydroxamic acid > phosphonic acid > carboxylic acid) towards some common metal oxides including aluminum, zirconium and iron oxides.

Self-assembly of metal/ metal oxide nano-thermites have been demonstrated using various surface modification approaches. Self-assembly driven by electrostatic attraction of metal and metal oxide was the more popularly reported approach. Yong et al modified MnO_2 nanowires with long chain polyelectrolyte, poly(diallyldimethylammonium chloride) (PDDA), to achieve positively charged surface, onto which negatively charged aluminum nanoparticles were attracted by electrostatic attraction.[102] Malchi et al created nano-thermite microspheres (Figure 2.7) containing n-Al and n-CuO, through surface modification using functionalized alkanoic acid and alkanethiol ligands, respectively, to create opposing charges for attraction to take place. [103] Kim et al created oppositely charged aerosols of n-Al and n-Fe_2O_3 with the help of atomizers and unipolar chargers to create bipolar coagulated nano-thermites. [104]

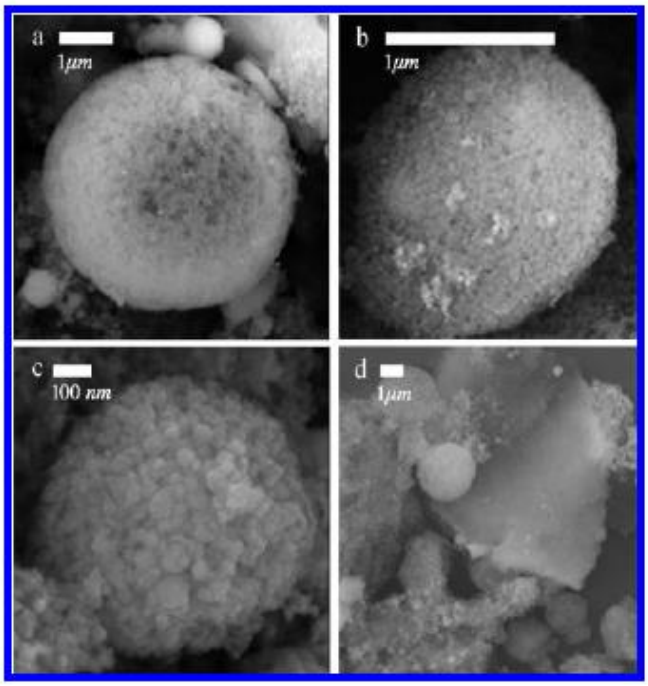

Figure 2.7: SEM images of n-Al/n-CuO microspheres created using electrostatic attraction, (a-c) showed the detail morphology of a single microsphere and (d) showed the modest yield of microspheres obtained from the process.[103]

Self-assembly with the help of bio-linkers such as protein cages and DNA has also been reported for the binary assembly of fuel and oxidizer. Slocik et al utilized cationized ferritin cages that are pre-loaded with either FeOOH or Ammonium Perchlorate (AP) to assemble on n-Al particles.[105] While Slocik et al reported successful self-assembly with exothermic reaction from the self-assembled n-Al with FeOOH or AP, combustion performance comparison was made using n-Al containing empty ferritin cages (without FeOOH or AP as the oxidizer) as the control. Reaction improvements in comparison to n-Al/FeOOH or n-Al/AP were not reported. Severac et al utilized the high specificity of oligonucleotide strands to bring about the assembly of n-Al and n-CuO through the hybridization of complimentary strands.[31] He reported an improved reaction exotherm using DSC studies while burn rate and pressure studies were not reported.

There were also reports on the use of poly-4-vinyl pyridine (P4VP) polymer containing pyridine as non-specific binding sites for both metal and metal oxide, to bring about the assembly of both. Shende et al [30] has applied the technique to Al/CuO while Cheng et al[19] has applied it to Al/Fe_2O_3. Shende et al reported an increased combustion wave speed from the self-assembled Al/CuO in comparison to randomly mixed Al/CuO. The research group led by Gangophadyay reported the successful assembly of Al/Bi_2O_3 and Al/MoO_3 using functionalized graphene oxide (GO) sheets.[106] The self-assembled Al/Bi_2O_3/GO showed improvement in reactivity (increased peak pressure, pressurization rate and burning rate) as well as a lowered sensitivity to ESD (Figure 2.8).[74]

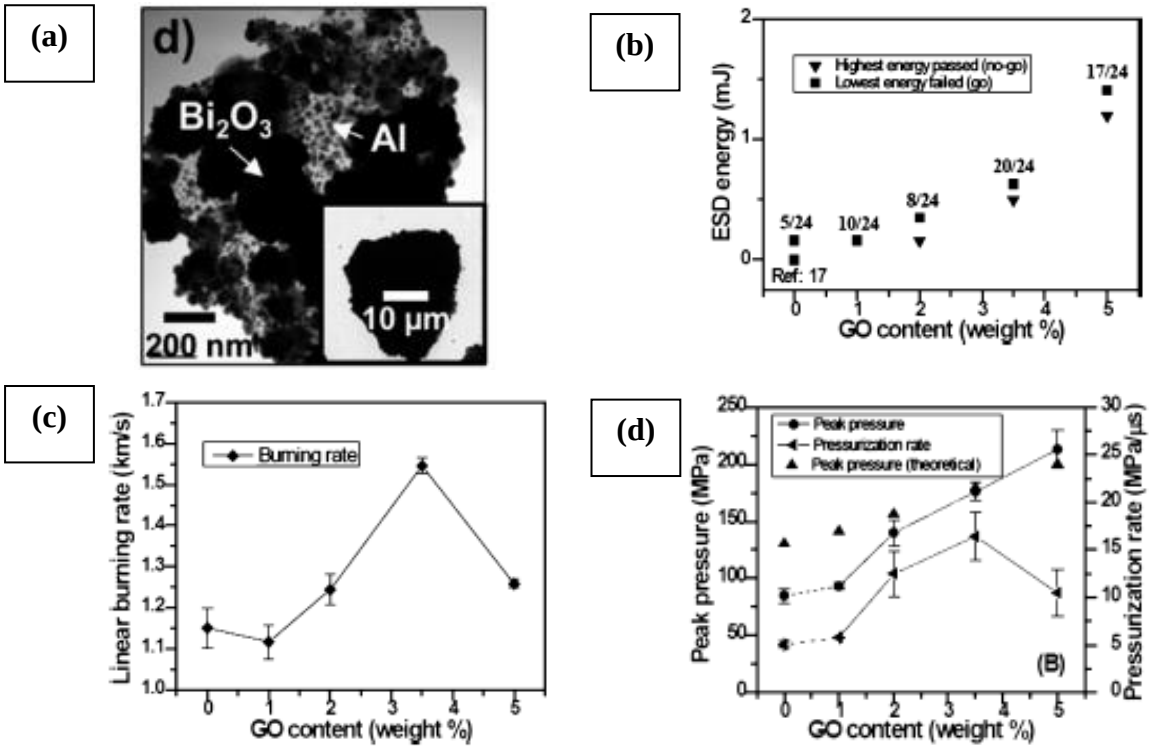

Figure 2.8: (a) TEM image of GO densely decorated with n-Al followed by Bi_2O_3 through self-assembly [106], (b) increase in ESD ignition threshold energy, (c) increase in burn rate, (d) increase in pressurization rate and peak pressure with inclusion of GO for self-assembly. [74]

2.5 Energetic Polymer Binder

Energetic composites having polymer matrix are often designed to engineer structurally viable composites that are moldable and machinable. Applications of such polymer-based energetic materials find use in applications such as polymer-bonded explosives (PBX), solid propellants and reactive casing/lining. Adding a binder to nano-thermite mixtures also helps to prevent the phase separation and inefficient burning of loose thermite powders and it improves the practical applicability of it. Common polymer matrixes that were often used include hydroxyl terminated polybutadiene (HTPB), carboxy terminated polybutadiene (CTPB), hydroxyl terminated polyether (HTPE) and epoxy. However, their inert nature could significantly bring down the energy and reactivity of any energetic composition. The research on the use of energetic polymers is emerging in view of pumping additional energy into the system without compromising the mechanical properties of the desired composite.

Energetic polymer are polymer containing explosophoric functional groups (such as NO_2, NF_2, N_3), which are chemical groups that gave organic compounds their explosive properties. Fluoropolymers, which contain the highly electronegative fluorine atoms in the hydrocarbon long chains, has also often been studied as a binder, as they could double as a strong oxidizer in the presence of metal and release a large amount of energy. Studies on the addition of energetic polymer to nano-aluminum or nano-thermites have been demonstrated for different purposes, including the enhancement of reactivity, tuning the pressure generation or even the reduction of sensitivity to ESD stimuli [68].

2.5.1 Fluoropolymer

Fluoropolymers have been used as oxidizers with metal fuels to form reactive mixtures. The driving force behind oxidation of the metal is the large enthalpy of formation (1510 kJ/mol) of the metal–fluorine bond, which results in the exothermic release of energy. The fluorination instead of oxidation of Al is usually preferred due to the stronger Al-F bond energy (664 ± 6 kJ/mol) that is higher than that of Al-O (512 ± 4 kJ/mol).

Polytetrafluoroethylene (PTFE), which is commercially known as Teflon, is one of the fluoropolymers that has been studied extensively with n-Al. It has one of the highest fluorine content of 72%. Processing of PTFE by conventional melt processing techniques was difficult due to the high melt viscosity (109 to 1011 Pa·s at 380 ºC). This led to the development of several co-polymers and terpolymers of tetrafluoroethylene (TFE), hexafluoropropylene (HFP) and vinylidene fluoride (VDF), which have been used quite extensively as binders for plastic-bonded explosives. [107] Among which, Viton A and THV have been more popularly studied in conjunction with n-Al or nano-thermites as a binder. Viton A is a copolymer of VDF and HFP, containing approximately 66% of fluorine. Viton is a commercially available product manufactured by DuPont and is also marketed as Fluorel by 3M, while THV is a terpolymer of TFE, HFP and VDF.

Foley et al[68] added Viton A to Al/CuO nano-thermites to study its effect on ESD ignition threshold. Foley et al desired to achieve safer nano-thermite composite with a higher ESD ignition threshold without diminishing the original combustion performance of Al/CuO nano-thermite through the use of a fluoropolymer coating. However, while they

have proven that Viton A coating could produce a safer nano-thermite composite with increased ignition threshold (from < 0.14 mJ to 22 mJ for a 10 weight% polymer coating), its peak pressure and pressurization rate decreased with the addition of Viton A. Seshadri et al [108] adopted FC2175 (chemically the same as Viton)as a binder for creating Al/NiO pellets and reported a reduction in combustion rate with the introduction of this fluoropolymer.

Besides perfluorinated polymers, perfluorinated hydrocarbon short chains have also been reportedly used as coating or surface modifiers in thermite compositions. Perfluorinated organosilanes (1H,1H,2H,2H-Perfluorodecyltriethoxysilane) coating was also adopted by Ke et al [16] on Al/Fe_2O_3 to create a hydrophobic passivation against aging. They also reported an improved energy release characteristic due to the Pre-Ignition Reaction (PIR) of Al with F in the fluorinated passivation coat. Kappagantula et al [109] and McCollum et al [110] have also both reported the use of a perfluorinated hydrocarbon coating on nano-thermites. Kappagantula et al [109] reported the improved reactivity and flame propagation speed of Al/MoO_3 by introducing perfluoro tetradecanoic acid (PFTD) coating on n-Al. They also reported that not all perfluorinated acid coating enhances the reactivity, and its effect is likely dependent on whether it could enhance the PIR of the system. Their conclusion was drawn from a reduced reactivity of the same nano-thermite system from using a very similar perfluorinated acid coating, perfluoro sebacic acid (PFS). On the other-hand, McCollum et al [110] reported that the effect of Perfluoropolyether (PFPE) coating on nano-thermite is dependent on the metal oxide used in the system, where PFPE could improve the reactivity of Al/MoO_3 but worsen that of Al/CuO.

Their reports are indications that the inter-reaction between the Al, metal oxide and fluoro-based compound are relatively complex and are not fully understood for full utilization of the benefits of adding perfluorinated compounds.

2.5.2 Nitrogen containing Polymer

Nitrocellulose, often in conjunction with nitroglycerin, is one of the earliest nitrogen-containing energetic binder used in PBX and propellants. It is a main ingredient in double-based propellant and is often used as a gas-generating binder for propellant

applications. Recently, nitrocellulose has been studied in thermite compositions to act as a gas-releasing binder. It was included as a binder in Al/Bi_2O_3 compositions for potential application as microthruster compositions by Staley et al [111]. A 5 to 10 wt% inclusion of nitrocellulose was able to improve the specific impulse of the nano-thermite composition with lesser probability of unwanted ignition during a high-g launch of the micro-thruster. The highly gasifying nitrocellulose was able to improve the thrust efficiency while still acting as a passivation to cushion the nano-thermites to improve its safety during launch. [111]

In a separate work by Wang et al [26], nitrocellulose was included as a binder to electrospray n-Al/n-CuO microparticles. Nitrocellulose content of up to 5 wt% was found to increase the maximum pressure and pressurization rate. Further increase in the amount of nitrocellulose was found to diminish its pressure generating performance. The gas produced from nitrocellulose was postulated to prevent the sintering of n-Al and n-CuO, thus improving their reaction rate. However, too much gas resulted in overpressurization and disintegration of the Al/CuO structure within each microparticle, resulting in inefficient reaction.

Other nitrogen containing energetic polymers including glycidyl azide polymer (GAP), poly(glycidyl nitrate) (PGN) and polyoxetanes such as poly(3-nitratomethyl-3-methyloxetane) (polyNIMMO),Poly(3-azidomethyl 3-methyl oxetane) (polyAMMO), poly-3,3-bis(3-azidomethyl)oxetane (polyBAMO), have reportedly been utilized as binders in explosive and propellant formulations. [107, 112] Among which, GAP is one of the most popular choices due to its higher availability and good binding properties. [107, 112] There was no published work on the application of GAP to nano-thermites.

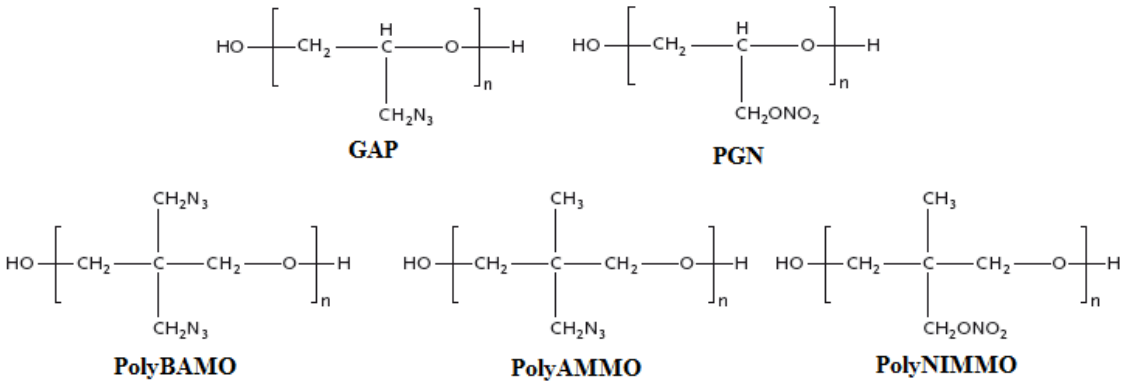

Figure 2.9: Chemical structure of common azido and nitro group containing energetic polymers [107, 112]

2.5.3 Other Performance Tuning Polymer Binder

(Acrylamidomethyl) cellulose acetate butyrate (AAMCAB) is neither a fuel nor oxidizer and does not react with Al. Bezmelnitsyn et al [113] reported the incorporation of AAMCAB in the Al/Fe_2O_3 nano-thermite to improve the sustained pressure over a longer period of time, which can facilitate its use in propellant applications. However, the combustion rate of the mixture was found to decrease with the addition of AAMCAB. As reported in their pressure measurements [113], the peak pressure were found to increase with increasing amount of AAMCAB (0 to 20 wt%) while reactivity (pressurization rate) was found to decrease with the addition of the polymer. Although the reactivity of Al/Fe_2O_3 was found to decrease with the introduction of this polymer, it shows increased peak pressure along with a longer duration of sustained pressure. The author [113] proposed the potential application as a propellant initiator with tunable balance between reactivity and pressure generation.

2.6 Summary

From the last few decades of published work on thermites, it is not difficult to understand that focus has been on reaping the benefits brought about by the availability of nano-sized metal and metal oxides. The huge improvement in the reactivity of metal and metal oxide in a thermite system was only made possible via the intimacy of mixing of these two components.

Among the vast selection of nano-thermite systems, Al/NiO is not among the most studied as compared to Al/CuO and Al/Fe_2O_3. Al/NiO were highlighted for studies mostly owing to their inherently lower gas generating nature, which could promise lower burn disturbances, an ideal case for certain applications including microinitiators. However, published work on this system is scarce at this point and no comparison studies have been made with other nano-thermite systems. The gasless characteristics of Al/NiO system has been mentioned by a few authors but they were all based on theoretical assumptions. There were no reported studies made on the pressure generation characteristics of n-Al/n-NiO.

Besides the total energy release and combustion performances, other aspects involving safety and storage stability are important factors limiting the actual applicability of a nanoenergetic material. However, there were no published data on the sensitivity of n-Al/n-NiO to external stimuli, making it impossible to gauge the safety of handling this nano-thermite material. This work aims to fill up the lacking data from the literature on the reactivity, pressure generation and sensitivity of n-Al/n-NiO, which are important characteristics to be understood before their practical applications.

Some factors, including coating and increased particle size, were found to be effective in decreasing the ESD sensitivity of some nano-thermites, but these techniques typically bring down the reactivity as well. This work aims to study the impact of better mixing homogeneity, brought about by self-assembly, on the sensitivity of nano-thermites, in hope of establishing both reduced sensitivity and improved reactivity.

The addition of a binder to the nano-thermite transforms it into a 3-D matrix that is more workable and possesses more practical applicability. Fluoropolymers, including Polytetrafluoroethylene (PTFE) and various copolymers of it with hexafluoropropylene (HFP) and vinylidene fluoride (VDF), have been studied with n-Al and other Al-based compositions due to the potential of yielding additional energy from Al-F reaction. The addition of fluorinated hydrocarbon compounds to nano-thermites have been reported to generate pre-ignition reaction in some cases and were useful in enhancing the reactivity of these materials. The interaction of Al, metal oxide and fluorine in the system is complex and has been receiving continuous research attention in recent years. The work

here aims to study how the inclusion of a fluoropolymer to the n-Al/n-NiO system impacts its reaction mechanism, pressure generation as well as sensitivity (safety) of the system.

References

1. Martirosyan, K., High-Density Nanoenergetic Gas Generators. In *Handbook of Nanoscience, Engineering, and Technology, Third Edition*, CRC Press: 2012; pp 739-758.
2. Rossi, C.; Rossi, C., Nanosized Aluminum as Metal Fuel. In *Al-Based Energetic Nanomaterials*, John Wiley & Sons, Inc.: 2015; pp 1-26.
3. Dreizin, E. L., Metal-based reactive nanomaterials. *Progress in Energy and Combustion Science* **2009,** *35* (2), 141-167.
4. Pantoya, M. L.; Granier, J. J., Combustion Behavior of Highly Energetic Thermites: Nano versus Micron Composites. *Propellants, Explosives, Pyrotechnics* **2005,** *30* (1), 53-62.
5. Fischer, S. H.; Grubelich, M. C., Theoretical Energy Release of Thermites, Intermetallics, and Combustible Metals. In *24th International Pyrotechnics Seminar* Monterey, CA., 1998.
6. Kuo, K. K.; Risha, G. A.; Evans, B. J.; Boyer, E., Potential Usage of Energetic Nano-sized Powders for Combustion and Rocket Propulsion. *MRS Proceedings* **2011,** *800*.
7. Zhao, N.; He, C.; Liu, J.; Gong, H.; An, T.; Xu, H.; Zhao, F.; Hu, R.; Ma, H.; Zhang, J., Dependence of catalytic properties of Al/Fe2O3 thermites on morphology of Fe2O3 particles in combustion reactions. *Journal of Solid State Chemistry* **2014,** *219* , 67-73.
8. Stiegman, A. E.; Park, C.-D.; Mileham, M.; Burgt, L. J. v. d.; Kramer, M. P., Dynamics of Al/Fe2O3 MIC Combustion from Short Single-Pulse Photothermal Initiation and Time-Resolved Spectroscopy. *Propellants, Explosives, Pyrotechnics* **2009,** *34*, 293 – 296.
9. Singh, S.; Singh, G.; Kulkarni, N.; Mathe, V. L.; Bhoraskar, S. V., Synthesis, characterization and catalytic activity of Al/Fe2O3 nanothermite. *J Therm Anal Calorim* **2015,** *119* (1), 309-317.
10. Plantier, K. B.; Pantoya, M. L.; Gash, A. E., Combustion wave speeds of nanocomposite Al/Fe2O3: the effects of Fe2O3 particle synthesis technique. *Combustion and Flame* **2005,** *140* (4), 299-309.
11. Patel, R.; Kim, S. J.; Kim, J. K.; Park, J. S.; Kim, J. H., Preparation of Al@Fe2O3 Core-Shell Composites Using Amphiphilic Graft Copolymer Template. *Korean Chemical Engineering Research* **2014,** *52* (2), 209-213.
12. Park, C.-D.; Mileham, M.; van de Burgt, L. J.; Muller, E. A.; Stiegman, A. E., The Effects of Stoichiometry and Sample Density on Combustion Dynamics and Initiation Energy of Al/Fe2O3 Metastable Interstitial Composites. *The Journal of Physical Chemistry C* **2010,** *114* (6), 2814-2820.
13. Menon, L.; Patibandla, S.; Ram, K. B.; Shkuratov, S. I.; Aurongzeb, D.; Holtz, M.; Berg, J.; Yun, J.; Temkin, H., Ignition studies of Al/Fe_2O_3 energetic nanocomposites. *Applied Physics Letters* **2004,** *84* (23), 4735-4737.

14. Mehendale, B.; Shende, R.; Subramanian, S.; Gangopadhyay, S.; Redner, P.; Kapoor, D.; Nicolich, S., Nanoenergetic Composite of Mesoporous Iron Oxide and Aluminum Nanoparticles. *Journal of Energetic Materials* **2006,** *24*, 341-360.
15. Luísa Durães, J. C. A. P., Radial Combustion Propagation in Iron(III) Oxide/Aluminum Thermite Mixtures. *Propellants, Explosives, Pyrotechnics* **2006,** *31* (1), 42-49.
16. Ke, X.; Zhou, X.; Hao, G.; Xiao, L.; Liu, J.; Jiang, W., Rapid fabrication of superhydrophobic Al/Fe2O3 nanothermite film with excellent energy-release characteristics and long-term storage stability. *Applied Surface Science* **2017,** *407*, 137-144.
17. Ferranti, L.; Thadhani, N. N., Dynamic Mechanical Behavior Characterization of Epoxy-Cast Al + Fe2O3 Thermite Mixture Composites. *Metallurgical and Materials Transactions A* **2007,** *38* (11), 2697-2715.
18. Fan, R.-H.; Lü, H.-L.; Sun, K.-N.; Wang, W.-X.; Yi, X.-B., Kinetics of thermite reaction in Al-Fe2O3 system. *Thermochimica Acta* **2006,** *440* (2), 129-131.
19. Cheng, J. L.; Hng, H. H.; Ng, H. Y.; Soon, P. C.; Lee, Y. W., Synthesis and characterization of self-assembled nanoenergetic Al-Fe2O3 thermite system. *Journal of Physics and Chemistry of Solids* **2010,** *71* (2), 90-94.
20. Cheng, J. L.; Hng, H. H.; Lee, Y. W.; Du, S. W.; Thadhani, N. N., Kinetic study of thermal- and impact-initiated reactions in Al–Fe2O3 nanothermite. *Combust. Flame* **2010,** *157*, 2241.
21. Zhang, K.; Rossi, C.; Petrantoni, M.; Mauran, N., A Nano Initiator Realized by Integrating Al/CuO-Based Nanoenergetic Materials With a Au/Pt/Cr Microheater. *Journal of Microelectromechanical Systems* **2008,** *17* (4), 832-836.
22. Zhang, K.; Rossi, C.; Ardila Rodriguez, G. A.; Tenailleau, C.; Alphonse, P., Development of a nano-Al ⁄ CuO based energetic material on silicon substrate. *Applied Physics Letters* **2007,** *91* (11), 113117.
23. Wu, M.-H.; Chiang, Y.-C. In *Al/CuO Nanothermite Shell Assembled via Depositing Aluminum Nanoparticles onto CuO Nanowire Array on a Copper Wire*, Proceedings of the 25th International Colloquium on the Dynamics of Explosions and Reactive Systems, Leeds, UK, 2-7 August 2015; Radulescu, M. I., Ed. Leeds, UK, 2015.
24. Weismiller, M. R.; Malchi, J. Y.; Yetter, R. A.; Foley, T. J., Dependence of flame propagation on pressure and pressurizing gas for an Al/CuO nanoscale thermite. *Proceedings of the Combustion Institute* **2009,** *32* (2), 1895-1903.
25. Wang, J.; Hu, A.; Persic, J.; Wen, J. Z.; Norman Zhou, Y., Thermal stability and reaction properties of passivated Al/CuO nano-thermite. *Journal of Physics and Chemistry of Solids* **2011,** *72* (6), 620-625.
26. Wang, H.; Jian, G.; Egan, G. C.; Zachariah, M. R., Assembly and reactive properties of Al/CuO based nanothermite microparticles. *Combustion and Flame* **2014,** *161* (8), 2203-2208.
27. Umbrajkar, S. M.; Schoenitz, M.; Dreizin, E. L., Exothermic reactions in Al–CuO nanocomposites. *Thermochimica Acta* **2006,** *451* (1–2), 34-43.
28. Sullivan, K.; Kuntz, J.; Gash, A., Electrophoretic deposition and mechanistic studies of nano-Al/CuO thermites. *Journal of Applied Physics* **2012,** *112* (2), 024316.
29. Stamatis, D.; Jiang, Z.; Hoffmann, V. K.; Schoenitz, M.; Dreizin, E. L., Fully Dense, Aluminum-Rich Al-CuO Nanocomposite Powders for Energetic Formulations In *44th AIAA/ASME/SAE/ASEE Joint Propulsion Conference & Exhibit*, Hartford, CT, 2008.
30. Shende, R.; Subramanian, S.; Hasan, S.; Apperson, S.; Thiruvengadathan, R.; Gangopadhyay, K.; Gangopadhyay, S.; Redner, P.; Kapoor, D.; Nicolich, S.; Balas, W.,

Nanoenergetic Composites of CuO Nanorods, Nanowires, and Al-Nanoparticles. *Propellants, Explosives, Pyrotechnics* **2008,** *33* (2), 122-130.
31. Séverac, F.; Alphonse, P.; Estève, A.; Bancaud, A.; Rossi, C., High-Energy Al/CuO Nanocomposites Obtained by DNA-Directed Assembly. *Adv. Funct. Mater.* **2012,** *22*, 323.
32. Sanders, V. E.; Asay, B. W.; Foley, T. J.; Tappan, B. C.; Pacheco, A. N.; Son, S. F., Reaction Propagation of Four Nanoscale Energetic Composites (Al/MoO3, Al/WO3, Al/CuO, and Bi2O3). *Journal of Propulsion and Power* **2007,** *23* (4), 707-714.
33. Petrantoni, M.; Rossi, C.; Salvagnac, L.; Conédéra, V.; Estève, A.; Tenailleau, C.; Alphonse, P.; Chabal, Y. J., Multilayered Al/CuO thermite formation by reactive magnetron sputtering: Nano versus micro. *Journal of Applied Physics* **2010,** *108* (8), 084323.
34. Petrantoni, M.; Rossi, C.; Conédéra, V.; Bourrier, D.; Alphonse, P.; Tenailleau, C., Synthesis process of nanowired Al/CuO thermite. *Journal of Physics and Chemistry of Solids* **2010,** *71* (2), 80-83.
35. Ohkura, Y.; Liu, S.-Y.; Rao, P. M.; Zheng, X., Synthesis and ignition of energetic CuO/Al core/shell nanowires. *Proceedings of the Combustion Institute* **2011,** *33* (2), 1909-1915.
36. Monk, I.; Schoenitz, M.; Jacob, R. J.; Dreizin, E. L.; Zachariah, M. R., Combustion characteristics of stoichiometric Al-CuO nanocomposite thermites prepared by different methods. *Combustion Science and Technology* **2016**.
37. Marin, L.; Nanayakkara, C. E.; Veyan, J. F.; Warot-Fonrose, B.; Joulie, S.; Esteve, A.; Tenailleau, C.; Chabal, Y. J.; Rossi, C., Enhancing the Reactivity of Al/CuO Nanolaminates by Cu Incorporation at the Interfaces. *ACS Appl Mater Interfaces* **2015,** *7* (22), 11713-8.
38. Malchi, J. Y.; Yetter, R. A.; Foley, T. J.; Son, S. F., The Effect of Added Al2O3on the Propagation Behavior of an Al/CuO Nanoscale Thermite. *Combustion Science and Technology* **2008,** *180* (7), 1278-1294.
39. He, S.; Chen, J.; Yang, G.; Qiao, Z.; Li, J., Controlled synthesis and application of nano-energetic material based on Al-CuO system.pdf>. *Central European Journal of Energetic Materials* **2015,** *12* (1), 129-144.
40. Glavier, L.; Taton, G.; Ducéré, J.-M.; Baijot, V.; Pinon, S.; Calais, T.; Estève, A.; Djafari Rouhani, M.; Rossi, C., Nanoenergetics as pressure generator for nontoxic impact primers: Comparison of Al/Bi2O3, Al/CuO, Al/MoO3 nanothermites and Al/PTFE. *Combustion and Flame* **2015,** *162* (5), 1813-1820.
41. Chiang, Y.-C.; Wu, M.-H., Assembly and reaction characterization of a novel thermite consisting aluminum nanoparticles and CuO nanowires. *Proceedings of the Combustion Institute* **2017,** *36* (3), 4201-4208.
42. Badiola, C.; Zhu, X.; Schoenitz, M.; Dreizin, E. L. In *Aluminum Rich Al-CuO Nanocomposite Materials Prepared by Arrested Reactive Milling at Cryogenic and Room Temperature*, 47th AIAA Aerospace Sciences Meeting including The New Horizons Forum and Aerospace Exposition, Aerospace Sciences Meetings, Orlando, Florida, American Institute of Aeronautics and Astronautics: Orlando, Florida, 2009.
43. Apperson, S.; Shende, R. V.; Subramanian, S.; Tappmeyer, D.; Gangopadhyay, S.; Chen, Z.; Gangopadhyay, K.; Redner, P.; Nicholich, S.; Kapoor, D., Generation of fast propagating combustion and shock waves with copper oxide/aluminum nanothermite composites. *Applied Physics Letters* **2007,** *91* (24), 243109.
44. Ahn, J. Y.; Kim, S. B.; Kim, J. H.; Jang, N. S.; Kim, D. H.; Lee, H. W.; Kim, J. M.; Kim, S. H., A micro-chip initiator with controlled combustion reactivity realized by

integrating Al/CuO nanothermite composites on a microhotplate platform. *Journal of Micromechanics and Microengineering* **2016,** *26* (1), 015002.
45. Ahn, J. Y.; Kim, J. H.; Kim, J. M.; Lee, D. W.; Park, J. K.; Lee, D.; Kim, S. H., Combustion characteristics of high-energy Al/CuO composite powders: The role of oxidizer structure and pellet density. *Powder Technology* **2013,** *241*, 67-73.
46. Puszynski, J. A.; Bulian, C. J.; Swiatkiewicz, J. J., Processing and Ignition Characteristics of Aluminum–Bismuth Trioxide Nanothermite System
Journal of Propulsion and Power **2007,** *23* (4), 698-706.
47. Baijot, V.; Glavier, L.; Ducéré, J.-M.; Djafari Rouhani, M.; Rossi, C.; Estève, A., Modeling the Pressure Generation in Aluminum-Based Thermites. *Propellants, Explosives, Pyrotechnics* **2015,** *40* (3), 402-412.
48. Zhang, R.; Xue, Y.; Jiang, J.-c.; Lei, X.-R. In *Performance of Laser Ignition of Nanocomposite Energetic Materials Al-MoO3*, Thirty-Third International Pyrotechnics Seminar, Fort Collins, Colorado, 16-21 July 2006; IPSUSA Seminars: Fort Collins, Colorado, 2006; pp 787-792.
49. Walter, K. C.; Pesiri, D. R.; Wilson, D. E., Manufacturing and Performance of Nanometric Al/MoO3 Energetic Materials. *Journal Of Propulsion And Power* **2007,** *23* (4).
50. Umbrajkar, S. M.; Seshadri, S.; Schoenitz, M., Aluminum-Rich Al–MoO3 Nanocomposite Powders Prepared by Arrested Reactive Milling. *Journal of Propulsion and Power* **2008,** *24* (2), 192-198.
51. Umbrajkar, S. M.; Chen, C.-M.; Schoenitz, M.; Dreizin, E. L., On problems of isoconversion data processing for reactions in Al-rich Al-MoO3 thermites. *Thermochimica Acta* **2008,** *477* (1-2), 1-6.
52. Son, S. F.; Asay, B. W.; Foley, T. J.; Yetter, R. A.; Wu, M. H.; Risha, G. A., Combustion of Nanoscale Al/MoO_3 Thermite in Microchannels. *Journal of Propulsion and Power* **2007,** *23* (4), 715-721.
53. Schoenitz, M.; Umbrajkar, S. M.; Dreizin, E. L., Kinetic Analysis of Thermite Reactions in Al-MoO3 Nanocomposites. *Journal of Propulsion and Power* **2007,** *23* (4), 683-687.
54. Granier, J. J. Combustion Characteristics Of Al Nanoparticles And Nanocomposite Al+Moo3 Thermites. Texas Tech University, 2005.
55. Dutro, G. M.; Yetter, R. A.; Risha, G. A.; Son, S. F., The effect of stoichiometry on the combustion behavior of a nanoscale Al/MoO3 thermite. *Proceedings of the Combustion Institute* **2009,** *32* (2), 1921-1928.
56. Dutro, G. M.; Son, S. F.; Tappan, A. S., The Effect of Microscale Confinement Diameter on the Combustion of an Al/MoO3 Thermite
In *44th AIAA/ASME/SAE/ASEE Joint Propulsion Conference & Exhibit*
Hartford, CT, 2008.
57. Bouma, R. H. B.; Meuken, D.; Verbeek, R.; Martinez Pacheco, M.; Katgerman, L., Shear Initiation of Al/MoO3-Based Reactive Materials. *Propellants, Explosives, Pyrotechnics* **2007,** *32* (6), 447-453.
58. Zhang, K.; Rossi, C.; Alphonse, P.; Tenailleau, C.; Cayez, S.; Chane-Ching, J.-Y., Integrating Al with NiO nano honeycomb to realize an energetic material on silicon substrate. *Applied Physics A: Materials Science & Processing* **2009,** *94* (4), 957-962.
59. Wen, J. Z.; Ringuette, S.; Bohlouli-Zanjani, G.; Hu, A.; Nguyen, N. H.; Persic, J.; Petre, C. F.; Zhou, Y. N., Characterization of thermochemical properties of Al nanoparticle and NiO nanowire composites. *Nanoscale Research Letters* **2013,** *8* (1), 184-184.

60. Zhang, D.; Li, X., Fabrication and Kinetics Study of Nano-Al/NiO Thermite Film by Electrophoretic Deposition. *The Journal of Physical Chemistry A* **2015,** *119* (20), 4688-4694.
61. Zhang, K.; Rossi, C.; Alphonse, P.; Tenailleau, C.; Cayez, S.; Chane-Ching, J.-Y., Integrating Al with NiO nano honeycomb to realize an energetic material on silicon substrate. *Applied Physics A* **2008,** *94* (4), 957-962.
62. Yan, Y.; Shi, W.; Jiang, H.; Xiong, J.; Zhang, W.; Li, Y., Fabrication and Characterization of Al/NiO Energetic Nanomultilayers. *Journal of Nanomaterials* **2015,** *2015*, 6.
63. Altham, J. A.; McLain, J. H.; Schwab, G. M., The Reactivity of Nickel Oxide. In *Zeitschrift für Physikalische Chemie*, 1971; Vol. 74, p 139.
64. Seshadri, P.; Mason, B.; Son, S.; Groven, L.; Gash, A., Burning Rates of Nano-Aluminum/ FC-2175/ Nickel Oxide Composites as a Function of Doping, Pressure and Magnetic Field. In *49th AIAA Aerospace Sciences Meeting including the New Horizons Forum and Aerospace Exposition*, American Institute of Aeronautics and Astronautics: 2011.
65. Rossi, C., Two Decades of Research on Nano-Energetic Materials. *Propellants, Explosives, Pyrotechnics* **2014,** *39* (3), 323-327.
66. Puszynski, J. A.; Bulian, C. J.; Swiatkiewicz, J. J., The Effect of Nanopowder Attributes on Reaction Mechanism and Ignition Sensitivity of Nanothermites. *MRS Proceedings* **2006,** *896*.
67. Greason, W. D., Electrostatic discharge characteristics for the human body and circuit packs. *Journal of Electrostatics* **2003,** *59* (3), 285-300.
68. Foley, T.; Pacheco, A.; Malchi, J.; Yetter, R.; Higa, K., Development of Nanothermite Composites with Variable Electrostatic Discharge Ignition Thresholds. *Propellants, Explosives, Pyrotechnics* **2007,** *32* (6), 431-434.
69. Weir, C.; Pantoya, M. L.; Ramachandran, G.; Dallas, T.; Prentice, D.; Daniels, M., Electrostatic discharge sensitivity and electrical conductivity of composite energetic materials. *Journal of Electrostatics* **2013,** *71* (1), 77-83.
70. Weir, C.; Pantoya, M. L.; Daniels, M. A., The role of aluminum particle size in electrostatic ignition sensitivity of composite energetic materials. *Combustion and Flame* **2013,** *160* (10), 2279-2281.
71. Johnson, C. E.; Higa, K. T.; Tran, T. T.; Albro, W. R., Thermite Initiation Processes and Thresholds. *MRS Proceedings* **2012,** *1405*.
72. Rossi, C.; Rossi, C., Applications of Al Nanoparticles: Nanothermites. In *Al-Based Energetic Nanomaterials*, John Wiley & Sons, Inc.: 2015; pp 33-61.
73. David G. Kelly; Pascal Beland; and, P. B.; Petre, C.-F. In *The Performance Modification of Aluminum Nanothermites Prepared Using Resonant Acoustic Mixing*, 42th International Pyrotecnics Society Seminar, 2016; pp 3-11.
74. Thiruvengadathan, R.; Staley, C.; Geeson, J. M.; Chung, S.; Raymond, K. E.; Gangopadhyay, K.; Gangopadhyay, S., Enhanced Combustion Characteristics of Bismuth Trioxide-Aluminum Nanocomposites Prepared through Graphene Oxide Directed Self-Assembly. *Propellants, Explosives, Pyrotechnics* **2015**, n/a-n/a.
75. Comet, M.; Pichot, V.; Spitzer, D.; Siegert, B.; Ciszek, F.; Piazzon, N.; Gibot, P. In *Elaboration and characterization of manganese oxide (MnO2) based "green" nanothermites*, 39th International Annual Conference of ICT, 2008; p 1.
76. Comet, M.; Pichot, V.; Siegert, B.; Schnell, F.; Ciszek, F.; Spitzer, D., Phosphorus-based nanothermites: A new generation of energetic materials. *Journal of Physics and Chemistry of Solids* **2010,** *71* (2), 64-68.

77. Puszynski, J. A., Reactivity of Nanosize Aluminum with Metal Oxides and Water Vapor. *MRS Proceedings* **2004,** *800*.
78. Wang, J.; Qiao, Z.; Yang, Y.; Shen, J.; Long, Z.; Li, Z.; Cui, X.; Yang, G., Core–Shell Al-Polytetrafluoroethylene (PTFE) Configurations to Enhance Reaction Kinetics and Energy Performance for Nanoenergetic Materials. *Chemistry – A European Journal* **2016,** *22* (1), 279-284.
79. Pisharath, S.; Zhang, F.; Ang, H. G., Influence of passivation on ageing of nano-aluminum: Heat flux calorimetry and microstructural studies. *Thermochimica Acta* **2016,** *635*, 59-69.
80. Park, K.; Rai, A.; Zachariah, M. R., Characterizing the coating and size-resolved oxidative stability of carbon-coated aluminum nanoparticles by single-particle mass-spectrometry. *Journal of Nanoparticle Research* **2006,** *8* (3), 455-464.
81. Foley, T. J.; Johnson, C. E.; Higa, K. T., Inhibition of Oxide Formation on Aluminum Nanoparticles by Transition Metal Coating. *Chemistry of Materials* **2005,** *17* (16), 4086-4091.
82. Jouet, R. J.; Warren, A. D.; Rosenberg, D. M.; Bellitto, V. J.; Park, K.; Zachariah, M. R., Surface Passivation of Bare Aluminum Nanoparticles Using Perfluoroalkyl Carboxylic Acids. *Chemistry of Materials* **2005,** *17* (11), 2987-2996.
83. Dubois, C.; Lafleur, P. G.; Roy, C.; Brousseau, P.; Stowe, R. A., Polymer-Grafted Metal Nanoparticles for Fuel Applications. *Journal of Propulsion and Power* **2007,** *23* (4), 651-658.
84. Sanders, V. E.; Asay, B. W.; Foley, T. J.; Tappan, B. C.; Pacheco, A. N.; Son, S. F., Reaction Propagation of Four Nanoscale Energetic Composites (Al/MoO3, Al/WO3, Al/CuO, and B12O3). *Journal of Propulsion and Power* **2007,** *23* (4), 707-714.
85. Puszynski, J. A.; Bulian, C. J.; Swiatkiewicz, J. J., Processing and Ignition Characteristics of Aluminum-Bismuth Trioxide Nanothermite System. *Journal of Propulsion and Power* **2007,** *23* (4), 698-706.
86. Barbee T.W.; Simpson R.L.; Gash A.E.; Satcher J.H. Nano-laminate-based-ignitors US20040060625 A1 2004.
87. Blobaum, K. J.; Wagner, A. J.; Plitzko, J. M.; Van Heerden, D.; Fairbrother, D. H.; Weihs, T. P., Investigating the reaction path and growth kinetics in CuOx/Al multilayer foils. . *J. Appl. Phys.* **2003,** *94*, 2923 - 2929.
88. Blobaum, K. J.; Reiss, M. E.; Plitzko, J. M.; Weihs, T. P., Deposition and characterization of a self-propagating CuOx/Al thermite reaction in a multilayer foil geometry. *J. Appl. Phys.* **2003,** *94*, 2915 - 2922.
89. Nicollet, A.; Lahiner, G.; Belisario, A.; Souleille, S.; Djafari-Rouhani, M.; Estève, A.; Rossi, C., Investigation of Al/CuO multilayered thermite ignition. *Journal of Applied Physics* **2017,** *121* (3), 034503.
90. Sullivan, K. T.; Worsley, M. A.; Kuntz, J. D.; Gash, A. E., Electrophoretic deposition of binary energetic composites. *Combustion and Flame* **2012,** *159* (6), 2210-2218.
91. Gash A.E.; Simpson R.L.; Tillotson T.M.; Satcher J.H.; Hrubesh L.W. In *Making Nanostructured Pyrotechnics in a Beaker*, Proceedings of the 27th International Pyrotechnics Seminar, 2000; pp 41-53.
92. Tillotson, T. M.; Gash, A. E.; Simpson, R. L.; Hrubesh, L. W.; Satcher, J. H.; Poco, J. F., Nanostructured energetic materials using sol-gel methodologies. *Journal of Non-Crystalline Solids* **2001,** *285* (1-3), 338-345.
93. Prentice, D.; Pantoya, M. L.; Gash, A. E., Combustion Wave Speeds of Solâˆ’Gel-Synthesized Tungsten Trioxide and Nano-Aluminum: The Effect of Impurities on Flame Propagation. *Energy & Fuels* **2006,** *20* (6), 2370-2376.

94. Badiola, C.; Schoenitz, M.; Dreizin, E. L., Synthesis of Aluminum-Rich Nanocomposite Powders at Cryogenic Temperatures. In *44th AIAA/ASME/SAE/ASEE Joint Propulsion Conference & Exhibit*, Hartford, CT, 2008.
95. Ward, T. S.; Chen, W.; Schoenitz, M.; Dreizin, E. L.; Dave, R., Nano-Composite Energetic Powders Prepared by Arrested Reactive Milling. In *43rd AIAA Aerospace Sciences Meeting and Exhibit*, Reno, Nevada, 2005.
96. Lehn, J.-M., Supramolecular Chemistry—Scope and Perspectives Molecules, Supermolecules, and Molecular Devices (Nobel Lecture). *Angewandte Chemie International Edition in English* **1988,** *27* (1), 89-112.
97. Whitesides, G.; Mathias, J.; Seto, C., Molecular self-assembly and nanochemistry: a chemical strategy for the synthesis of nanostructures. *Science* **1991,** *254* (5036), 1312-1319.
98. Whitesides, G. M.; Grzybowski, B., Self-Assembly at All Scales. *Science* **2002,** *295* (5564), 2418-2421.
99. Folkers, J. P.; Gorman, C. B.; Laibinis, P. E.; Buchholz, S.; Whitesides, G. M.; Nuzzo, R. G., Self-Assembled Monolayers of Long-Chain Hydroxamic Acids on the Native Oxide of Metals. *Langmuir* **1995,** *11* (3), 813-824.
100. Laibinis, P. E.; Whitesides, G. M.; Allara, D. L.; Tao, Y. T.; Parikh, A. N.; Nuzzo, R. G., Comparison of the structures and wetting properties of self-assembled monolayers of n-alkanethiols on the coinage metal surfaces, copper, silver, and gold. *Journal of the American Chemical Society* **1991,** *113* (19), 7152-7167.
101. Soares, J. W.; Steeves, D. M.; Singh, J.; Im, J.; Whitten, J. E. In *Thiol adsorption on metal oxides: an approach for selective deposition on zinc oxide nanoparticles*, 2011; pp 79400K-79400K-7.
102. Yang, Y.; Wang, P.-p.; Zhang, Z.-c.; Liu, H.-l.; Zhang, J.; Zhuang, J.; Wang, X., Nanowire Membrane-based Nanothermite: towards Processable and Tunable Interfacial Diffusion for Solid State Reactions. *Sci. Rep.* **2013,** *3*.
103. Malchi, J. Y.; Foley, T. J.; Yetter, R. A., Electrostatically Self-Assembled Nanocomposite Reactive Microspheres. *ACS Applied Materials & Interfaces* **2009,** *1* (11), 2420-2423.
104. Kim, S. H.; Zachariah, M. R., Enhancing the Rate of Energy Release from NanoEnergetic Materials by Electrostatically Enhanced Assembly. *Advanced Materials* **2004,** *16* (20), 1821-1825.
105. Slocik, J. M.; Crouse, C. A.; Spowart, J. E.; Naik, R. R., Biologically Tunable Reactivity of Energetic Nanomaterials Using Protein Cages. *Nano Letters* **2013,** *13* (6), 2535-2540.
106. Thiruvengadathan, R.; Chung, S. W.; Basuray, S.; Balasubramanian, B.; Staley, C. S.; Gangopadhyay, K.; Gangopadhyay, S., A Versatile Self-Assembly Approach toward High Performance Nanoenergetic Composite Using Functionalized Graphene. *Langmuir* **2014,** *30* (22), 6556-6564.
107. Ang, H. G.; Pisharath, S., *Energetic Polymers*. Wiley: 2012.
108. Seshadri, P. Combustion characteristics of nanoenergetic materials composed of aluminum, nickel oxide and a fluoroelastomer. Purdue University, 2011.
109. Kappagantula, K. S.; Farley, C.; Pantoya, M. L.; Horn, J., Tuning Energetic Material Reactivity Using Surface Functionalization of Aluminum Fuels. *The Journal of Physical Chemistry C* **2012,** *116* (46), 24469-24475.
110. McCollum, J.; Pantoya, M. L.; Iacono, S. T., Activating Aluminum Reactivity with Fluoropolymer Coatings for Improved Energetic Composite Combustion. *ACS Applied Materials & Interfaces* **2015,** *7* (33), 18742-18749.

111. Staley, C. S.; Raymond, K. E.; Thiruvengadathan, R.; Herbst, J. J.; Swaszek, S. M.; Taylor, R. J.; Gangopadhyay, K.; Gangopadhyay, S., Effect of Nitrocellulose Gasifying Binder on Thrust Performance and High-g Launch Tolerance of Miniaturized Nanothermite Thrusters. *Propellants, Explosives, Pyrotechnics* **2014,** *39* (3), 374-382.
112. Provatas, A., Energetic Polymers and Plasticizers for Explosive Formulation - A Review of Recent Advances. DSTO, Ed. Commonwealth of Australia, 2000.
113. Bezmelnitsyn, A.; Thiruvengadathan, R.; Barizuddin, S.; Tappmeyer, D.; Apperson, S.; Gangopadhyay, K.; Gangopadhyay, S.; Redner, P.; Donadio, M.; Kapoor, D.; Nicolich, S., Modified Nanoenergetic Composites with Tunable Combustion Characteristics for Propellant Applications. *Propellants, Explosives, Pyrotechnics* **2010,** *35* (4), 384-394.

Chapter 3

Experimental Methods

The fabrication processes of Al/NiO nano-thermites as well as the various characterization techniques used are described in this section. Solvent mixing with ultrasonication was used to disperse and prepare the nano-thermite powder. The Al and NiO nanoparticles used were characterized using SEM, BET, XRD and TGA. The prepared nano-thermites with different compositions (varying ER) were studied for their heat of reaction using a bomb calorimeter and they were thermally analyzed using a DSC. Self-assembly of the binary nano-thermite system was attempted through surface functionalization of n-Al and n-NiO using organosilanes having complimentary functional ends and the procedures are detailed in this section. Surface functionalized nanoparticles were characterized using TGA, FTIR and SEM while self-assembled nano-thermites were studied using SEM/EDX, DSC and dynamic pressure measurements. Both physically mixed and self-assembled nano-thermite prepared at ER 1.2 were studied using non-isothermal kinetics method described by Kissinger and Ozawa-Flynn-Wall to estimate their activation energy. The procedure detailing the addition of THV, a fluoropolymer, to n-Al/n-NiO is included in this section. The composite powders were studied for their thermal and pressure characteristics using DSC and dynamic pressure measurements. Finally the sensitivity of n-Al/n-NiO as well as surface functionalized n-A/n-NiO and n-Al/n-NiO/THV to external stimuli (ESD, friction and impact) were studied and the test methods are reported.

3.1 Preparation of Al/NiO Nano-Thermite

3.1.1 Physical Mixing of n-Al and n-NiO

n-NiO was supplied by Sigma Aldrich (Stock number 637130, with average particle size <50 nm) and n-Al (spherical with BET average particle size of 78 nm) by Army Research, Development and Engineering Centre (ARDEC). All the raw materials were characterized via XRD, SEM, BET and particle sizer. Characterization techniques and conditions are specified in the following section.

All the Al/NiO nano-thermite powder mixtures were prepared via ultrasonic dispersion in reagent grade 2-propanol (Reagent grade, ≥99.7%). All the n-Al/n-NiO prepared via this technique as termed physically mixed nano-thermites throughout this report. Both n-NiO and n-Al were pre-sonicated independently in 2-propanol for 20 mins before they were combined and further mixed under ultrasonication for 1 hr. All ultrasonication were performed in Elma S60H Elmasonic with ultrasonic frequency of 37 kHz and 150 W power. Powder suspensions were poured over a large crystalizing dish and dried over 50 ^{o}C hotplate. Due to the ESD-sensitivity of nano-thermites mixture, the nano-thermite powders were collected using an ESD-dissipative brush (Fisherbrand anti-static brush, Catalogue No. 15078213). The mixing was conducted in a laboratory equipped with anti-static flooring and any personnel handling it should be equipped with an anti-static laboratory coat and shoes as safety precautions. Collected powder was dried in a 60 ^{o}C oven under vacuum conditions for 6 hrs before further tests.

The reaction between NiO and Al follows the equation:

$$3NiO + 2Al \rightarrow Al_2O_3 + 3Ni \quad (3.1)$$

A mixture prepared with the stoichiometric ratio as per the equation is defined as having an Equivalence Ratio (ER) of 1. The ER is an easy metric to define the mixture's fuel to oxidizer ratio with respect to its stoichiometric composition. Al/ NiO of varying ER between 0.8 and 2.0 were prepared, taking into account the weight percentage of active aluminum for the n-Al in use (measured via full oxidation in a Thermo-Gravimetric Analyzer (TGA)).

$$\text{Equivalence Ratio} = \frac{\left(\frac{\text{Mass fuel}}{\text{Mass oxidiser}}\right)_{\text{actual}}}{\left(\frac{\text{Mass fuel}}{\text{Mass oxidiser}}\right)_{\text{stoichiometric}}} \quad (3.2)$$

In a typical process to prepare 1 g of nano-thermites with ER 1, 0.2538 g of n-Al (based on a 70.8 % active Al content) and 0.7462 g of n-NiO were each sonicated in 25 ml of 2-propanol using a sonicator bath for 20 mins. They were combined into a round bottom flask and further ultrasonicated for 1 hr. Final suspension was emptied into a 230 mm crystallizing dish positioned on a grounded anti-static mat and ambient dried in a fumehood. Dried powder was collected using an ESD-dissipative brush and further dried under vacuum at 60 ^{o}C for 6 hrs.

3.1.2 Surface Functionalization and Self-Assembly of n-Al and n-NiO

Other than preparing physically mixed n-Al/n-NiO, self-assembled n-Al/n-NiO were also prepared for our studies in this report. The aim is to create a self-assembled nano-thermite with improved mixing homogeneity. The effect of self-assembly on reaction kinetics, pressure generation characteristics and sensitivity were studied. To achieve self-assembly, surface functionalization of n-Al and n-NiO were performed using organosilanes having complimentary functional ends.

The nanoparticles were first surface functionalized through silanization with silane coupling agents. The proposed method takes the advantage of the hydroxyl groups on the surface of n-NiO as well as on the insulating oxide shell of the n-Al particles. These aluminum oxide layers are spontaneously formed in air on the Al nanoparticles, and the oxide reacts readily with moisture to form hydroxide (-OH) at the most outside layer of the nanoparticles.[1, 2]. These hydroxyl groups are reactive and could be utilized for the surface modification of the particles with a silane coupling agent. The chosen silane coupling agent can come with different functional groups.

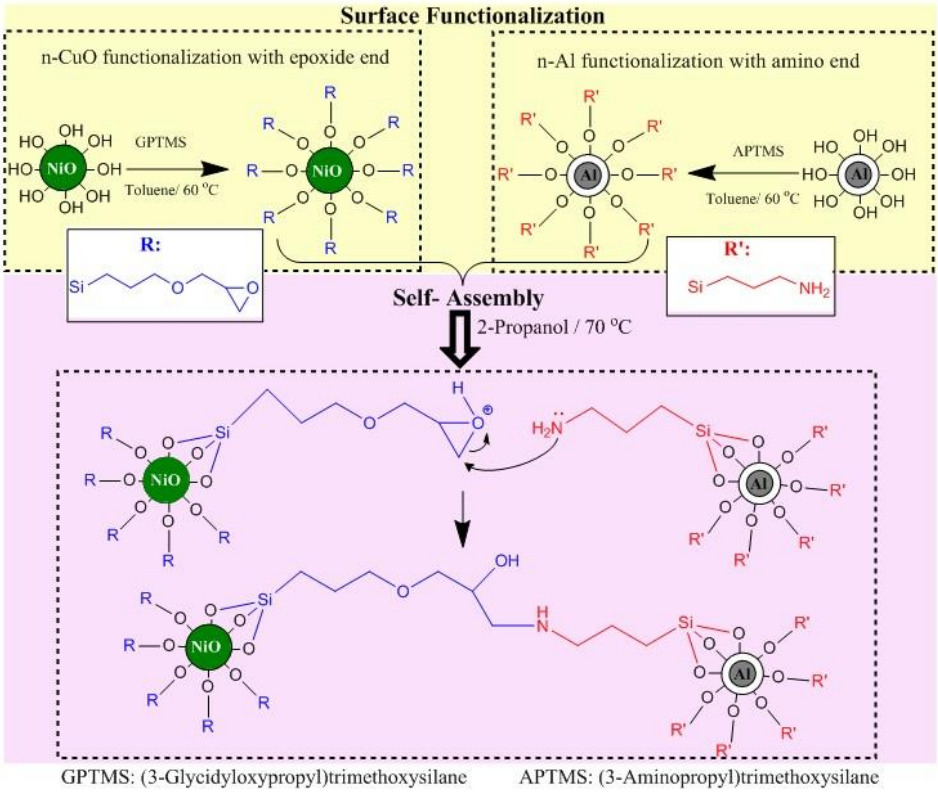

Figure 3.1: Schematic diagram for surface functionalization and self-assembly approach of n-NiO and n-Al

Silanization of the nanoparticle surfaces were performed on n-Al and n-NiO independently with amino and epoxide functional endings, respectively. Functionalized nanoparticles were brought together to effect a binary nano-thermite self-assembly. The intended approach of surface functionalization, followed by self-assembly, is shown in Figure 3.1.

3.1.2.1 Surface Modification of nano-Nickel Oxide

1 g of n-NiO powder was ultra-sonicated in 100 ml of toluene for 10 mins prior to addition of 750 mg of 3-Glycidoxypropyl Trimethoxysilane (GPTMS) that was pre-dissolved in 20 ml of toluene. The reaction was carried out at 60 °C under flowing N_2 gas and proceeds under continuous stirring and ultra-sonication for 3 hrs. The suspension was centrifuged to remove the supernatant and the n-NiO was successively washed twice with toluene and once with acetone. The retrieved n-NiO that was grafted with GPTMS (n-NiO-GPTMS) was ambient dried followed by oven-drying at 60 °C for 6 hrs. The procedure was made with reference to what was reported by Garcia et al[3] as well as Feng

et al[4]. All ultrasonication were performed in Elma S60H Elmasonic with ultrasonic frequency of 37 kHz and 150 W power.

3.1.2.2 Surface Modification of nano-Aluminum

1 g of n-Al powder was ultra-sonicated in 100 ml of toluene for 10 mins prior to addition of 1800 mg of 3-Aminopropyl Trimethoxysilane (APTMS) that was pre-dissolved in 20 ml of toluene. The reaction was carried out at 60 °C under flowing N_2 gas and proceeds under continuous stirring and ultra-sonication for 4 hrs. The suspension was centrifuged to remove the supernatant and n-Al was successively washed twice with toluene and once with acetone. The retrieved n-Al that was grafted with APTMS (n-Al-APTMS) was ambient dried followed by oven-drying at 60 °C for 6 hrs.

3.1.2.3 Self-Assembly of n-Al-APTMS with n-NiO-GPTMS

To effect the self-assembly of n-Al-APTMS with n-NiO-GPTMS, we proposed a reaction between the functional groups grafted on the nanoparticles. We proposed a reaction condition suitable for the ring opening of epoxide by the amino group to take place as shown in Figure 3.2. It has been reported that effective hydrolysis of epoxides can be conducted in water with short reaction time and high yield.[5] They reported the use of different solvent having a great impact on the yield of product, with most alcohol proving to be relatively effective. Thus, we proposed the use of isopropanol to effect the reaction between APTMS and GPTMS. The reaction was carried out and monitored using FTIR to confirm the feasibility of this reaction.

Appropriate amounts (total weight of 1 g, ratio of two components is determined by the desired ER) of n-Al-APTMS with n-NiO-GPTMS were each dispersed in 50 ml of isopropanol under ultrasonication for 10 min. Both suspensions were combined in a round bottom flask for reaction at 70 ^{o}C for 6 hrs under continuous nitrogen gas purging with constant stirring. After reaction, the nano-thermite suspension was dispensed onto an electrically grounded shallow metal tray and dried under ambient conditions. Dried nanothermite powder was retrieved using a conductive brush and further dried under vacuum at 50 ^{o}C for 24 hrs.

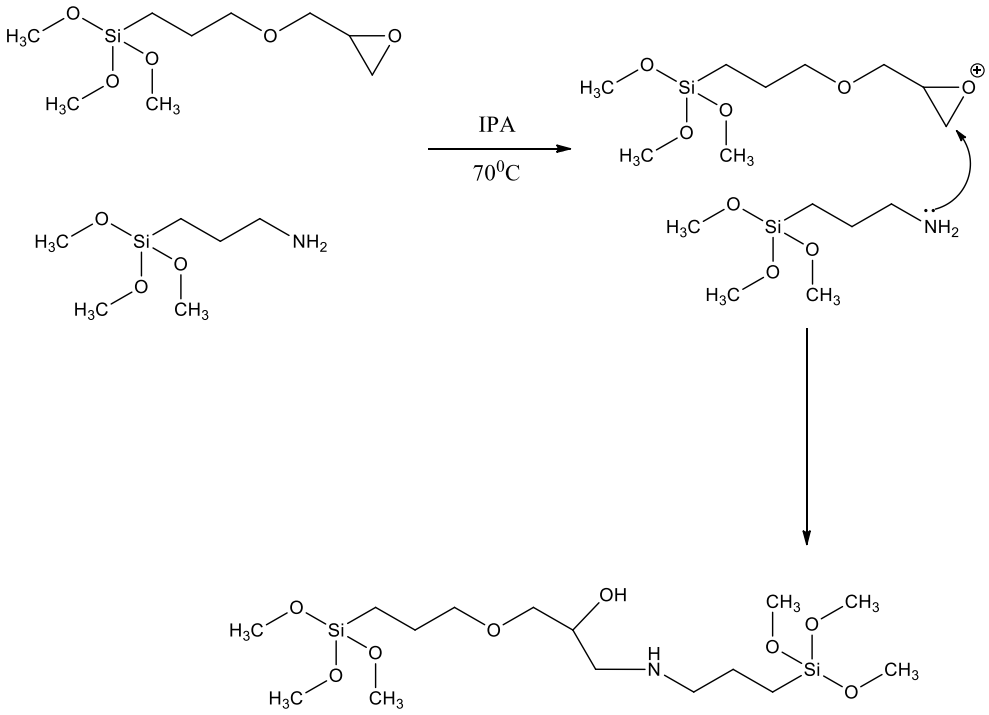

Figure 3.2: Plausible reaction route of GPTMS and APTMS.

3.1.3 Addition of Fluoropolymer (THV) to n-Al/n-NiO

n-Al/n-NiO were coated with THV powder to study the effect of the polymeric coating on the pressure generation characteristic as well as the sensitivity of the nano-thermite. THV is a terpolymer of tetrafluoroethylene, hexafluoropropylene and vinylidene fluoride, with 70.5 weight% fluorine content (3M Dyneon® THV-221AZ). Al/NiO with optimized equivalence ratio of 1.2, yielding a calorimetric heat output of 3649 J/g was utilized throughout our study in varying percentage of THV (0 to 40 weight%).

3.1.3.1 Preparation Procedure of n-Al//n-NiO/THV composite powder

A THV in acetone solution of 0.02 g/mL was first prepared. Next, a predetermined amount of THV-acetone solution was then added to the physically mixed n-Al/n-NiO in 2-propanol suspension (~30 mL). For instance, a Al/NiO with 20 wt% THV was prepared by adding 12.5 ml of THV/acetone solution (equivalent to 0.25 g THV) to 1 g of n-Al/n-NiO nano-thermite (n-Al/n-NiO in 2-propanol suspension prepared in advance according to procedure described in earlier section). The reaction mixture was then stirred for 1

hour at room temperature before it was cast onto a flat stainless-steel plate or large 23mm glass crystallizing dish (vessel placed on a grounded ESD mat) under ambient conditions. The sample was then collected in powder form using an anti-static brush.

3.2 Characterization of Al and NiO Nano-Particles

3.2.1 Particle Size and Morphology

3.2.1.1 Scanning Electron Microscopy (SEM)

Scanning electron micrographs of the nanoparticles were taken using a Field Emission Scanning Electron Microscope (JEOL JSM-7600F-FESEM, Tokyo, Japan). All nanoparticles were dispersed in isopropanol through ultrasonication for 10 mins before cast drying onto a silicon wafer. All prepared samples were platinum coated at 20mA for 20sec prior to SEM observation.

3.2.1.2 Surface Area Analysis (BET method)

Surface area measurements of the nano-particles were performed using a Micromeritics Tristar II 3020 Automated Gas Sorption System by nitrogen gas adsorption. All samples were degassed under vacuum at 60 ^{o}C for 8 hrs prior to measurements. The surface area was calculated using the Brunauer, Emmett and Teller (B.E.T.) theory. Through the introduction of gas into the sample, we could obtain an estimate of the number of molecules that is required to cover the adsorbent surface with a monolayer of adsorbed molecules. This is then multiplied by the cross-sectional area of the adsorbate molecule to obtain the sample's surface area. This BET calculation method is widely known and used for specific surface area calculations.[6]

Average Particle Size (APS) is calculated from the BET surface area assuming nonporous spherical particles with uniform sizes. It was thus only a good estimation if the particles have a spherical morphology and are relatively uniform in size.

The equation for APS calculation using the BET specific surface area: [7]

$$\text{APS (in nm)} = \frac{6000}{(\text{BET Surface Area in } m^2/g) \times (\text{density in } g/cm^3)} \quad (3.3)$$

3.2.1.3 Particle Size Distribution

Particle size distributions of the nano-aluminum and nano-nickel oxide particles were measured using a Laser Diffraction Particle Size Analyzer (Horiba, Partica LA-950), which has a measuring range of 10 nm to 3000 µm. Two light sources (650nm and 405 nm) were shone on the particle suspension and the scattered light angle and intensity were measured and related to their particle sizes using the MIE scattering theory. The nanoparticle suspensions were prepared in 2-propanol and ultra-sonicated for 30 mins prior to their measurement. The measurement results collected were displayed in terms of volume distribution. This technique provides an estimation of the size distribution, when they are suspended in 2-propanol. 2-propanol was used as the dispersion medium during the intermixing of the two nanoparticles to prepare the nano-thermites.

3.2.2 Chemical Analysis

3.2.2.1 X-Ray Diffraction (XRD)

The powder XRD patterns were recorded using a Bruker D8 Advance Powder X-Ray Diffractometer (under ambient conditions) using a filtered Cu-Kα radiation (λ = 1.5418 Å). All samples were in powder form and were measured without further processing. Samples were scanned between 2 Theta angle of 20 to 100 degrees at a step size of 0.02 degrees and a scan rate of 0.5s/step. The XRD patterns were used for the identification of the crystal phase(s) of the nano-aluminum and nano-nickel oxide. All phase identifications were done using the Match! Software that is integrated with the latest ICDD database.

Average crystallite size of the Al and NiO samples can be obtained from the width of the

lattice reflections, using the Debye–Scherrer formula (Equation 3.4).[8, 9]

$$d = \frac{K\lambda}{B\cos\theta} \tag{3.4}$$

Where,

d is the estimated crystallite size in nm, λ is radiation wavelength, 0.15406 nm for Cu Kα X-ray.

K is the shape factor, which is typically a number close to unity and depends on factors including the shape of the crystallite and their size distribution [10], but it is never clear from the literature on the exact value to be applied in each case. [11] It will be taken as 1 in our calculations to provide an estimate of the crystallite size.

B is the measured line broadening full width at half maximum (FWHM) in radians, θ is Bragg's angle.

3.2.3 Active Aluminum Content

As the nano-sized aluminium particles in use are passivated with a thin layer of alumina, the active aluminium weight content of them need to be measured in order to correctly measure the weight of Al used in the formulation preparations. Nano aluminum sample was heated up in a TGA up to 1200 ºC in oxygen at a heating rate of 5 ºC/min, to measure the percentage weight gain from complete oxidation of the Al samples as represented by the following equation.

$$4Al + 3O_2 \rightarrow 2Al_2O_3 \tag{3.5}$$

As the weight gain is due to the new oxide formed from the metallic aluminum in the sample, the percentage of active (free) metallic aluminum in the sample can be derived from the percentage weight gain:[12, 13]

$$\text{Active Al \%} \times \frac{\text{Weight of O in } 2Al_2O_3}{\text{Weight of } 4Al} = \text{Weight gain\%} \tag{3.6}$$

Or

$$\text{Active Al \%} = \text{Weight gain\%} \times R \tag{3.7}$$

$$\text{where } R = \frac{\text{Weight of } 4Al}{\text{Weight of O in } 2Al_2O_3} = 1.125$$

3.3 Thermal-Kinetic Studies of Al/NiO Nano-Thermites

3.3.1 Heat of Reaction

The total heat releases of the Al/NiO nano-thermites having different ERs were measured using the bomb calorimeter (Parr Instrument Company, Model 6200). A bomb calorimeter is typically used to either measure the heat of combustion of a material, upon combustion in oxygen, or the calorific heat output of a material if it gets ignited in an inert environment. For a thermite material, containing both sources of fuel and oxidizer, its total calorific heat output can be measured in an inert environment. The Parr bomb calorimeter Model 6200 is an isoperibol calorimeter where the enclosed bomb is placed within a bucket of water, surrounded by a jacket that is maintained at a constant temperature. The system provides an adiabatic condition by preventing heat lost from the bomb and bucket to its surrounding. With the known heat capacity of the bomb and bucket, the measured temperature increase can be used to calculate the calorific heat output of the reaction

The nano-thermite powders were fired inside a 350 cm^3 (Parr Model 1108) high pressure oxygen combustion vessel. Ignition was performed using a nichrome wire (Parr Part No. 45C10) as the fuse at an argon filling pressure of 3.0 MPa. The calorimeter has been standardized using benzoic acid. Energy was computed, taking into account the fuse wire consumed, through wire length measurement before and after the experiment.

3.3.2 Thermal Analysis

Differential Scanning Calorimetric (DSC) data of the nano-thermite powder with varying ER were obtained from a Setaram Labsys DSC. Approximately 20 mg of the samples were taken in an alumina crucible and subjected to a heating profile of 5 ^{o}C/min up to 1000 ^{o}C. All the tests were performed under inert atmosphere (Argon) with a purging rate of 50 mL/min. The recorded heat flux versus temperature profile of the material heated at such a slow and controlled heating rate provides an insight to the transitions of the material as the reaction proceeds.

3.3.3 Kinetic Model

The non-isothermal method can be utilized to obtain the solid-state kinetic data via DSC data processing, where samples were heated at one or more constant heating rates (usually linear) and following the course of the reaction. The reaction kinetics of the Al/NiO having ER 1.2 were studied by performing DSC using four different heating rates (2, 3, 4, 5 and 8°C per min). The activation energy and pre-exponential factor were calculated using model-free methods including Kissinger and Ozawa-Flynn-Wall methods. The test using Kissinger's method is conducted according to ASTM standard (ASTM E2890-12)[14]. The test method described by Ozawa-Flynn-Wall was simultaneously applied to the same data according to ASTM standard (ASTM E698-16)[15] to confirm the results. The variation in activation energy with respect to conversion is studied using Ozawa-Flynn-Wall's method.

Kinetic analysis and deriving the kinetic model of novel nano-thermite system is a key input for modeling their performance aspects such as combustion front velocity. Non-isothermal method, which involves heating the samples at a few constant heating rates, was employed to obtain the solid-state kinetic data of the nano-thermite reaction. The general expressions for heterogeneous decomposition of the solid as a function of time or temperature are:

$$\frac{d\alpha}{dt} = k\, f(\alpha) \qquad (4.3a)$$

$$\frac{d\alpha}{dT} = \frac{k}{\beta} f(\alpha) \qquad (4.3b)$$

where:

α = fraction reacted or conversion (dimensionless)

t= time (s)

T= temperature (K)

k = specific rate constant at temperature T, and

f(α) = conversion function (dimensionless)

β = linear heating rate (Ks^{-1})

α is generated from DSC curves whereby α, at a given temperature (T)is calculated by:

$$\alpha(T) = \frac{AUC_0^T}{AUC_0^\infty} \qquad (4.3c)$$

where:

AUC_0^T = Area under the curve from 0 to T

AUC_0^∞ = Total area under the curve

The Arrhenius equation defines the rate constant, k, as:

$$k = A\, e^{(-E_a/RT)} \qquad (4.4)$$

where:

R is the real gas constant(8.314 J mol^{-1} K^{-1}),

T is the absolute temperature in Kelvin (K)

E_a is the activation energy (J mol^{-1})

A is the frequency or pre-exponential factor (s^{-1})

Combining Equations 4.3b and 4.4:

$$\frac{d\alpha}{dT} = \frac{A}{\beta} e^{(\frac{-Ea}{RT})} . f(\alpha) \qquad (4.5)$$

Two types of Model-free techniques were used for processing our data. The first being those described by Kissinger as well as Ozawa-Flynn-Wall, where the peak temperature of the DSC curve is related to its heating rate and concludes in one activation energy, assuming a single simple mechanism through the reaction process. While a second type of technique, also call isoconversional method, takes into consideration the conversion and rate of conversion data and concludes in a set of activation energies in variation with the conversion. Isoconversional methods described by Ozawa-Flynn-Wall was utilized for our calculation.

3.3.3.1 Model-Free Methods: Kissinger and Ozawa-Flynn-Wall

In the methods described in this section, the reaction peak temperatures were related to their heating rates using equations described by Kissinger as well as Ozawa-Flynn-Wall to calculate the activation energy and pre-exponential factor. In Kissinger's paper [16] , he ascribed the derivative of the maximum reaction rate, which is happening at peak temperature (T_m), to be zero since the reaction rate starts to decline after reaching its maximum. He also assumed a first order reaction where n equates to 1 in the reaction-order expression of:

$$f(\alpha) = (1-\alpha)^n \qquad (4.6)$$

Equation 4.5 can be expressed as Equation 4.7 from the assumptions made:

$$ln \frac{\beta}{T_m^2} = ln\left\{\frac{AR}{E_a}\right\} - \frac{E_a}{R\,T_m} \qquad (4.7)$$

$$E_a = -R\left[\frac{d\left(ln\frac{\beta}{T_m^2}\right)}{d\left(\frac{1}{T_m}\right)}\right] \quad (4.8)$$

The kinetic parameters including activation energy (E_a) and pre-exponential factor (A) can be obtained from a plot of Ln β/T_m^2 versus $1/T_m$ for a series of experiments at different heating rates. While activation energy (E_a) describes the energy barrier opposing a reaction, pre-exponential factor (A) is a measure of the probability that a molecule having energy E_a will participate in a reaction. The Kissinger Method is adopted in the ASTM test standard (ASTM E2890)[14] for obtaining the kinetic parameters of activation energy and pre-exponential factors.

Another isoconversional method formulated by Ozawa in 1965, which was also derived and published independently by Flynn and Wall in 1966, was popularly adopted for calculation of activation energies using thermal analysis conducted at constant heating rates. Flynn et al introduced a correction factor to improve the accuracy of their mathematic estimations, which was later popularly quoted as the Ozawa-Flynn-Wall or Flynn-Wall-Ozawa method.[17-22] The method were adopted in the ASTM standard (ASTM E698-16)[15]as a standard test for characterizing the hazard potentials of thermally unstable materials by calculating their activation energies and pre-exponential factors. Activation energy and pre-exponential factors are calculated from the slope and the intercept of a log β versus $1/T_m$ plot using Equations 4.9a and b.

$$E_a = -2.19R\left[\frac{d(log_{10}\beta)}{d\left(\frac{1}{T_m}\right)}\right] \quad (4.9a)$$

$$A = \frac{\beta E e^{\frac{E}{RT}}}{RT^2} \quad (4.9b)$$

Equation 4.9a is further refined by including a correction factor D to obtain a more accurate approximation of the activation energy and expressed as Equation 4.10. D value

is obtained from a table provided in ASTM E698-16[15], using the first approximation of E_a.

$$E_a = -2.303\frac{R}{D}\left[\frac{d(log_{10}\beta)}{d\left(\frac{1}{T_m}\right)}\right] \quad (4.10)$$

3.3.3.2 Model-Free Isoconversional Methods: Ozawa-Flynn-Wall

The kinetic analysis based on isoconversional methods allows the kinetic parameters to be evaluated for different constant extents of conversion without evaluating any particular form of the reaction model. Thermal decomposition of nanothermite is a complex solid state reaction. A single set of Arrhenius parameters for an overall process will not be capable of reflecting the inherent complexity of the nanothermite decomposition reactions. The ability of isoconversional methods to show this type of reaction complexity is a critical step toward the ability to explain mechanistic conclusions from kinetic data. The isoconversional methods described by Ozawa-Flynn-Wall was used to study the variation of activation energy with conversion.

Ozawa et al [19]derived two methods from the theoretical considerations, where the first is based solely on the relation between peak temperature and heating rate while the second method uses the conversion as well as rate of conversion and calculates the E_a at each conversion throughout the reaction process. Ozawa's first method was used in the previous section and the second will be adopted here.

The expression used by Ozawa-Flynn-Wall is described as follows [19]:

$$\log\beta = \log\frac{AE_a}{g(\propto)R} - 2.315 - 0.4567\ \frac{E_a}{R\,T} \quad (4.11a)$$

E_a can be calculated from the slope of a log β vs 1/T plot at each conversion, α, according to the following expression:

$$\log\beta_{\alpha} = \log\frac{A_{\alpha}E_{a\alpha}}{g(\propto)R} - 2.315 - 0.4567\ \frac{\mathrm{E}_{a\alpha}}{\mathrm{R\ T}_{\alpha}} \quad (4.11b)$$

3.3.4 Reaction Product and Intermediates Analysis

The compositions of the reaction products were analyzed using Bruker D8 Advance powder XRD to develop an understanding of the reaction mechanism. All samples were scanned between 20 to 100 degrees at a step size of 0.02 degrees at a scan rate of 0.5s/step. Any change in reaction mechanism with a change in the nano-thermite's composition (varying ER) can be understood through this study.

The composition of the reaction products of Al/NiO ER 1.2 heated in a DSC at 5 ^{o}C per minute to different temperatures (475 ^{o}C, 600 ^{o}C, 765 ^{o}C, 1000 ^{o}C) were analyzed using the powder XRD. All analyses were done using Match program that is linked with PDF-2, an ICDD (International Centre for Diffraction Data) database.

3.4 Study of surface functionalized nanoparticles and self-assembled n-Al/n-NiO

3.4.1 Chemical Analysis

The amount of surface modifier grafted on the nanoparticles was quantified by weight lost using the TGA. Approximately 10 mg of samples were heated in alumina crucibles in a Shimadzu DTG-60H at a heating rate of 10 ^{o}C/min to 500 ^{o}C in purified air with a constant flow of 50 mL/min. The weight lost from room temperature to 100 ^{o}C were attributed to loss of adsorbed moisture. Maximum weight lost from 100 ^{o}C to around 400 ^{o}C of each surface functionalized sample was measured. The weight lost from the pristine nanoparticle was also measured and subtracted from the total weight lost for computation of weight normalized percentage weight lost due to the additional grafting for each nanoparticle sample.

Fourier Transform Infrared Spectroscopy (FTIR) was used for chemical functional group identification of the grafted nanoparticles. The FTIR from Perkin Elmer (Frontier L1280034), with a universal ATR attachment, was utilized for our studies. The spectra were collected over 4000–400 cm^{-1} using 16 scans and a resolution of 8 cm^{-1}. This was used to check the grafting of the organosilanes on n-Al and n-NiO. The reactivity of n-Al-APTMS and n-NiO-GPTMS to GPTMS and APTMS, respectively were also checked using TGA and FTIR.

3.4.2 Homogeneity of Mixing

The homogeneity of mixing of the self-assembled n-Al/n-NiO was characterized using SEM and EDX mapping. A FESEM (JEOL JSM-7600F-FESEM, Tokyo, Japan) equipped with X-ray source from INCA to provide Energy Dispersive X-ray Spectroscopy (EDX) for chemical analysis was used. Elemental mapping of SEM images were performed to study the homogeneity of the intermixing of self-assembled n-Al/n-NiO in comparison to physically mixed ones. Elemental mapping of Al and Ni were performed to indicate the presence of n-Al and n-NiO, respectively. The elemental maps of Al and Ni were post-processed via superimposing the different color coded images using the freeware ImageJ [23].

3.4.3 Thermal and Kinetic Studies

The self-assembled as well as physically mixed nano-thermites were studied for their thermal profiles using a NETZCH DSC 404 F3 Pegasus® system. Approximately 10 mg of the samples were taken in an alumina crucible and subjected to a heating profile of 5 ^{o}C/min up to 1000 ^{o}C under constant argon flow (50 mL/min). The recorded heat flux versus temperature profile of the material were plotted.

Different heating rates (2, 3, 4, 5, 8 ^{o}C/min) of n-Al/n-NiO as well as the self-assembled n-Al-APTMS/ n-NiO-GPTMS were conducted in a DSC for calculation of their activation energies using the model-free kinetic methods described by both Kissinger and Ozawa-Flynn-Wall. This will help us understand if the organosilanes grafting pose any

change to the activation energy barrier of the thermite reaction. The methods were described in greater details in the earlier Section (3.3.3).

3.4.4 Pressure Generation Characteristics

The dynamic pressure measurement was conducted using a 240 cm^3 high pressure combustion vessel (Parr Model 1104B). It has an attached pressure transducer (Kistler Model 211B2), having measuring capability up to 5000 psi and a sensitivity of 1.058 mV/psi. The vessel was pre-filled with 250 psi of argon before each firing test. Each ignition was performed using 10cm of Nichrome fuse wire (Parr Part No. 45C10). Data acquisition was conducted at 2000 Hz for a duration of 5 seconds using a Parr Dynamic Pressure Recording system (Model A365CEE). Approximately 0.25 g of powder sample was used for each test.

3.4.5 Sensitivity to Stimulus

The effect of organosilane surface functionalization on the sensitivity of these n-Al/n-NiO to ESD, friction and impact were investigated. Self-assembled n-Al-APTMS/n-NiO-GPTMS were tested for their sensitivity to these external stimuli and compared to unfunctionalized n-Al/n-NiO prepared by physical mixing. The sensitivity measured indicates the stability of these materials when subjected to unwanted external stimuli and is a reflection of the level of safety precaution required in handling these hazardous materials.

3.4.5.1 BAM Friction Test

Sample (approx. 10 mm^3) was placed onto a rough porcelain plate (25 × 25 × 5 mm) that is clamped onto the moving platform of the friction apparatus. The friction force between the moving porcelain plate and a static porcelain peg (10 × 15 mm) (curvature radius 10 mm) causing initiation of sample was determined. A set of 9 weights allows friction forces ranging from 5 to 360 N to be determined. The minimum force of friction is determined when at least one sample out of six ignites, turns black, makes a cracking sound or explodes from the test.

Figure 3.3: BAM Friction Tester

3.4.5.2 BAM Fall Hammer Impact Test

Sample (approx. 40 mm^3) was placed in the plunger assembly, consisting of two steel rollers, a hollow steel collar and a centering ring for fixation. The assembly is placed onto a small anvil. The impact energy (energy = work × distance = mass × acceleration × distance) can be varied by changing the drop height (10 to 100 cm) and the mass (0.5 to 10 kg). The minimum impact energy is determined by one which has at least one out of six samples explodes.

Figure 3.4: BAM Fall Hammer Impact Tester

3.4.5.3 Electrostatic Discharge (ESD) Sensitivity Test

The ESD tests were performed using XSpark 10 featuring a static spark gap geometry (spark gap of around 1 mm). A small amount of sample (approx. 10 mg) is placed in between two metal electrodes. By selecting appropriate capacitor and voltage level, energy is then released as an electric spark through the sample. The ‘Damped’ discharge

mode is used and the time profile of input energy and fraction of energy consumed by the spark gap are measured by high voltage and current probes connected to the oscilloscope. By varying voltage and capacity, a series of trials were performed until at least 10 consecutive 'no-go' trials were observed. Based on the data obtained, the minimal initiation energy (MIE) and maximum threshold energy (E_{min}) can be determined using Winspark 2.0 software.

Figure 3.5: Electrostatic Discharge (ESD) Sensitivity Tester

3.5 Study of n-Al/n-NiO/THV composite powder

n-Al/n-NiO/THV composite powders were studied for the effect of adding THV fluoropolymer on the pressure generation characteristic as well as the sensitivity of the nano-thermite. n-Al/n-NiO with optimized equivalence ratio of 1.2 was mixed with varying percentage of THV (0, 10, 20, 30 and 40 weight percent) and studied.

3.5.1 Thermal and Pressure generation studies

The n-Al/n-NiO/THV composite powders were subjected to a heating profile in a DSC and their respective thermal responses were analyzed. Studies were performed using a NETZCH DSC 404 F3 Pegasus® system. Approximately 10 mg of the samples were taken in an alumina crucible and subjected to a heating profile of 5 ^{o}C/min up to 1000 ^{o}C under constant argon flow (50 mL/min). In an effort to understand the reaction mechanism of the nano-thermite reaction in the presence of the fluoropolymer, the reaction products were analyzed using powder XRD.

The pressure-time analyses of these n-Al/n-NiO/THV composite powders were studied using a dynamic pressure measurement system, by firing 0.25g of each sample inside a high strength Parr 1104B combustion vessel, containing 250 psi of argon. Their reaction products were analyzed using powder XRD to understand the difference in the reaction mechanism between slow heating (performed in DSC) and isochoric combustion through instantaneous thermal ignition (performed in enclosed combustion vessel).

Thermochemical calculations were performed using EXPLO5 program to predict the adiabatic combustion temperature as well as the amount of gaseous products from the reaction of Al/NiO/THV in varying compositions. The calculations were performed using isochoric combustion of the different thermite compositions using EXPLO5 codes. The calculations were done using the default loading density of 0.200 g/cm^3. We assumed a 70 % active Aluminum content and included corresponding amount of Al_2O_3 in the compositions.

3.5.2 Sensitivity to Stimulus

The effect of THV fluoropolymer addition on the sensitivity of these nano-thermites to ESD, friction and impact were also investigated. The test methodologies were as described earlier in Section 3.4.5. n-Al/n-NiO containing 30 wt% of THV was selected for the test to understand if the addition of fluoropolymer could reduce their sensitivity and improve the safety in handling such hazardous materials.

References

1. Karlsson, P.; Palmqvist, A. E. C.; Holmberg, K., Surface modification for aluminium pigment inhibition. *Advances in Colloid and Interface Science* **2006,** *128-130*, 121-134.
2. Li, L. J.; Pi, P. H.; Wen, X. F.; Cheng, J.; Yang, Z. R., Aluminum pigments encapsulated by inorganic-organic hybrid coatings and their stability in alkaline aqueous media. *Journal of Coatings Technology Research* **2008,** *5* (1), 77-83.
3. García-Cerda, L. A.; Romo-Mendoza, L. E.; Quevedo-López, M. A., Synthesis and characterization of NiO nanoparticles and their PMMA nanocomposites obtained by in situ bulk polymerization. *J Mater Sci* **2009,** *44* (17), 4553-4556.
4. Feng, G.; Jiang, L.; Wen, P.; Cui, Y.; Li, H.; Hu, D., A new ion-exchange adsorbent with paramagnetic properties for the separation of genomic DNA. *Analyst* **2011,** *136* (22), 4822-4829.

5. Wang, Z.; Cui, Y.-T.; Xu, Z.-B.; Qu, J., Hot Water-Promoted Ring-Opening of Epoxides and Aziridines by Water and Other Nucleopliles. *The Journal of Organic Chemistry* **2008,** *73* (6), 2270-2274.
6. Cook, M. A., *The science of high explosives*. Reinhold: New York, 1958.
7. Yu, C.; Zhang, W.; Shen, R.; Xu, X.; Cheng, J.; Ye, J.; Qin, Z.; Chao, Y., 3D ordered macroporous NiO/Al nanothermite film with significantly improved higher heat output, lower ignition temperature and less gas production. *Materials & Design* **2016,** *110*, 304-310.
8. Rossi, C., Front Matter. In *Al-Based Energetic Nanomaterials*, John Wiley & Sons, Inc.: 2015; pp i-xi.
9. Rossi, C.; Rossi, C., Nanosized Aluminum as Metal Fuel. In *Al-Based Energetic Nanomaterials*, John Wiley & Sons, Inc.: 2015; pp 1-26.
10. Langford, J. I.; Wilson, A. J. C., Scherrer after sixty years: A survey and some new results in the determination of crystallite size. *Journal of Applied Crystallography* **1978,** *11* (2), 102-113.
11. Borchert, H.; Shevchenko, E. V.; Robert, A.; Mekis, I.; Kornowski, A.; Grübel, G.; Weller, H., Determination of Nanocrystal Sizes: A Comparison of TEM, SAXS, and XRD Studies of Highly Monodisperse CoPt3 Particles. *Langmuir* **2005,** *21* (5), 1931-1936.
12. Rossi, C.; Rossi, C., Applications: Al Nanoparticles in Gelled Propellants and Solid Fuels. In *Al-Based Energetic Nanomaterials*, John Wiley & Sons, Inc.: 2015; pp 27-31.
13. Sun, J.; Simon, S. L., The melting behavior of aluminum nanoparticles. . *Thermochim. Acta* **2007,** (463), 32-40.
14. International, A. *Standard Test Method for Kinetic Parameters for Thermally Unstable Materials by Differential Scanning Calorimetry Using the Kissinger Method*; ASTM: 2012.
15. International, A., Standard Test Method for Kinetic Parameters for Thermally Unstable Materials Using Differential Scanning Calorimetry and the Flynn/Wall/Ozawa Method. ASTM 2016.
16. Kissinger, H. E., Variation of Peak Temperature With Heating Rate In Differential Thermal Analysis. *Journal of Research of the National Bureau of Standards* **1956,** *57* (4), 217-221.
17. Ozawa, T., Estimation of activation energy by isoconversion methods. *Thermochimica Acta* **1992,** *203*, 159-165.
18. Ozawa, T.; Koto, T., A simple method for estimating activation energy from derivative thermoanalytical curves and its application to thermal shrinkage of polycarbonate. *Journal of thermal analysis* **1991,** *37* (6), 1299-1307.
19. Ozawa, T., Kinetic analysis of derivative curves in thermal analysis. *Journal of thermal analysis* **1970,** *2* (3), 301-324.
20. Takeo, O., A New Method of Analyzing Thermogravimetric Data. *Bulletin of the Chemical Society of Japan* **1965,** *38* (11), 1881-1886.
21. Flynn, J. H., The isoconversional method for determination of energy of activation at constant heating rates. *Journal of thermal analysis* **1983,** *27* (1), 95-102.
22. Flynn, J. H.; Wall, L. A., A quick, direct method for the determination of activation energy from thermogravimetric data. *Journal of Polymer Science Part B: Polymer Letters* **1966,** *4* (5), 323-328.
23. https://imagej.nih.gov/ij/ (accessed 26 Aug 2016).

Chapter 4

Results and Discussion

n-Al and n-NiO were characterized for their chemical composition, particle morphology, particle size and size distribution. The active aluminum content of n-Al was measured using TGA to be 70.8 wt %. The heat of reaction for Al/NiO (stoichiometric ratio) has a measured value of 3309 J/g, which is very close to its theoretical value of 3440 J/g, indicating a near complete reaction. Fuel-rich compositions were shown to display higher heat of reaction due to the formation of Al_xNi_y intermetallic. The thermal responses of Al/NiO nano-thermites were analyzed using a DSC and their respective reaction products were analyzed using a powder XRD to predict their reaction mechanism. Surface functionalization and self-assembly of n-Al and n-NiO using organosilanes with complimentary end groups (epoxide/ amino) was attempted. The self-assembled n-Al/n-NiO showed a better intermixing of the binary composite powder from their SEM/EDX photographs. They displayed preference for pre-aluminum melting reaction as well as an increased heat release rate from their DSC profiles. The self-assembly process was shown to increase the gas release rate of organosilane-functionalized nano-thermites. However, the overall pressurization rate was not shown to be better than unfunctionalized n-Al/n-NiO. The activation energy of self-assembled n-Al-APTMS/n-NiO-GPTMS was found to be higher than physically mixed n-Al/n-NiO. 30 wt% THV addition to n-Al/n-NiO (ER 1.2) could reduce the sensitivity of n-Al/n-NiO to both ESD and friction and preserve its reactivity.

4.1 Characterization of n-Al, n-NiO and Al/NiO Nano-Thermite

4.1.1 X-Ray Diffraction

n-Al, n-NiO and the as-prepared nano-thermite were characterized using XRD to confirm their compositions. The spectrum of n-Al conforms to aluminum (ICDD PDF 01-072-3440) and the spectrum of n-NiO conforms to that of NiO, bunsenite (ICDD PDF 04-001-9373). Although n-Al was covered with a thin layer of aluminum oxide, its amorphous nature did not make it identifiable via the XRD spectrum. Calculated average crystallite sizes using the Scherrer formulae (Equation 3.4) from the XRD spectra are 34 nm and 9 nm for n-Al and n-NiO, respectively. Calculations were performed using the respective (111) peak and the assumption of K = 1. The prepared nano-thermite mixture (prepared at its stoichiometric ratio) contained only the Al and NiO phases without any additional peaks indicating no changes resulting from the preparation technique. The XRD spectra are shown in Figure 4.1.

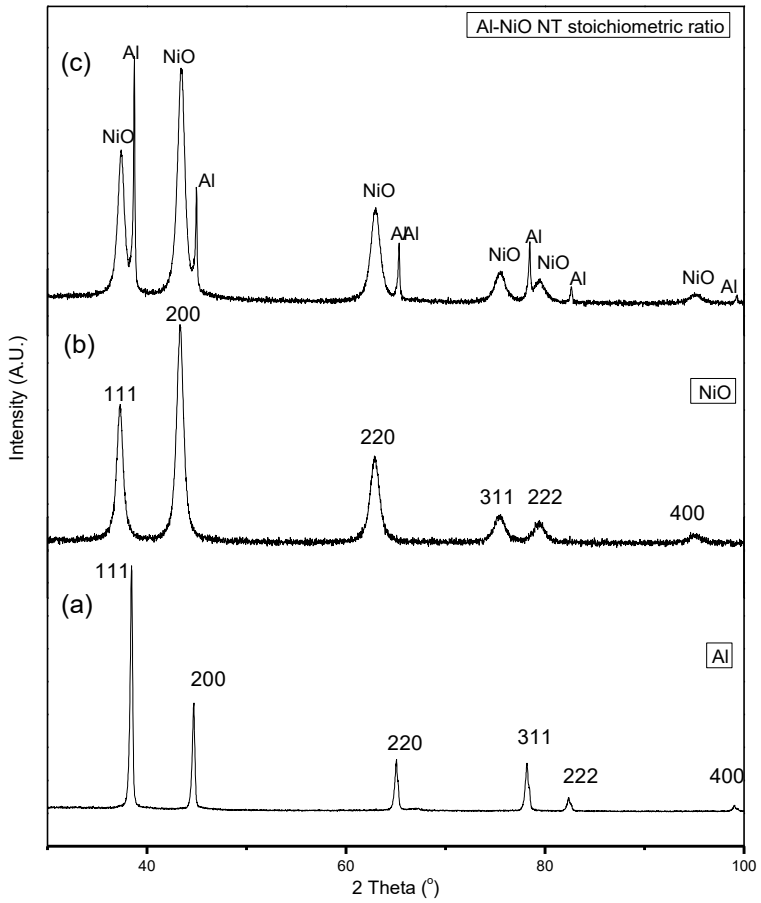

Figure 4.1: XRD spectra of (a) n-Al, (b) n-NiO and (c) n-Al/n-NiO nano-thermite at ER 1.

4.1.2 Scanning Electron Microscopy

The SEM images (Figure 4.2) show n-Al powders having a spherical morphology while n-NiO appeared as irregular clusters of nanoparticles that remained inseparable through ultrasonication. n-Al powders have a primary particle size range of 20 – 310 nm while that of n-NiO powders were not measurable due to their aggregated form. The nano-thermite mixture showed that n-Al and n-NiO were relatively well mixed. The SEM micrographs taken at both 50,000× and 100,000× of the nano-particles and their mixture are shown in Figure 4.2.

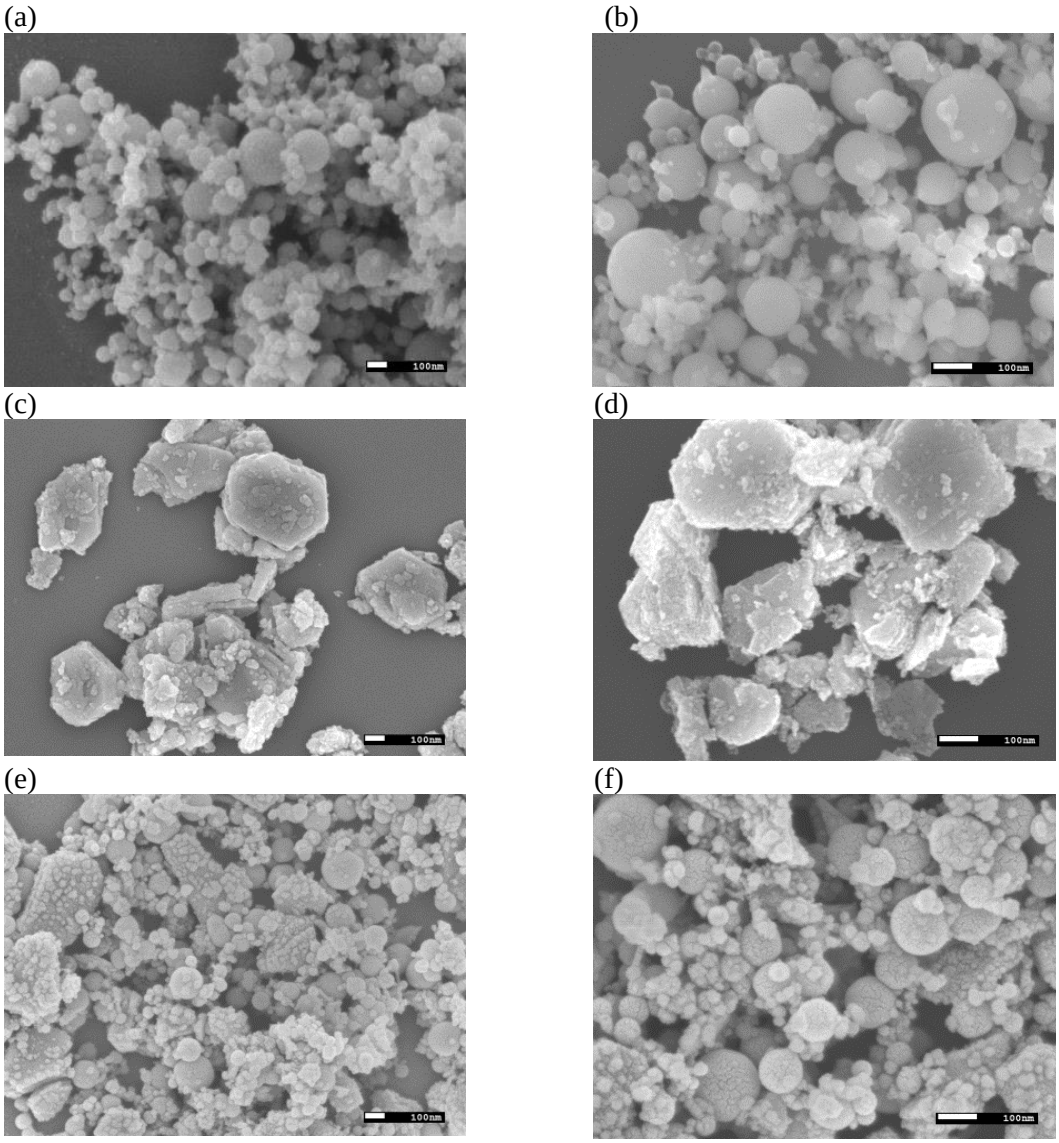

Figure 4.2: SEM micrographs of (a-b) n-Al, (c-d) n-NiO and (e-f) n-Al/n-NiO nano-thermite at ER 1 taken at 50,000× and 100,000× magnifications.

4.1.3 Surface Area Analysis

The n-Al and n-NiO had measured BET specific surface area of 28.74 ± 0.06 m^2/g(APS equivalent to 77 nm) and 72.09 ± 0.67 m^2/g (APS equivalent to 12 nm) from their surface area analysis. The average particle sizes were calculated using Equation (3.3) with the assumption that the nanoparticles are non-porous and spherical with uniform size.

4.1.4 Particle size distribution

While the SEM images gave us the best visualization of the primary particle size of the n-Al and n-NiO, a better representation of the size distribution of the particles in their suspended form within isopropanol would be to measure using a laser diffraction particle size analyzer. Through the diffracted light angle and intensity, the particle size of the sample is estimated. Each sample was measured five times. The volumetric size distributions of n-Al as well as n-NiO, suspended in isopropanol, are plotted in Figure 4.3. The statistical size information of the samples are tabulated in Table 4.1.

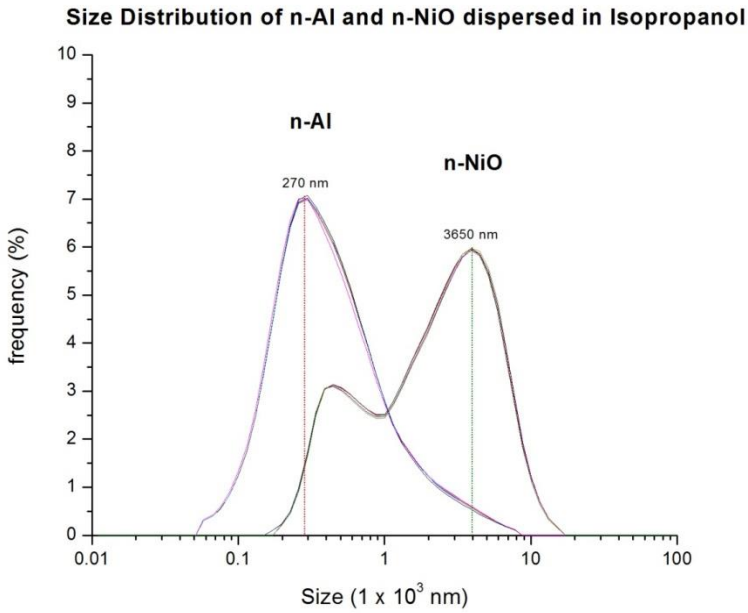

Figure 4.3: Particle size distribution of n-Al and n-NiO suspended in isopropanol measured using Laser Diffraction Particle Size Analyzer

Table 4.1: The mean, mode, D10, D50 (Median), D90, as well as the particle size range were measured for n-Al and n-NiO

Size (nm)						
Sample	**Mean**	**Mode**	**D10**	**D50**	**D90**	**Range**
n-Al	615	270	144	352	1302	58 - 7700
n-NiO	2805	3650	408	2229	6050	172 - 15172

The n-Al have a particle size range of 58 to 7700 nm and a measured mode size of 270 nm, meaning that it has the highest proportion of particles displaying a size of 270 nm. The n-NiO has a measured particle size range of 172 to 15172 nm. This is a clear indication that the particles exist as hard agglomerates and could not be dispersed into their individual particles. The measured mode size of 3650 nm indicates that most particles exist as aggregates of around this size. We noted that the particle size range measured via laser diffraction is much higher than that measured via electron microscopy. This is expected because the particle size measured via electron microscopy is based on the counting of particles with varying dimensions and gives a number distribution. However, a volume distribution is reported from the size measurement using laser diffraction. A size distribution measured based on volume can display a much larger average size from just a small fraction of particles with very large volume within the population. The deviation of sizes in number and volume distributions is especially common for particles with polydispersed size.

4.1.5 Active Aluminum

The n-Al powder has an active aluminum content of 70.8 weight% from weight gain measurement (63.029 weight%) through complete oxidation measured using TG-DTA (Figure 4.4). Calculations were made using Equation (3.7). The weight change with its accompanying DTA signal showed a two-step oxidation that is typical of n-Al powder. The multiple step oxidation displayed by Al powder has been well described by Dreizin et al [1] and a typical TGA curve of Al going through oxidation with a schematic showing their respective transitions is shown in Figure 4.5. The active aluminum content is used

for the calculation of the required Al/NiO sample weight ratio to prepare the nano-thermites with the respective ER.

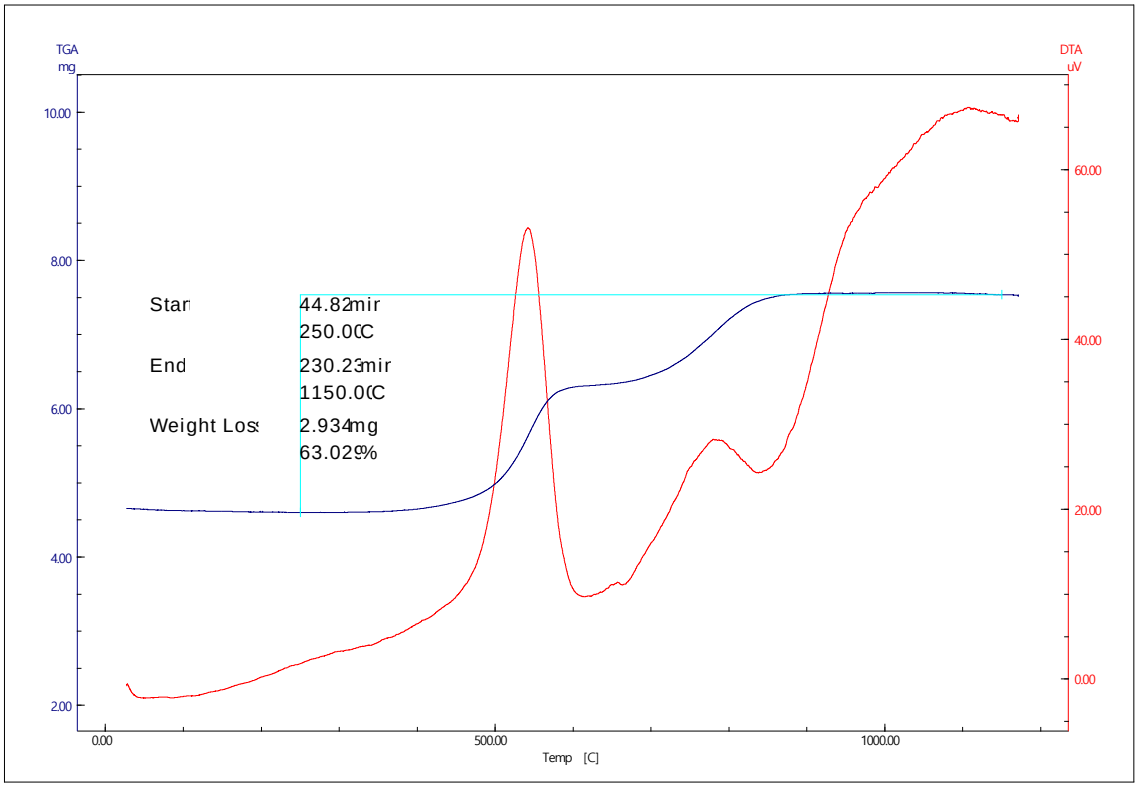

Figure 4.4: TG-DTA signal of n-Al showing complete oxidation in oxygen. Total weight gain is used for computing the active aluminum content of the n-Al.

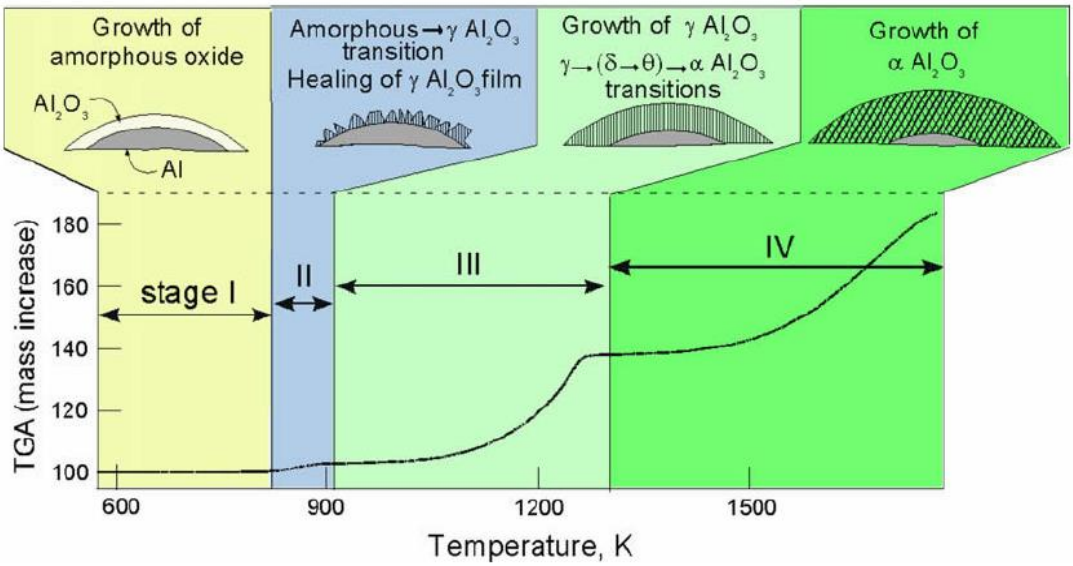

Figure 4.5: TGA signal showing the change in mass of Al powder (micron-sized) going through oxidation. The different stages of oxidation as well as their respective changes in the growing alumina phases are shown.[1]

4.2 Heat of Reaction for Al/NiO Nano-Thermite

The heats of reactions for Al / NiO nano-thermite mixtures with varying ER were measured using the bomb calorimeter and the results are tabulated in Table 4.2. The total calorific heat outputs were found to increase with increasing aluminum content from ER 0.8 to 1.2 (Figure 4.6). Further increase in aluminum content did not increase the energy output until a slight increase (of 3 %) is observed for ER 1.7 while subsequent increase in aluminum content (ER 1.7 to 2.0) did not change its energy output further. The theoretical heat of reaction for the reaction between Al and NiO as depicted in Equation (3.1) is 3440J/g.[2] The average measured heat output from the Al/NiO ER 1 (stoichiometric ratio) mixture prepared has a value of 3309 J/g, which is very close to its theoretical value, indicating an almost complete reaction. The increase in heat output for fuel-rich mixtures (having ER >1) is likely a result of additional energy generation from the formation of Al_xNi_y intermetallic due to the excess Al remaining after the complete redox reaction between Al and NiO. The intermetallic reaction between Al and Ni is a highly exothermic process and has been commonly adopted in research for energetic applications such as microinitiators.[3] The formation of the intermetallic is further confirmed by the XRD analysis in a separate study conducted on the reaction products of samples heated in a DSC (reported in the next section).

The theoretical values for the reaction between Al and NiO with varying ER is computed through summation of the theoretical heat of reaction values of Al/NiO reaction (3440 J/g) with the Al/Ni intermetallic reaction to form AlNi (1381 J/g) as depicted in Equation 4.1. For the simplicity of calculation, the energy difference from the formation of other Al_xNi_y intermetallic is ignored. The calculated total heat output against ER is plotted in Figure 4.7. This is an interesting trend to observe as despite of displaying a maximum calculated heat output at the stoichiometric mixing ratio (ER 1) for Al and NiO, the total heat output actually peaks at ER 2.5 due to the additional heat output from the formation of Al_xNi_y intermetallic. The heat of reaction between Al and NiO plateaus off (in Figure 4.6) instead of decrease when ER increases beyond 1 because of the additional energy released from the formation of Al_xNi_y intermetallic. The intermetallic is formed from the remaining Al in excess as well as the formed Ni (reduced product of NiO).

Table 4.2: The average calorific heat output of Al/NiO prepared with varying weight ratio for ER 0.8-2.0.

Equivalence Ratio (ER)	n-Al Wt %	n-NiO Wt %	Average Calorific energy output (J/g)
0.8	16.15	83.85	2769 ± 55
0.9	17.81	82.19	2788 ± 67
1.0	19.41	80.59	3309 ± 10
1.1	20.94	79.06	3440 ± 58
1.2	22.42	77.58	3649 ± 40
1.3	23.84	76.16	3611 ± 23
1.4	25.21	74.79	3607 ± 53
1.7	29.05	70.95	3721 ± 29
2.0	32.51	67.49	3702 ± 10

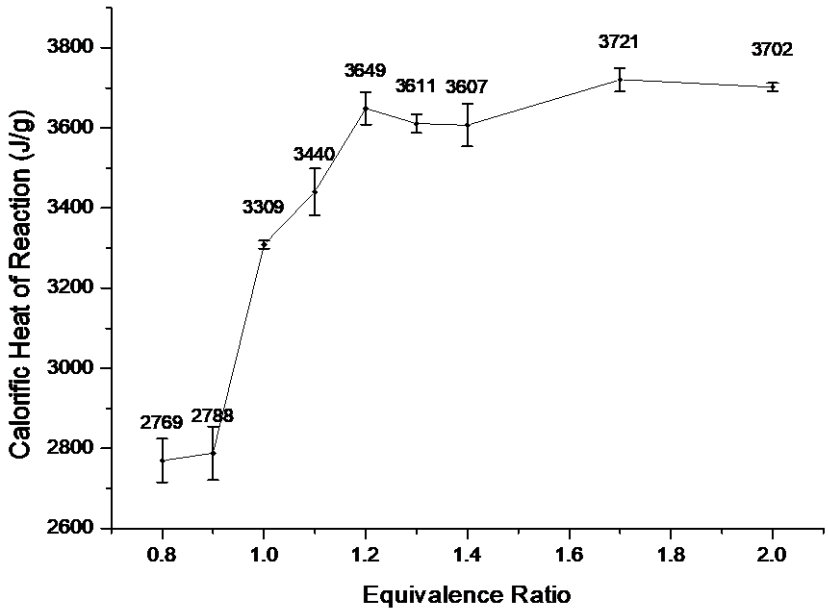

Figure 4.6: Calorific Heat output of Al/NiO nano-thermites having varying ER (0.8 – 2.0) measured using a Bomb Calorimeter (in Argon).

Ni + Al → AlNi Theoretical Heat of Reaction: 1381 J/g [2] (4.1)

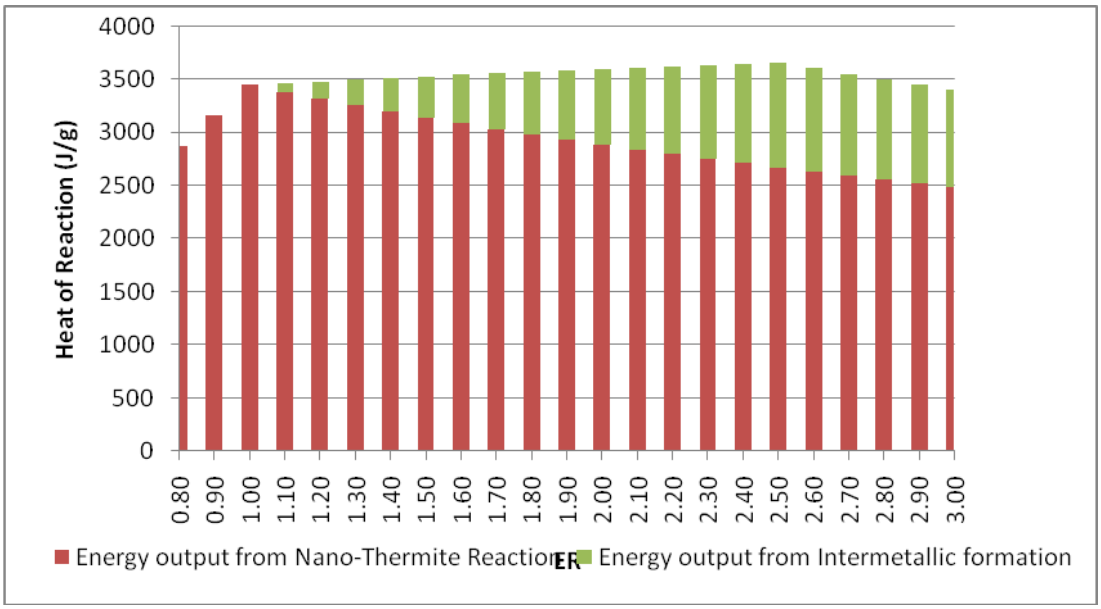

Figure 4.7: Calculated total energy output of Al/NiO with varying ER (0.8-3.0) resulting from nano-thermite reaction between Al and NiO as well as the intermetallic reaction between Al (in excess) and Ni (product of nano-thermite reaction).

4.3 Thermal Analysis and Product Analysis for Al/NiO Nano-Thermite

4.3.1 Differential Scanning Calorimetry

Nano-thermites with varying ER (0.8 to 2.0) were heated to 1000 ^{o}C in a DSC at 5 ^{o}C/min under Argon (Figure 4.8). The DSC profiles of the Al/NiO nano-thermites displayed a two stage exothermic reaction ascribed to the two-stage oxidation of n-Al. The first reaction exotherm had an average onset temperature of 474 ± 3 ^{o}C and peak temperature of 523 ± 3 ^{o}C while the second reaction exotherm had an average onset temperature of 694 ± 16 ^{o}C and peak temperature of 749 ± 26 ^{o}C for the Al/NiO having different ER (0.8 to 2.0). The n-Al melting endotherm, with an average onset temperature of 655 ^{o}C, is observed in all the DSC profiles and appears more prominently in an Al-rich composition (i.e. ER 2.0). It indicates the existence of Al, in its molten state, after the first reaction exotherm.

Al is known to go through multiple stages of oxidation that is accompanied with alumina phase change at different temperature.[1] The n-Al used for this work exhibited a two-stage oxidation when heated to 1000 ^{o}C in oxygen where the first stage oxidation took place at an onset temperature of 476 ^{o}C and the second with an onset of 676 ^{o}C. The first-stage oxidation took place with the amorphous alumina transforming to gamma phase and growing till a critical thickness before it breaks and exposing new aluminum to the oxidizing environment, which indicates a slowing of the oxidation process before it began again with a display of the second oxidation exotherm. The second exotherm took place after the melting of Al at 660 ^{o}C, representing the oxidation of Al in its molten state at this stage. The conditions are similar to what the n-Al are experiencing in the Al/NiO reaction where Al gets oxidized by the NiO present, while NiO experiences reduction by the Al present.

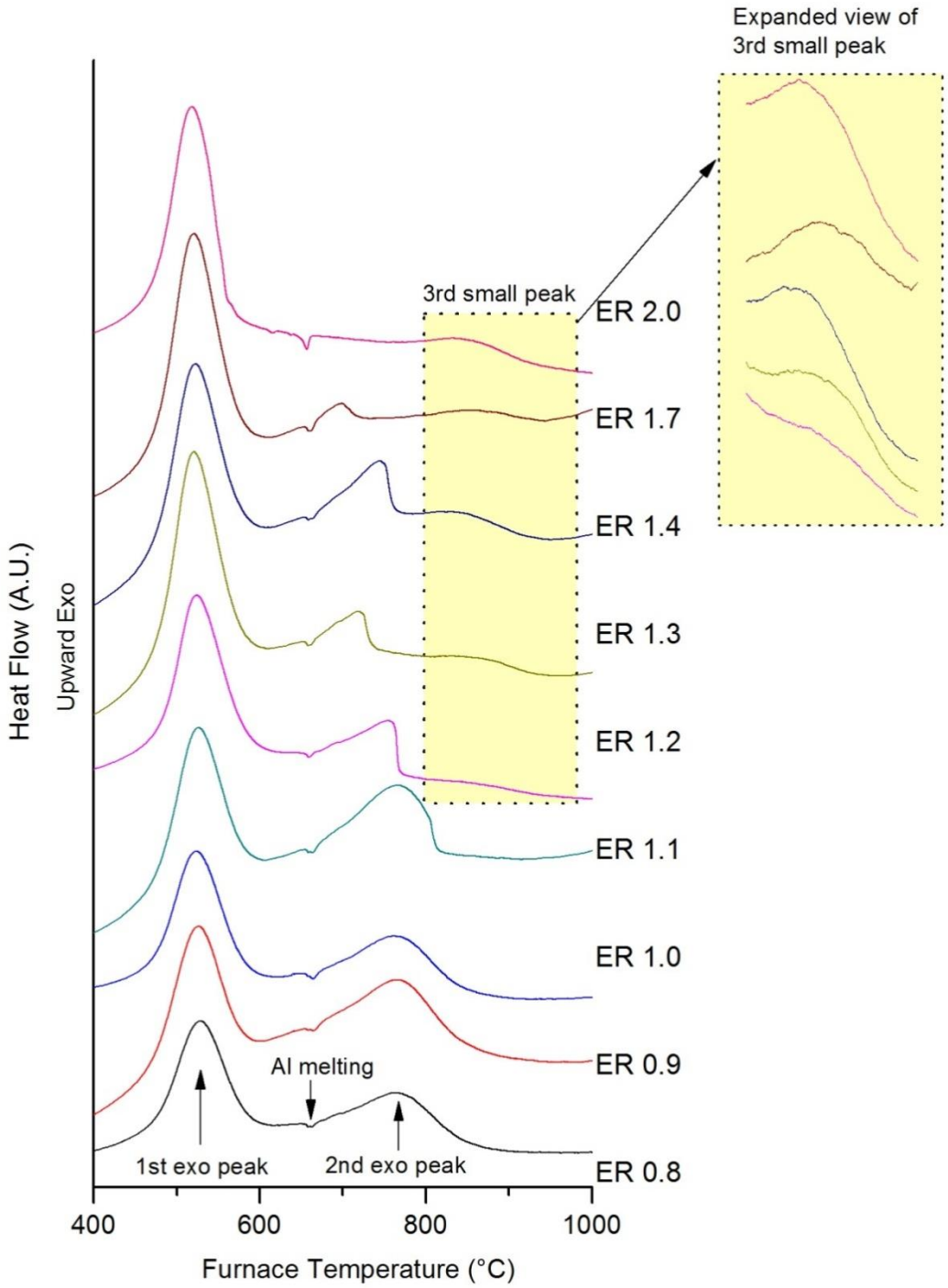

Figure 4.8: DSC profiles of n-Al/n-NiO nano-thermites with varying ER (0.8-2.0)

The energy released in the first exotherm increases while that in the second exotherm decreases with increasing Al content (from ER 0.8 to 2.0) until the complete disappearance of the second exotherm took place for ER2.0. The absence of a second exotherm in ER 2.0 is due to the low amount of NiO present in the reactant mixture,

indicating an insufficiency of oxidizer for the second stage oxidation of Al to take place. The DSC profiles of Al/NiO with higher aluminum contents (ER 1.2 to 2.0) also exhibited a third small exotherm with an onset temperature around 800 ^{o}C. The energy released from each exotherm is calculated through integration of the area under each curve and the values are plotted in Figure 4.9. The higher proportion of heat release from the first exotherm in comparison to the second exotherm indicates that it is the major heat releasing reaction exotherm. The interesting fact that an increasing amount of energy is found released from the first exotherm in an increasingly fuel-rich environment (as ER increased from 0.8 to 2.0) is an indication that a fuel-rich environment encourages the pre-aluminum melting oxidation to take place.

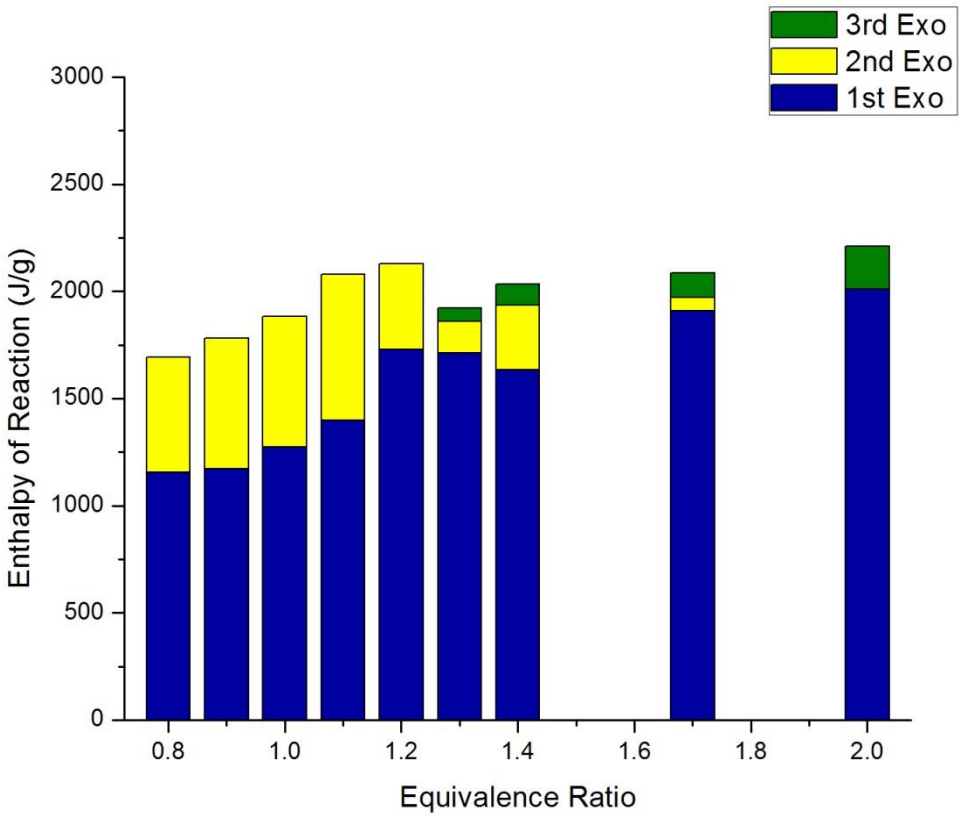

Figure 4.9: Energy measured from DSC exotherms (1st, 2nd and 3rd exotherms) for reaction between n-Al and n-NiO in varying ER

4.3.2 X-Ray Diffraction

In an attempt to understand the difference in the reaction of Al/NiO prepared with different ER, their reaction products were subjected to XRD composition analysis (Figure 4.10). It was found that Al/NiO, which was prepared in its stoichiometric ratio (ER 1.0), showed a complete redox reaction to form Ni and Al_2O_3, according to Equation (4.2a). Al_xNi_y intermetallic were detected, but only in fuel rich compositions (ER 1.2 and above) that were heated to 1000 ^oC, indicating that an excess of Al is a prerequisite for the formation of the intermetallic. Al/Ni intermetallic phases that were detected include Ni_2Al_3, AlNi, Ni_3Al, $Ni_{0.879}Al_{0.121}$.

On the contrary, a $NiAl_2O_4$ double oxide was formed in fuel-lean compositions (ER 0.8, 0.9) (Figure 4.10). The $NiAl_2O_4$ spinel is a result of solid state reaction between NiO and Al_2O_3occurring at high temperatures, which forms at the interface between NiO and Al_2O_3 through the counter diffusion of Al and Ni ions through the spinel layer. [4]

In an attempt to understand how the reaction progressed through the increasing temperature in a DSC, the reaction products for ER 1.2 was selected for further analysis by heating the sample at 5 ^oC/min in a DSC to different temperatures (475 ^oC, 600 ^oC, 765 ^oC, 1000 ^oC) as shown in Figure 4.11. The analysis confirms that the AlxNiy intermetallic was formed only at a high temperature, after 765 ^oC. It corresponds well to the third reaction exotherm in the DSC profile, which also explains why a third exotherm only appears in fuel-rich compositions (ER 1.2 to 2.0). At a reaction onset temperature of 800 ^oC, the Al that is remaining in excess (since ER1.2 is a fuel-rich composition), exist in its molten form and diffuse into Ni (formed as a product from the Al/NiO redox reaction) to form the intermetallic.

When the Al/NiO ER 1.2 nano-thermite mixture was heated to 765 ^oC, all NiO has completely reacted by this temperature as shown in the complete disappearance of NiO from the XRD spectrum. This indicated that the redox reaction between NiO and Al has completed by this temperature, leaving an excess of Al unreacted at this temperature. All Al has fused with Ni to form AlxNiy intermetallic when the mixture reaches 1000 ^oC as displayed by the disappearance of Al and appearance of Ni_3Al and $Ni_{0.879}Al_{0.121}$ intermetallic in the XRD spectrum. At 475 ^oC, Ni has begun to appear, indicating that the redox reaction between Al and NiO has begun at this temperature. However, Al_2O_3 remained undetected using the XRD at this temperature due to its amorphous nature at

475 ^{o}C. γ-Al_2O_3 was only detected when the reaction was allowed to reach 600 ^{o}C, where the conversion of amorphous Al_2O_3 to γ-Al_2O_3 would have taken place.

In summary:

Fuel-lean mixture (ER0.8-0.9)

$$\mathbf{3NiO + 2Al \rightarrow Al_2O_3 + 3Ni} \quad (4.2a)$$

$$\mathbf{Al_2O_3 + NiO_{unreacted} \rightarrow NiAl_2O_4} \quad (4.2b)$$

NiO (which is in excess) that remain unreacted after the first reaction (Equation 4.2a), further reacts with Al_2O_3 in a second reaction (Equation 4.2b)

Stoichiometric Ratio (ER 1.0)

$$\mathbf{3NiO + 2Al \rightarrow Al_2O_3 + 3Ni} \quad (4.2a)$$

Fuel-Rich mixture (ER1.1 – 2.0)

$$\mathbf{3NiO + 2Al \rightarrow Al_2O_3 + 3Ni} \quad (4.2a)$$

$$\mathbf{Ni + Al_{unreacted} \rightarrow Ni_xAl_y} \quad (4.2c)$$

Al (which is in excess) that remain unreacted after the first reaction (Equation 4.2a), further reacts with Ni in the second reaction (Equation 4.2c). Equation (4.2c) is an exothermic reaction and is displayed as the third exotherm (onset temperature of 800 ^{o}C) in the DSC.

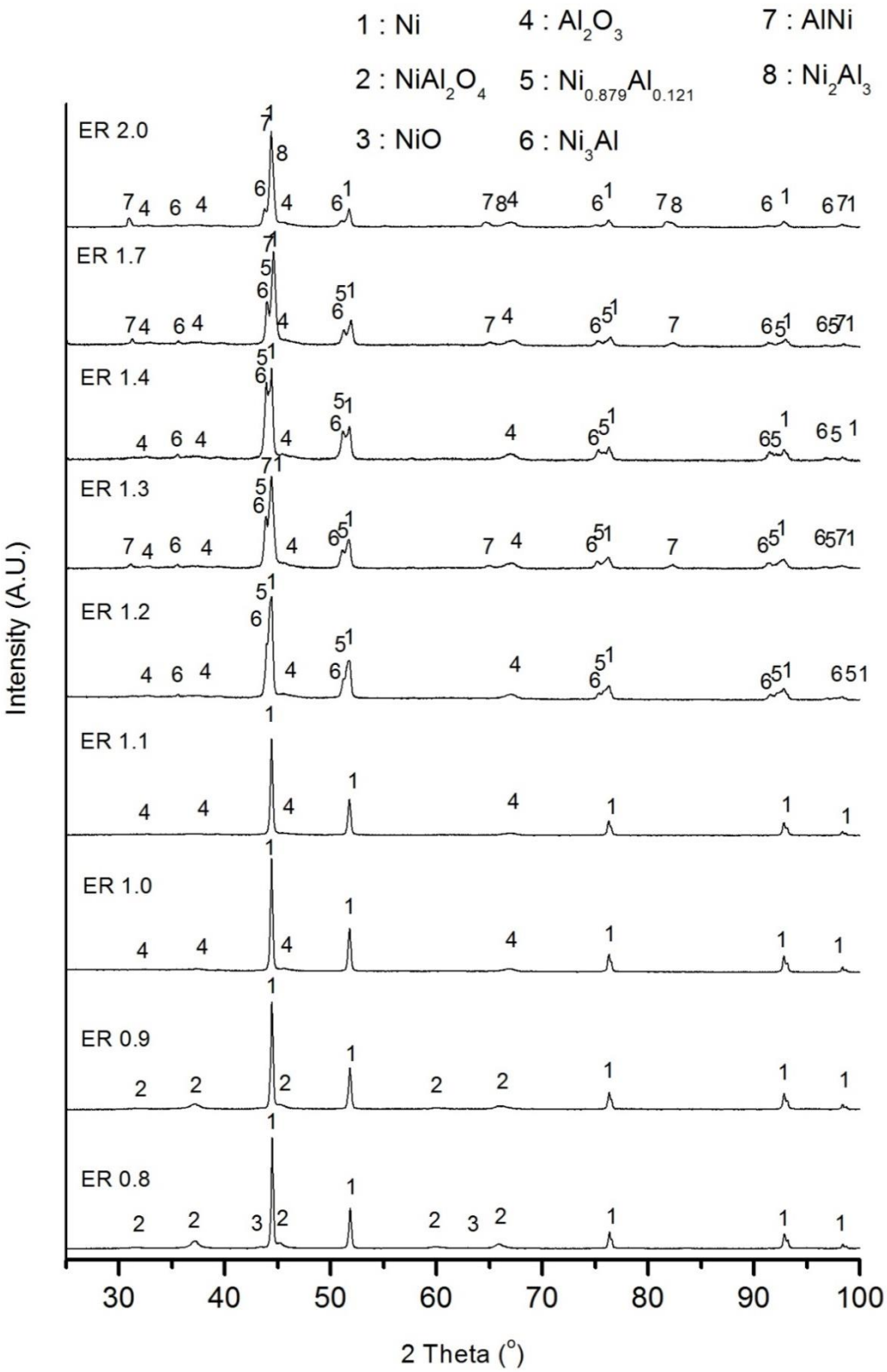

Figure 4.10: XRD spectra of reaction products from Al/NiO with varying ER (0.8 to 2.0) heated to 1000 ºC

(a)

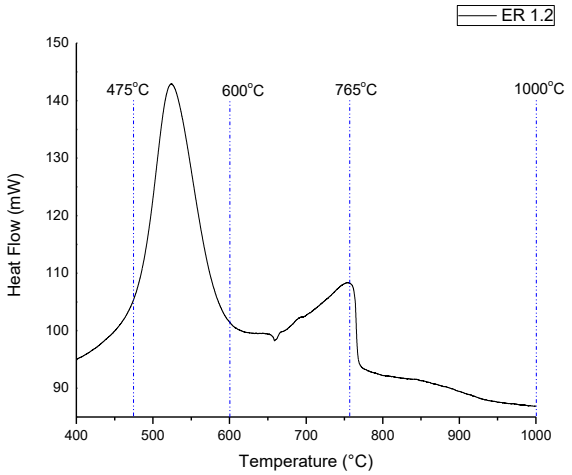

(b)

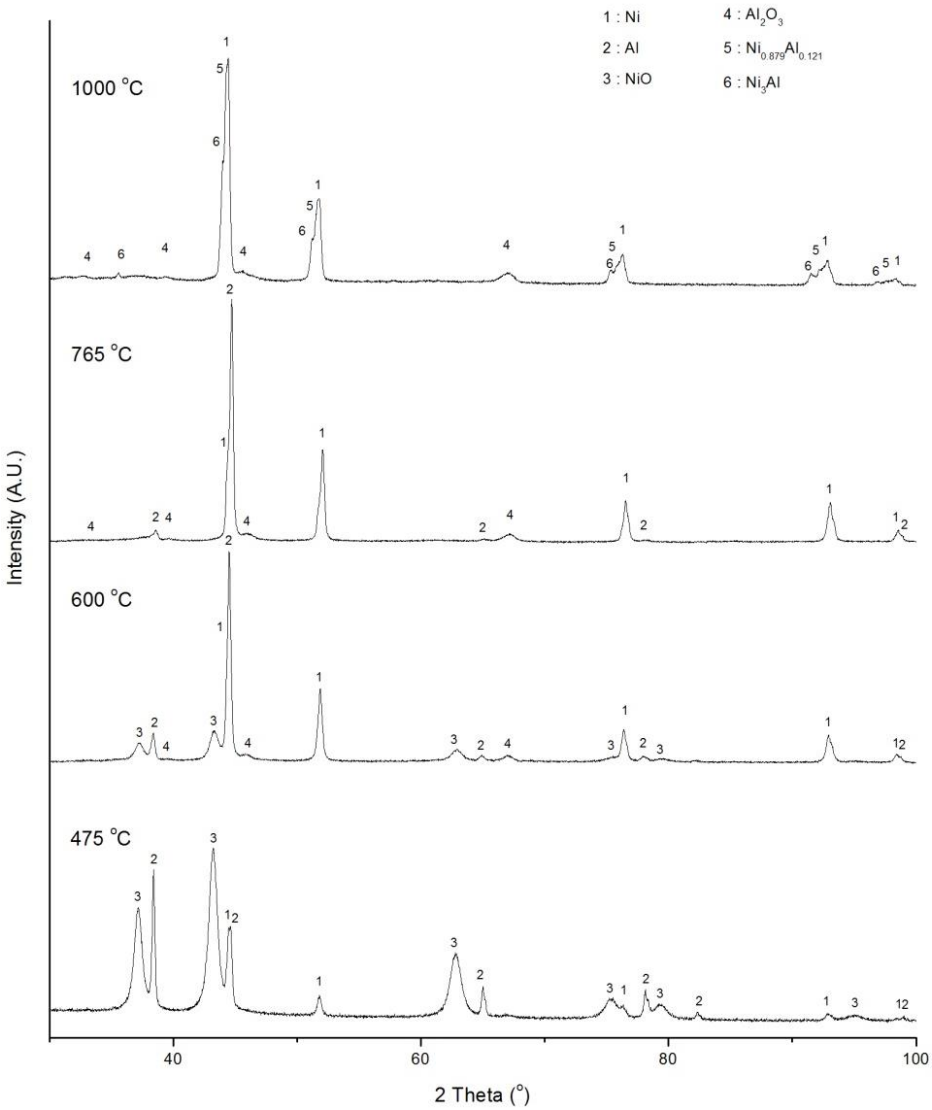

Figure 4.11: (a) Reaction of Al/NiO ER 1.2 in a DSC (conducted at 5 °C/min in Argon) were stopped at 4 different temperatures (475, 600, 765, 1000 °C) with product retrieved for XRD analysis (b) XRD spectra of reaction products from Al/NiO (ER 1.2), heated to different temperatures indicated in (a)

4.4 Surface Functionalization and Self-Assembly of n-Al/ n-NiO using organosilane

4.4.1 Introduction

The aim of this study is to investigate the effect of grafting and self-assembly on n-Al/n-NiO using organosilane surface modification. Self-assembled n-Al/n-NiO were prepared and compared to physically mixed n-Al/n-NiO, which serves as the control. All samples were prepared in a mixing ratio with ER1.2 in a similar manner. n-Al and n-NiO were each dispersed in isopropanol for 15 mins via sonication before they were combined in a Round-Bottom flask and stirred for 6 hrs at 70 ^{o}C under nitrogen atmosphere.

Two other samples namely the physically mixed silane grafted and self-assembled (reduced grafting) were prepared to isolate the effect of grafting and grafting percentage on the nano-thermite system. Both n-Al and n-NiO in the physically mixed silane grafted sample were grafted with organosilanes having the same function end group (amino) to avoid interaction. Heating during its mixing was excluded to avoid any interaction between the grafted organosilane while mixing duration was kept the same. The effect of grafting percentage was investigated by reducing the grafting percentage on n-NiO from 2.5 to 1.3 wt%. The n-NiO-GPTMS with reduced grafting was used in the preparation of the sample while all other conditions were kept the same as the others. The samples studied are tabulated in Table 4.3.

Table 4.3: The sample names and their respective compositions used for this study. All n-Al /n-NiO were prepared in ER 1.2.

Sample Name	Composition
Self-assembled	n-Al-APTMS (2.1 wt%) + n-NiO-GPTMS (2.5 wt%)
Physically mixed	n-Al + n-NiO
Physically mixed silane grafted	n-Al-APTMS (2.1 wt%) + n-NiO-APTMS (1.8 wt%)
Self-assembled (Reduced grafting)	n-Al-APTMS (2.1 wt%) + n-NiO-GPTMS (1.3 wt%)

4.4.2 Surface Functionalization

4.4.2.1 Surface Functionalization of n-Al with APTMS

Surface functionalization of n-Al with (3-Aminopropyl) Trimethoxysilane (APTMS) were conducted as described in the procedure detailed in Section 3.4. The reaction is described in the schematic diagram as shown in Figure 4.12. The FTIR spectrum of the n-Al grafted with APTMS (Figure 4.13) indicates the presence of asymmetrical and symmetrical stretching vibration of the C- H bond in methylene group at 2847, 2940 cm^{-1}. Si-O-Si bond was observed at around 1096 cm^{-1}, indicating the condensation reaction between silanol groups. The n-Al-APTMS showed a weight lost of 3.2 % from the TGA as shown in Figure 4.14. A deduction of the the observed weight loss in pristine n-Al (1.7 %) concluded in a net weight lost of 1.5% from the APTMS grafting.

APTMS-modified n-Al were reacted with (3-Glycidoxypropyl) Trimethoxysilane (GPTMS) to determine if the amino groups of the grafted APTMS remained active for reaction with the epoxide group on GPTMS. APTMS-modified n-Al and GPTMS were mixed in 2-propanol and subjected to heating at 70 ^{o}C for 6 hrs. The nanoparticles were washed thrice with 2-propanol and dried overnight at 60 ^{o}C. The TGA analysis of the resulting nanoparticles shows a further weight loss of 1.6% (Figure 4.14). The additional weight lost is likely a result of the additional organic presence of GPTMS that were grafted from the ring opening reaction of epoxide (on GPTMS) by the amino moiety on the n-Al-APTMS. The nanopaarticles retained their spherical morphology and no significant difference in size was detected from the SEM images of n-Al and n-Al grafted with APTMS (Figure 4.15).

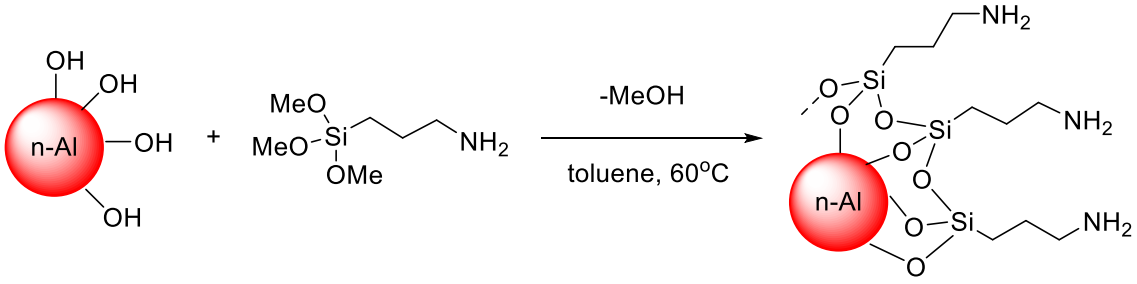

Figure 4.12: Schematic drawing on the surface functionalization of n-Al with APTMS

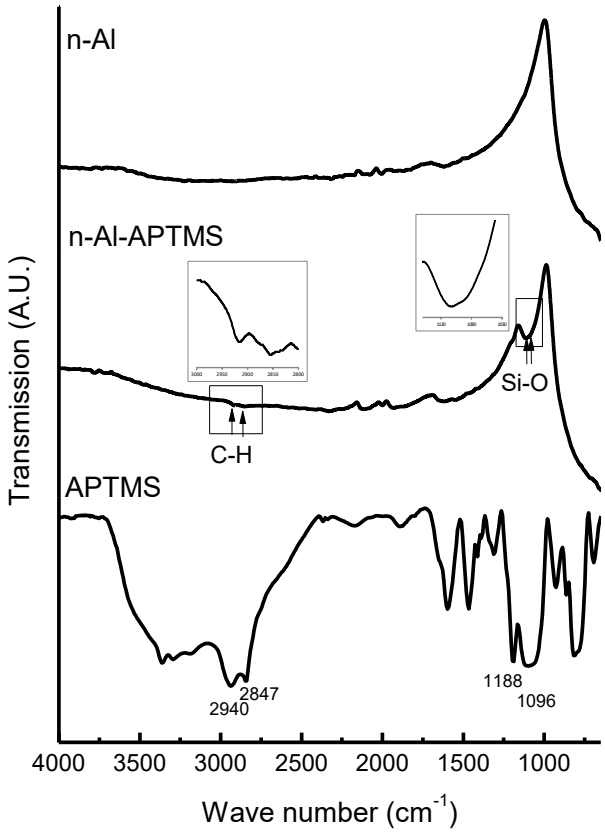

Figure 4.13: FTIR spectra of pristine n-Al, n-Al grafted with APTMS and original APTMS

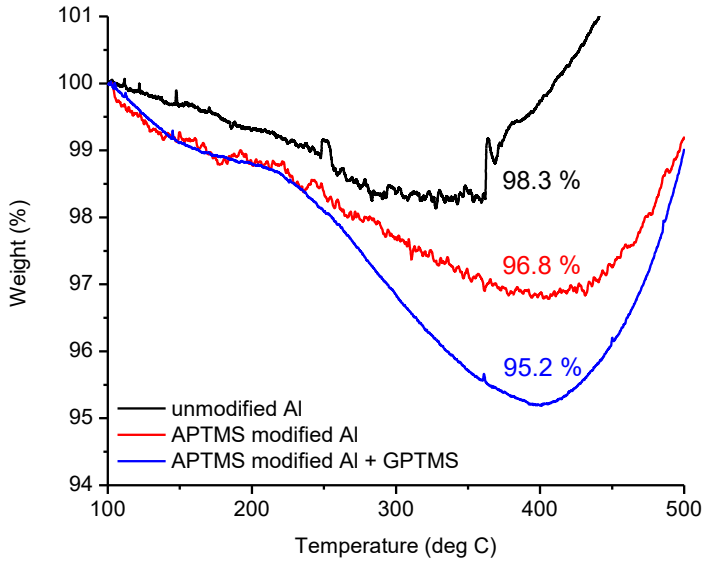

Figure 4.14: Maximum percentage weight loss of n-Al, n-Al functionalized with APTMS (n-Al-APTMS) and n-Al-APTMS that has reacted with GPTMS as measured from a TGA from 100 to approximately 400 ^{o}C.

(a) 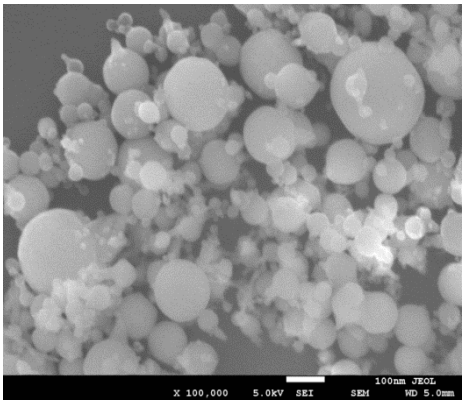 (b) 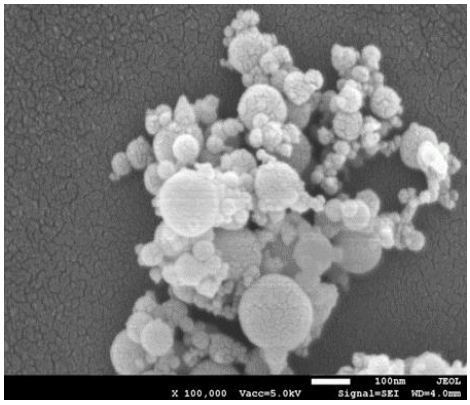

Figure 4.15: FESEM images of (a) n-Al and (b) n-Al functionalized with APTMS, both images taken at 100,000 x magnification

The particle size distribution of n-Al-APTMS was measured using laser diffraction and the result is shown in comparison with n-Al before modification (Figure 4.16). n-Al-APTMS showed an increase in the upper limit of its size range (58-8816 nm) in comparison to n-Al (58-7700 nm). Since both n-Al and n-Al-APTMS have much smaller primary particle size (20-310 nm), evident from their SEM photos, we conclude that the larger size detected using the laser diffraction are due to the presence of agglomerates and the size distribution results indicate the presence of larger agglomerates in n-Al-APTMS. The surface modification may have slightly affected their dispersion in isoproponal.

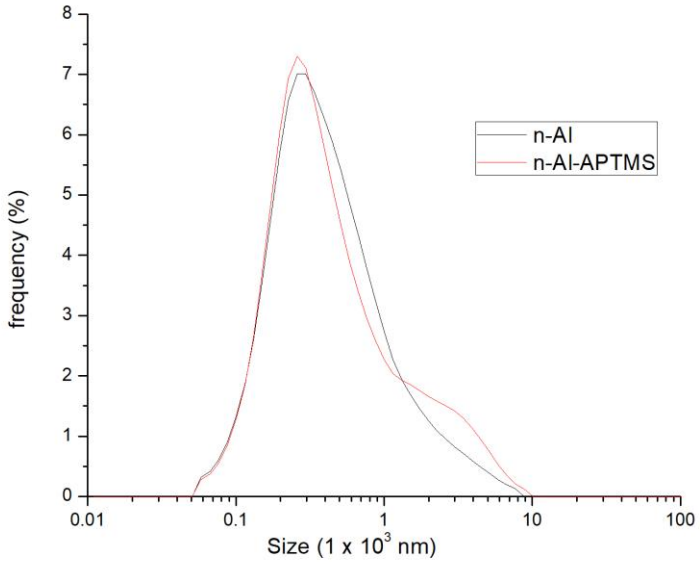

Size (nm)						
Reading	**Mean**	**Mode**	**D10**	**D50**	**D90**	**Range**
n-Al	615	270	144	352	1302	58 - 7700
n-Al-APTMS	758	256	146	348	1960	58 - 8816

Figure 4.16: Particle size distribution of n-Al-APTMS, in comparison with n-Al, measured by laser diffraction.

4.4.2.2 Surface Functionalization of n-NiO with GPTMS

Surface functionalization of n-NiO with (3-Glycidoxypropyl) Trimethoxysilane (GPTMS) were conducted as described in the procedure detailed in Section 3.4. The reaction is described in the schematic diagram as shown in Figure 4.17. The FTIR spectrum of the n-NiO grafted with GPTMS (Figure 4.18) indicates the presence of asymmetrical and symmetrical stretching vibration of the C- H bond in methylene group at 2839, 2943 cm^{-1}. Si-O-Si bond was observed at around 1088 cm^{-1}, indicating the condensation reaction between silanol groups. The n-NiO-GPTMS showed a weight lost of 4.7 % from the TGA as shown in Figure 4.19. A deduction of the the observed weight loss in pristine n-NiO (2.2 %) concluded in a net weight lost of 2.5% from the APTMS grafting.

GPTMS-modified n-NiO were reacted with APTMS to determine if the epoxide groups of the grafted GPTMS remained active for reaction with the amino group on APTMS.

APTMS-modified n-Al and GPTMS were mixed in 2-propanol and subjected to heating at 70 ^{o}C for 6 hrs. The nanoparticles were washed thrice with 2-propanol and dried overnight at 60 ^{o}C. The TGA analysis of the resulting nanoparticles shows a further weight loss of 2.1% (Figure 4.19). The additional weight lost is likely a result of the additional organic presence of APTMS that were grafted from the ring opening reaction of epoxide groups on the GPTMS-grafted n-NiO by the amino moiety on the APTMS. The nanopaarticles retained their morphology and no significant difference in size was detected from the SEM images of n-NiO and n-NiO grafted with GPTMS (Figure 4.20). The particle size distribution of n-NiO-GPTMS was measured using laser diffraction and the result is shown in comparison with n-NiO before modification (Figure 4.21). The particles did not show significant difference before and after modification with both displaying the same size range and slight difference in their actual statistical size.

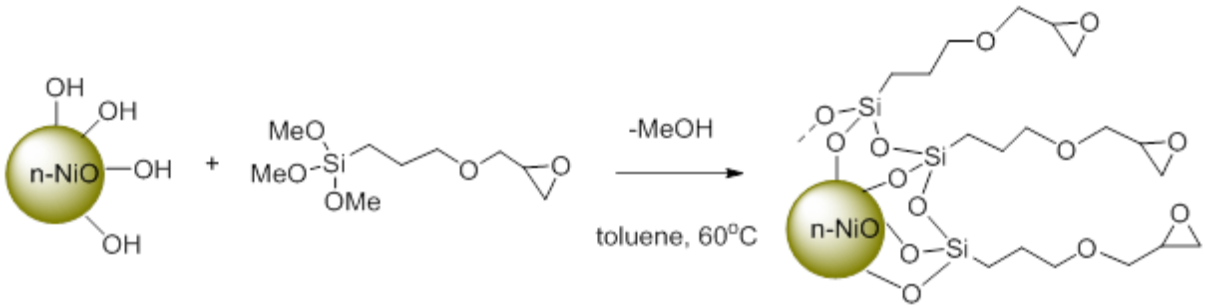

Figure 4.17: Schematic drawing on the surface functionalization of n-NiO with (3-Glycidoxypropyl) Trimethoxysilane (GPTMS)

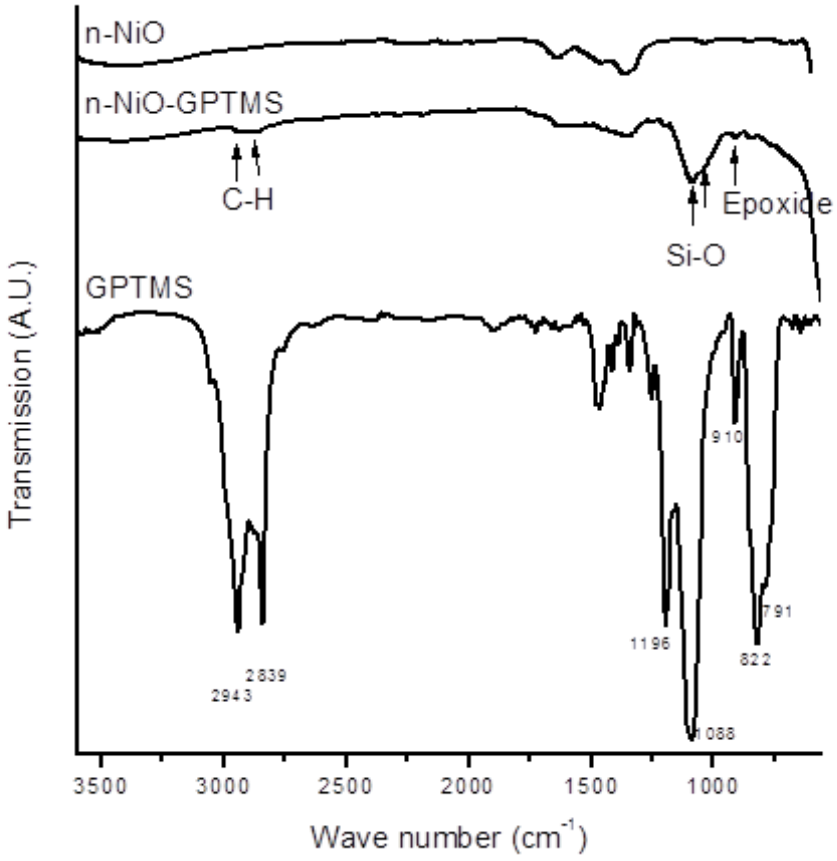

Figure 4.18: FTIR spectra of pristine n-NiO, n-NiO grafted with (3-Glycidoxypropyl) Trimethoxysilane (GPTMS) and original GPTMS

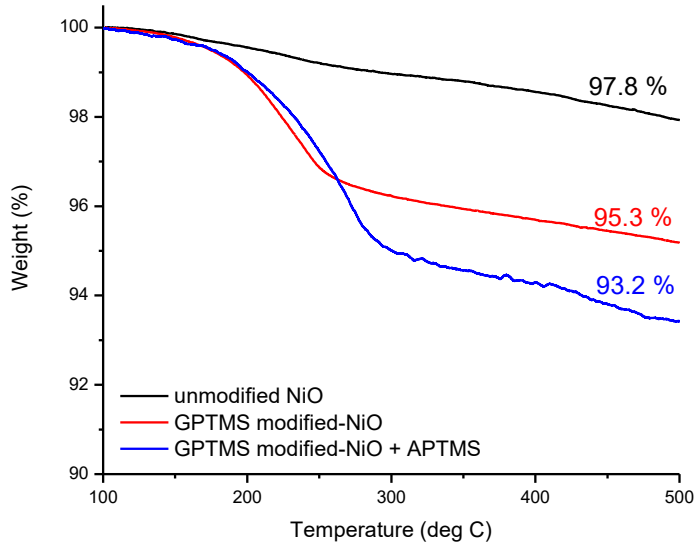

Figure 4.19: Percentage weight loss of n-NiO, n-NiO functionalized with GPTMS (n-NiO-GPTMS) and n-NiO-GPTMS that has reacted with APTMS as measured from a TGA from 100 to 500 ^{o}C.

(a) (b)

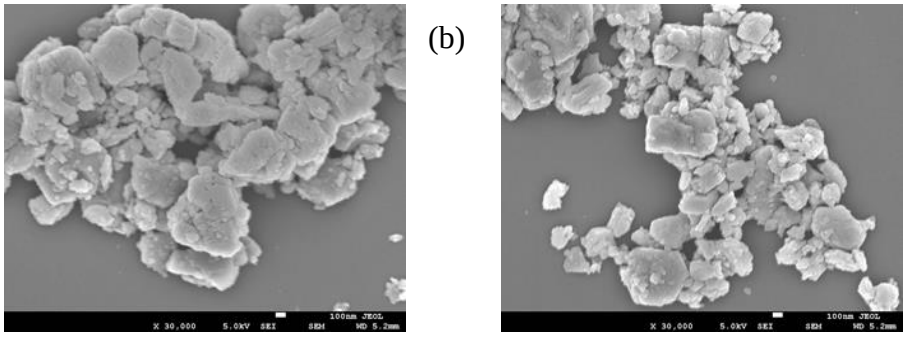

Figure 4.20: FESEM images of (a) n-NiO and (b) n-NiO functionalized with GPTMS, both images taken at 30,000 x magnification

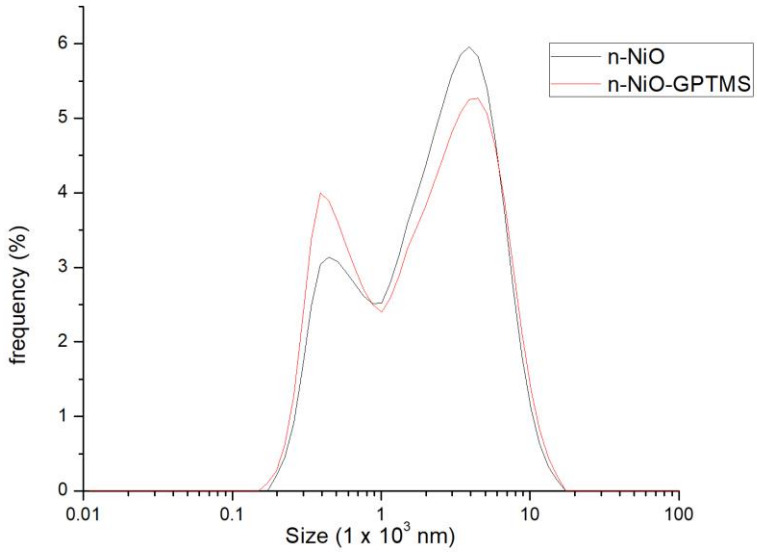

Size (nm)						
Reading	**Mean**	**Mode**	**D10**	**D50**	**D90**	**Range**
n-NiO	2805	3650	408	2229	6050	172 - 15172
n-NiO-GPTMS	2722	3756	363	1970	6246	172 - 15172

Figure 4.21: Particle size distribution of n-NiO-GPTMS, in comparison with n-NiO, measured by laser diffraction.

4.4.3 Al/ NiO intermixing

Secondary electron images for both self-assembled n-Al-APTMS/ n-NiO-GPTMS and physically mixed n-Al/n-NiO were taken at 50,000× and 100,000× for comparison.

Although n-Al has a more spherical appearance in comparison to the mostly irregular n-NiO, it is not easy to discern the homogeneity of mixing between the two samples using the SEM images. Elemental mapping of Al and Ni of images taken at 20,000× distinguished the difference in mixing homogeneity of n-Al/n-NiO in the two samples. The self-assembled sample displayed a good intermixing of n-Al and n-NiO (Figure 4.22 d) while large clusters of n-Al were observed in the physically mixed sample (Figure 4.23 d).

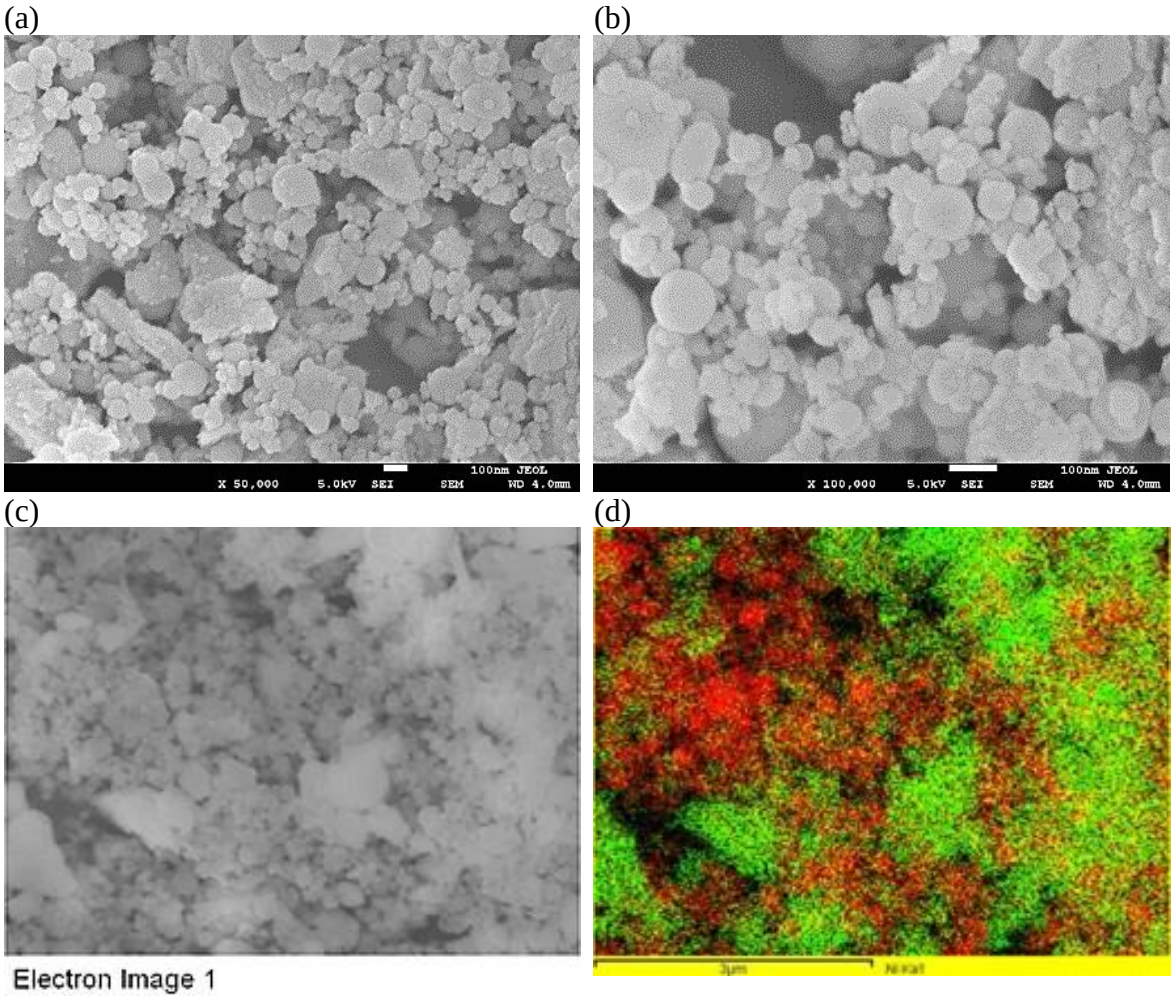

Figure 4.22: SEM pictures of self-assembled n-Al-APTMS/n-NiO-GPTMS at (a) 50,000 x, (b) 100,000 x and (c-d) 20,000 x with corresponding Elemental mapping of Al (Red) and Ni (Green).

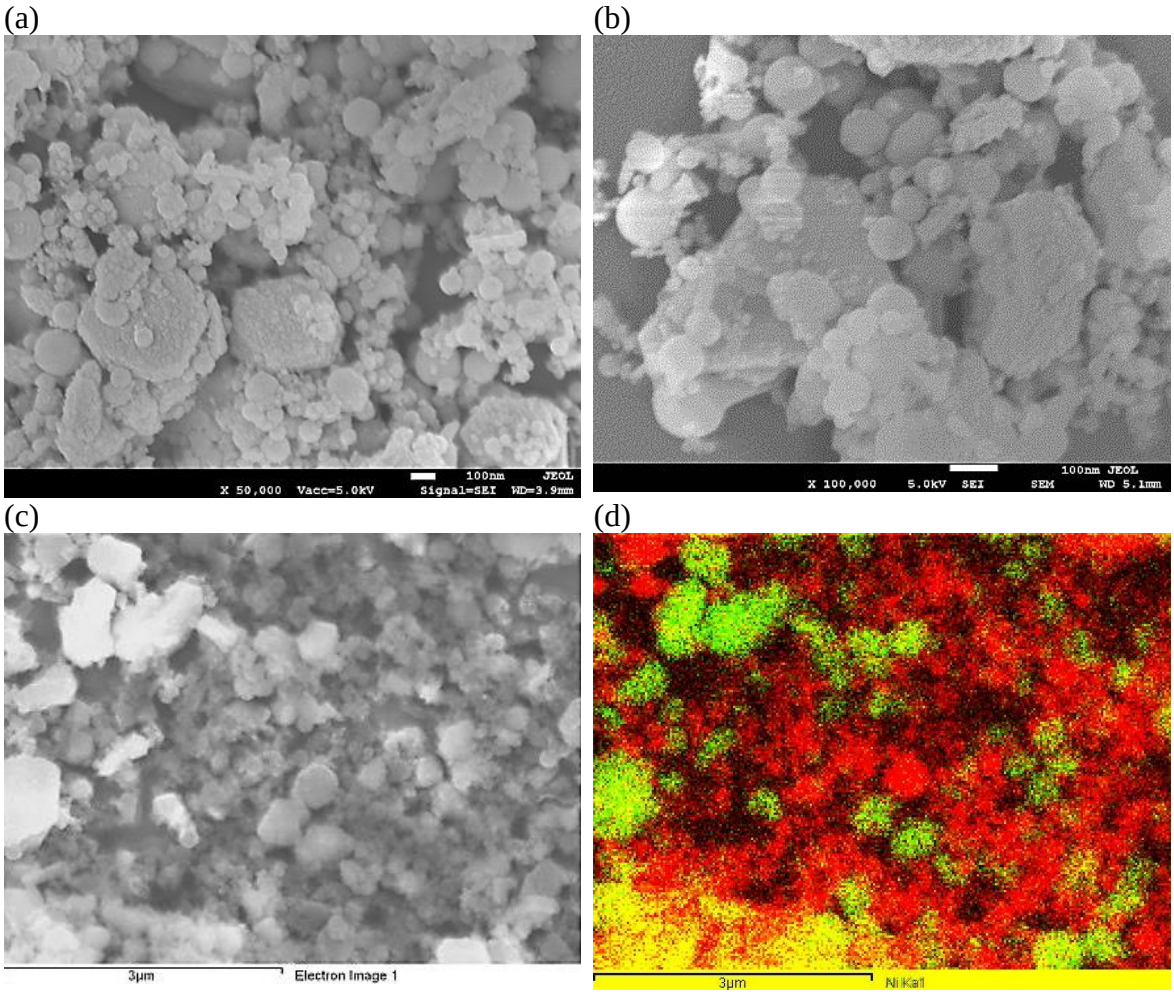

Figure 4.23: SEM pictures of Physically mixed n-Al/n-NiO at (a) 50,000 x, (b) 100,000 x and (c-d) 20,000 x with corresponding Elemental mapping of Al (Red) and Ni (Green).

4.4.4 Thermal Analysis

The self-assembled n-Al-APTMS/n-NiO-GPTMS showed a different DSC profile from the physically mixed n-Al/n-NiO (Figure 4.24). The self-assembled sample showed a sharper exotherm spanning across a small temperature range (500-605 ^{o}C) with the absence of a second exotherm, which typically appears in physically mixed samples. This shows complete Al/NiO redox reaction taking place before aluminum melting and indicates a complete reaction at the reactants' nanoscale level. Since both DSC profiles were collected at the same constant heating rate of 5 ^{o}C/min, the sharper exotherm spanning across a narrower temperature range indicates a faster heat releasing rate of the self-assembled nano-thermite. In the physically mixed nano-thermite, only a portion of the total energy release came from the reaction between Al and NiO at the nanoscale

level (first exotherm). Unreacted n-Al subsequently went through melting at 650 ºC and sintering before further reaction took place between the bulk Al and NiO (2nd exotherm). The complete reaction before aluminum melting was achieved via improved Al/NiO mixing at the nano-scale level, which was not achieved via physical mixing.

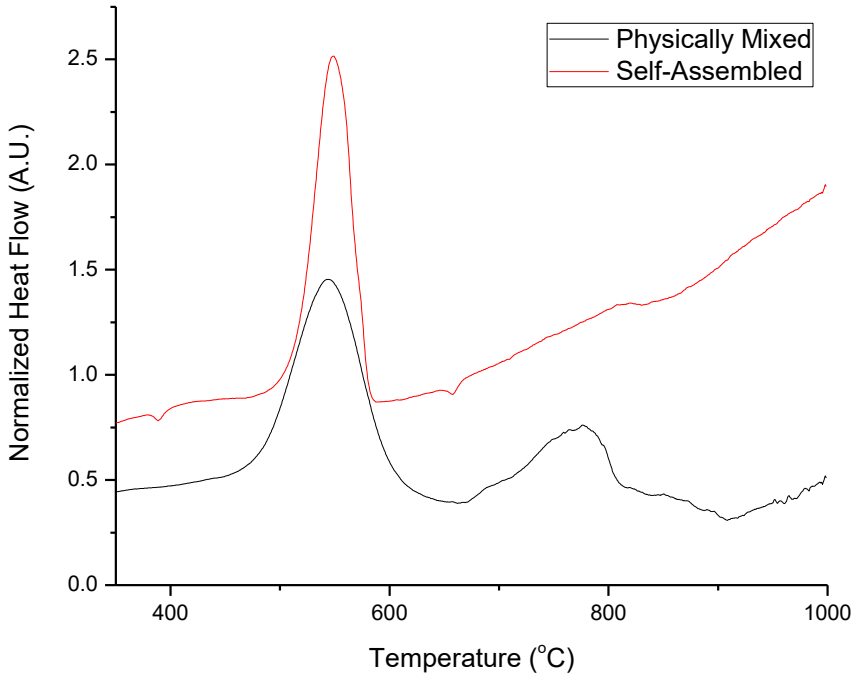

Figure 4.24: DSC profiles of physically mixed and self-assembled n-Al/n-NiO

The self-assembled n-Al-APTMS/n-NiO-GPTMS was also measured for its Heat of Reaction using the Bomb Calorimeter. The self-assembled n-Al-APTMS/n-NiO-GPTMS have a Heat of Reaction of 3073 ± 7 J/g, and is lower than that of that of the physically mixed n-Al/n-NiO, which has a Heat of Reaction at 3649 ± 40 J/g. The lowered heat of reaction of the self-assembled n-Al-APTMS/n-NiO-GPTMS is likely due to the energy dilution brought about by the inert silane grafting. However, we also noted a smaller standard deviation of the measured heat of reaction for the self-assembled system, which indicate a system with better sample homogeneity.

4.4.5 Pressure Generation

The maximum pressure (Pmax), pressurization rate (dP/dt) and time to Pmax for the various samples were plotted as shown in Figure 4.25 (values tabulated in Table 4.4).

There is no significant difference in the maximum pressure among the different samples. In general, grafted samples may show slightly lowered weight normalized Pmax due to the 2-3 weight% of added organosilane. The highest pressurization rate is observed for the ungrafted n-Al/n-NiO nano-thermites at 0.58 kPsi/s. Organosilane-grafted n-Al/n-NiO that were physically mixed showed a 68 % reduction in its pressurization rate. This indicates that the addition of organosilane grafting on the nanoparticles could negatively impact its pressurization rate.

However, organosilane grafted n-Al/n-NiO that were self-assembled gave a very much higher pressurization rate (144 % increase) in comparison to the physically mixed grafted nanoparticles. This is a display of the mixture's improved reactivity from the self-assembly process. Between the two self-assembled samples, the one with reduced organosilane grafting on n-NiO showed an improvement in its pressurization rate. It indicates that the pressurization rate could be further improved with a better control of the grafting content.

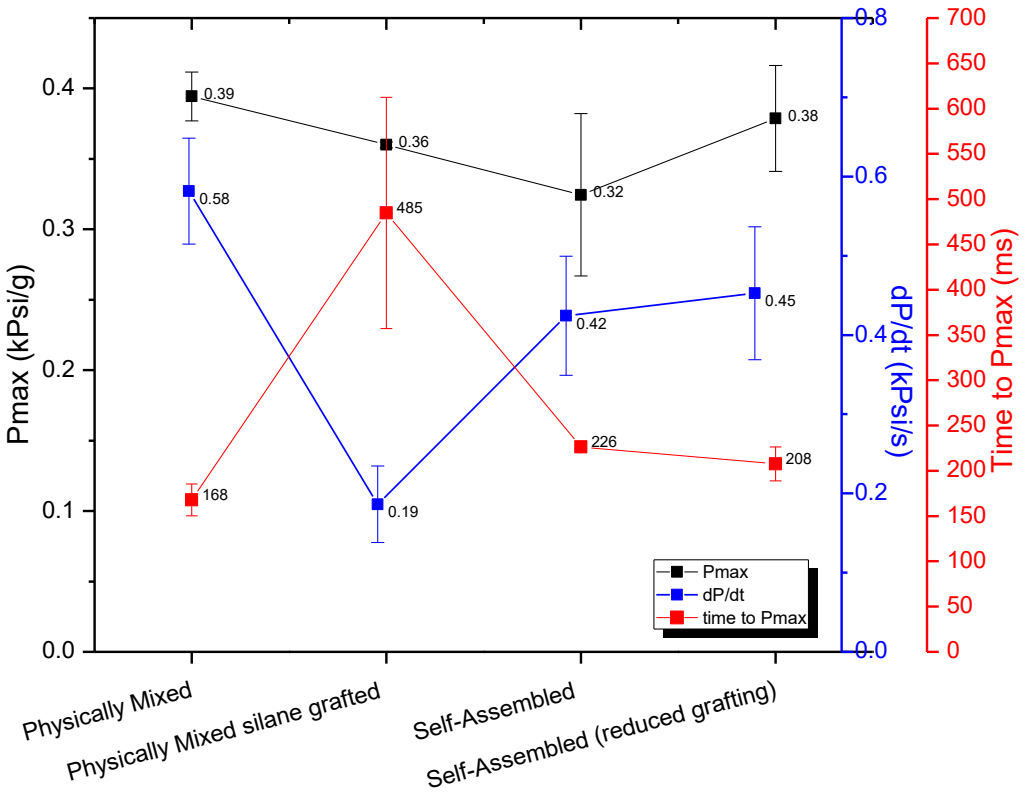

Figure 4.25: Plot on the maximum pressure (Pmax), pressurization rate (dP/dt) and time to reach maximum pressure (Time to Pmax) for n-Al/n-NiO prepared using various methods

Table 4.4: Summarized Dynamic Pressure Measurement data including maximum pressure (Pmax), pressurization rate (dP/dt) and time to reach maximum pressure (Time to Pmax) for n-Al/n-NiO prepared using various methods

Pressure Parameters	Physically mixed	Physically mixed silane grafted	Self-assembled	Self-assembled (Reduced grafting)
Pmax (kPsi/g)	0.394 ± 0.017	0.360 ± 0.002	0.324 ± 0.058	0.379 ± 0.038
dp/dt (kPsi/s)	0.581 ± 0.067	0.186 ± 0.048	0.424 ± 0.075	0.453 ± 0.084
Time to Pmax (ms)	168 ± 18	485 ± 128	226 ± 5	208 ± 19

4.4.6 Reaction Kinetics

In this study, the data from non-isothermal DSC experiments were analyzed to calculate kinetic parameters based on model-free techniques. The technique relates the peak temperature of the DSC curve to its heating rate and calculates the activation energy. Methods described by both Kissinger and Ozawa-Flynn-Wall were utilized. The kinetic parameters were obtained using equations described by these two methods in order to compare and cross-check the accuracy of our calculations. The activation energies for the thermal decomposition of both the physically mixed n-Al/n-NiO and self-assembled n-Al-APTMS/ n-NiO-GPTMS nano-thermites were investigated and compared to understand their reaction kinetics.

4.4.6.1 Model-Free Methods: Kissinger and Ozawa-Flynn-Wall

The reaction kinetics of physically mixed n-Al/n-NiO and self-assembled n-Al-APTMS/ n-NiO-GPTMS, both with ER 1.2, were studied. As the self-assembled sample with reduced grafting was shown to display better pressurization rate, it is adopted for the kinetic studies in this section. The prepared samples were heated at 5 different heating rates (β) (2, 3, 4, 5 and

8 °C/min). The peak temperatures of the main exotherm were recorded and used as inputs for the respective calculations. Activation energy (E_a) and pre-exponential factor (A) can be obtained from a plot of Ln β/T_m^2 versus $1/T_m$ for a series of experiments conducted at different heating rates using the method described by Kissinger. The same set of data was also subjected to the calculations described by Ozawa-Flynn-Wall for the estimation of E_a and A, in order to cross-check the calculations. The plots for calculation of E_a and A using Kissinger for the various n-Al/n-NiO nano-thermites are as shown in Figure 4.26a. The plots obtained using Ozawa-Flynn-Wall's technique is shown in Figure 4.26b. All the obtained results are summarized in Table 4.5.

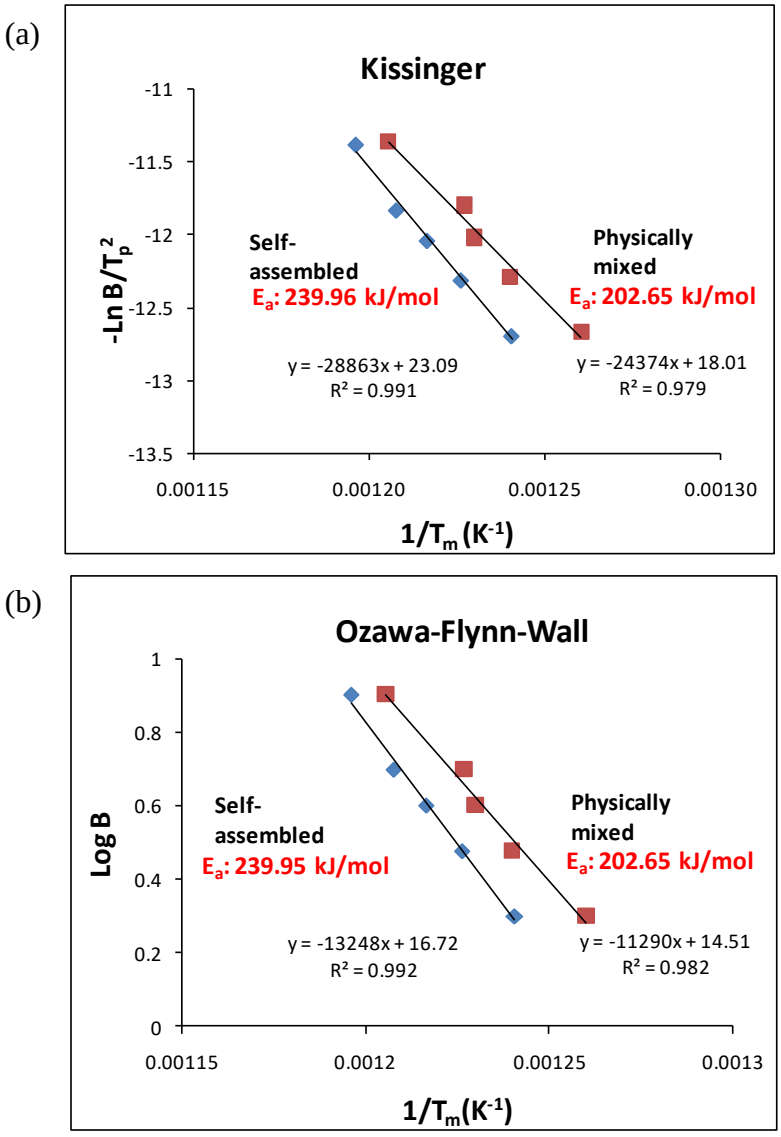

Figure 4.26: Best-fit linear plot for calculation of Ea for the various n-Al/n-NiO (self-assembled n-Al-APTMS/n-NiO-GPTMS with reduced grafting; physically mixed n-Al/n-NiO) using (a) Kissinger and (b) Ozawa-Flynn-Wall.

From the slope (= E_a/R) of the plots as shown in Figure 4.26, E_a of 203 kJ/mol and 240 kJ/mol were obtained for the physically mixed n-Al/n-NiO and self-assembled n-Al-APTMS/ n-NiO-GPTMS, respectively. The results were obtained using the peak temperature of the main exotherm, occurring before aluminum melting. The post-aluminum melting exotherms were always of a much smaller scale (if present) and is not further analyzed here. The main reaction exotherm is a result of the solid-state reaction between n-Al and n-NiO and is a diffusion controlled process. n-Al-APTMS/ n-NiO-GPTMS nano-thermites possess higher activation energy in comparison to the n-Al/n-NiO. We could conclude that the surface grafting of n-Al and n-NiO with the organosilanes resulted in a barrier to the interdiffusion of Al and O at the reaction interface. A similar increase on the activation energy of nano-thermites from n-Al surface grafting was also reported by Puszynski et al [5] , where n-Al were grafted with oleic acid which increased the E_a of Al/BiO_2 from 222 to 245 kJ/mol.

The accuracy of the calculated E_a of n-Al/n-NiO using Kissinger's method was confirmed via the use of a second method, i.e. Ozawa-Flynn-Wall, giving a very close estimation at less than 0.009 kJ/mol (0.004%) of variation. Our calculated activation energy is relatively close to reported values made by John Wen et al[12] and Udhayabanu et al [6] for n-Al/n-NiO. John Wen et al reported an estimated E_a value of 216.3 kJ/mol while Udhayabaru et al reported a value of 277 kJ/mol.

The calculations conducted above were using T_m, taking place at the peak of a reaction, and is on the basis that activation energy does not vary with conversion as the reaction progressed. However, the assumption that the activation energy remains constant with conversion for solid-state reactions is arguable as they are unlike homogeneous reactions (i.e. in liquid or gas reactions) which could only occur between freely moving reactants experiencing random collisions, making their reactivity unaffected by product formation. Isoconversional techniques, as reported in the next section, could estimate the changes in activation energies with conversion as the reaction progresses.

Table 4.5: Summary of activation energy and pre-exponential factor for both first and second exotherm using methods by Kissinger and Ozawa-Flynn-Wall

Reaction Exotherm	β(°C/min)	T_m (°C)	Kissinger		Ozawa-Flynn-Wall	
			E_a(kJ/mol)	A (s^{-1})	E_a(kJ/mol)	A (s^{-1})
n-Al/n-NiO	2	520.5	202.65	1.27×10^{12}	202.65	1.63×10^{12}
	3	533.5				
	4	540.0				
	5	542.0				
	8	556.5				
n-Al-APTMS/ n-NiO-GPTMS	2	533.0	239.96	1.35×10^{13}	239.95	3.08×10^{14}
	3	542.5				
	4	549.0				
	5	555.0				
	8	563.0				

4.4.6.2 Model-Free Isoconversional Method by Ozawa-Flynn-Wall

We plotted ln β versus 1/T at each conversion (α=0.10, 0.20, 0.30, 0.40, 0.50, 0.60, 0.70, 0.80, 0.90) for the various n-Al/n-NiO samples. The one performed for physically mixed n-Al/n-NiO is shown in Figure 4.27 (The ones performed for self-assembled n-Al-APTMS/n-NiO-GPTMS were not shown) The E_a s are obtained from the slopes of the lines, which equates to $0.457E_A/R$ (Refer to Equation (4.11b)). Table 4.6 shows the respective E_as calculated at each conversion for the various samples. The E_a versus conversion plots are shown in Figure 4.28.

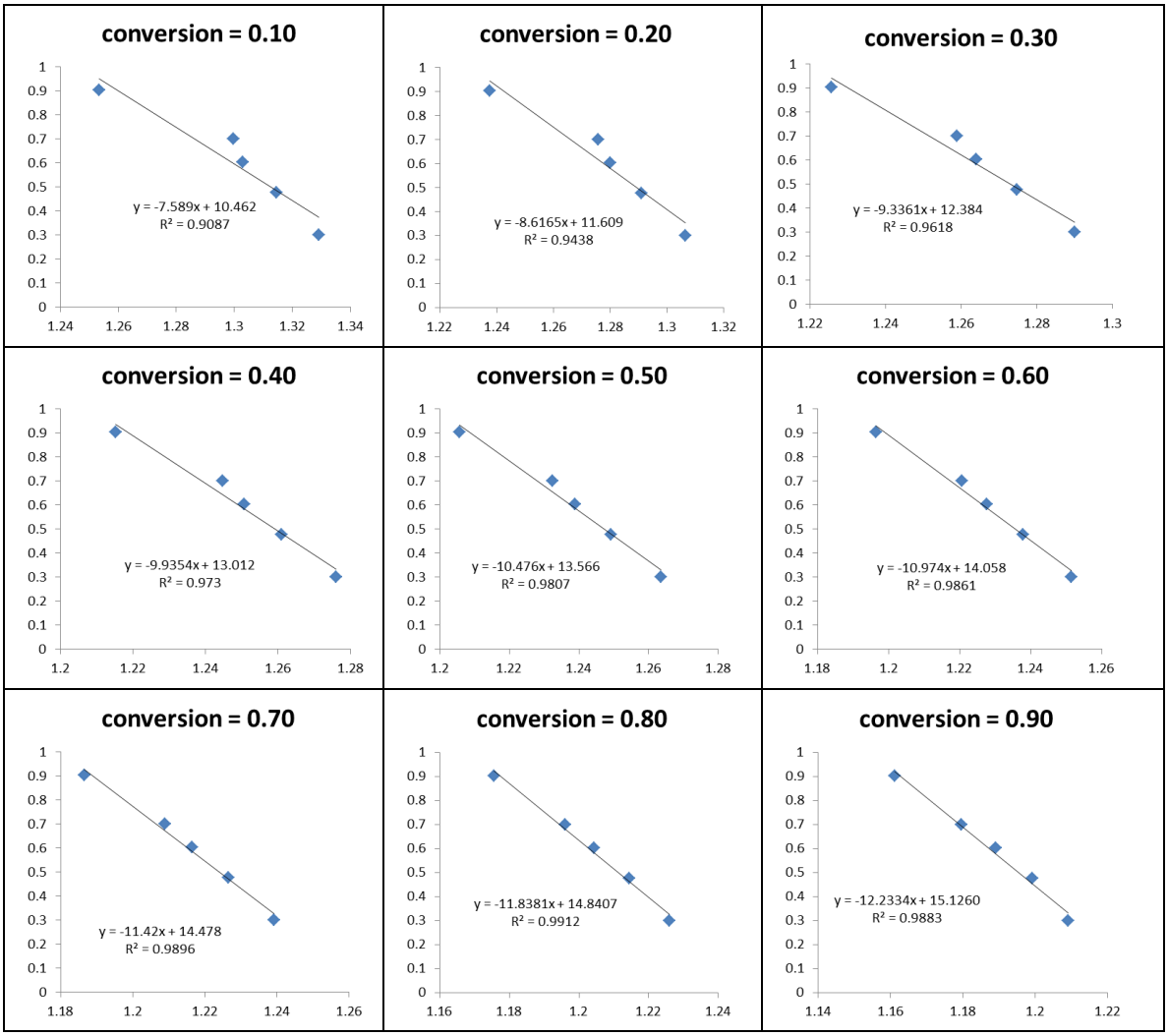

Figure 4.27: Plots to calculate activation energy at each conversion using the slopes obtained in each best-fit linear plot using Ozawa-Flynn-Walls mathematical expressions for the physically mixed n-Al/n-NiO.

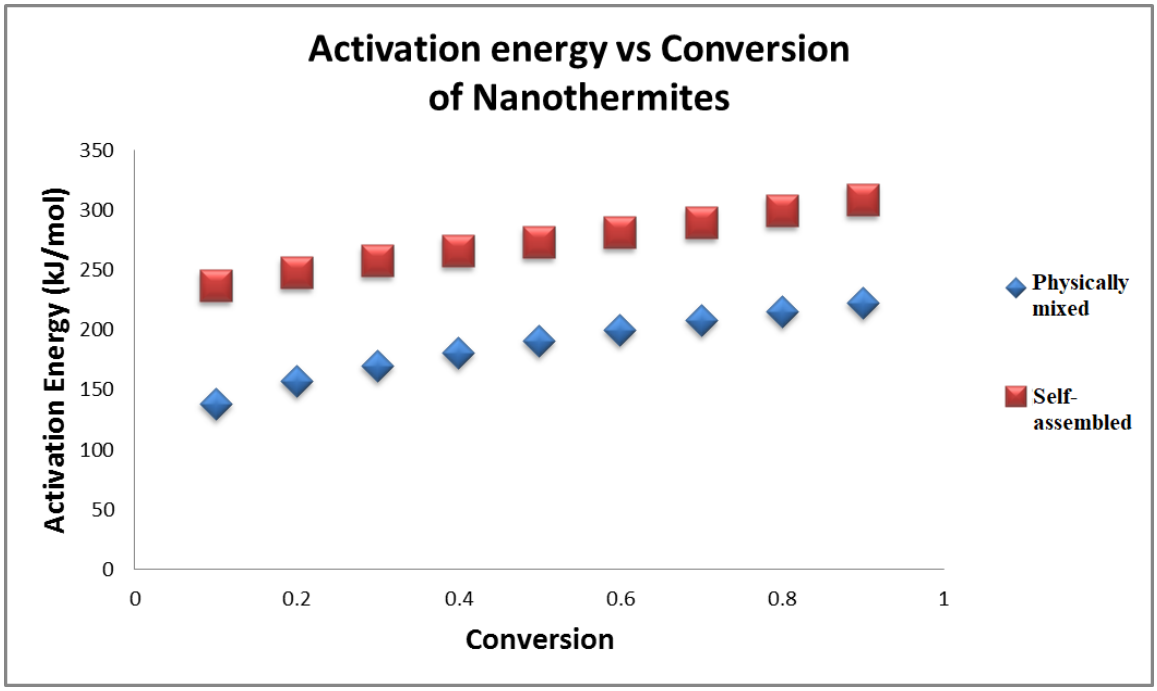

Figure 4.28: Plot showing activation energy versus conversion for physically mixed n-Al/n-NiO and self-assembled n-Al-APTMS/n-NiO-GPTMS using Ozawa-Flynn-Wall's method.

Table 4.6: Summary Table for calculated Activation Energy (E_a) for various conversions (α) of physically mixed n-Al/n-NiO and self-assembled n-Al-APTMS/n-NiO-GPTMS using Ozawa-Flynn-Wall's method.

α	Physically mixed (n-Al/n-NiO)	Self-assembled (n-Al-APTMS/n-NiO-GPTMS)
	E_a	E_a
0.1	138.07	235.58
0.2	156.76	247.12
0.3	169.85	256.27
0.4	180.76	264.45
0.5	190.60	272.36
0.6	199.64	280.07
0.7	207.76	288.54
0.8	215.37	298.08
0.9	222.57	307.23

The E_a showed a gradual increase from 138 kJ/mol to 223 kJ/mol as the reaction progressed for physically mixed n-Al/n-NiO. A similar dependency of Ea on conversion was observed for self-assembled n-Al-APTMS/ n-NiO-GPTMS. The increasing energy barrier for the reaction as more products were formed indicates the increasing barrier for inter-diffusion of Al and O to take place as more products are formed at the reaction interface. Al_2O_3 and Ni, which are solid products (500-600 ^oC) formed from the reaction hinders the diffusion of Al and O for further conversion of the remaining reactants to products. The dependence of Ea on conversion is not altered for organosilane grafted n-Al and n-NiO.

Our estimated activation energy of 203 kJ/mol for Al/NiO is also similar to published values for other nano-thermite systems. Puszynski et al[5] and Sun et al[7] reported activation energies of Al/Fe_2O_3, Al/Bi_2O_3 and Al/MoO_3 nano-thermites to be in the range of 205 to 260 kJ/mol. The activation energy of Al/O_2 (240 kJ/mol) reaction reported by Sun et al [7] also falls in a similar range. Results suggested similar rate-limiting step in all these reactions (i.e. Al/NiO, Al/MoO_3, Al/Fe_2O_3, Al/Bi_2O_3 and Al/O_2). The most probable rate-limiting step in a pre-aluminum melting Al oxidation reaction, either with another metal oxide oxidizer or gaseous oxygen, is the diffusion rate of O and Al inwards and outwards, respectively, through the alumina shell.

4.4.6.3 Conclusion of Reaction Kinetics Study

The estimated activation energy is a reflection of the thermal energy barrier required to be overcome before a reaction could take place. The activation energy was estimated using both non-isoconversional as well as isoconversional techniques. Both types of techniques have been adopted by various authors to study nano-thermites. Isoconversional techniques gave a realistic understanding on how the activation energy varies as the reaction progressed. The main energy-releasing reaction exotherm of n-Al/n-NiO took place before aluminum melting. We estimated the activation energy of n-Al/n-NiO to be 203 kJ/mol. Self-assembled n-Al/n-NiO nano-thermites that were prepared using n-Al and n-NiO that were surface-functionalized with organosilanes were also analyzed, and were shown to display increased activation energy at 240 kJ/mol. This

indicates that the surface functionalization did increase the energy barrier to the inter-reaction of Al and NiO, which is a solid-state reaction and a diffusion controlled process.

4.5 Addition of fluoropolymer to n-Al/n-NiO nano-thermite

Nano-thermites in its loose powder form could face some difficulty for practical usage. The inclusion of a polymeric binder can transform nano-thermites into 3-Dimensional composites giving it a structural form. However, the inclusion of an inert hydrocarbon polymeric binder, which often acts as a heat sink, can drastically decrease the ignitability as well as combustion rate of a reactive mixture. The decomposition of such organic species generates gaseous products and it is unknown how it may impact the pressure characteristics of a low-gas generating composition like Al/NiO nano-thermites. The aim of our studies is to characterize the pressure-generating properties of n-Al/n-NiO coated with THV221AZ fluoropolymer.

4.5.1 Thermal Analysis of Fluoropolymer THV221AZ

THV221AZ is a commercial fluorothermoplastic marketed by 3M (Dyneon®). It is a terpolymer consisting of tetrafluoroethylene (TFE), hexafluoropropylene (HFP) and vinylidene fluoroide (VDF) and has fluorine content in the range of 70.5 weight%. Specific gravity of THV221AZ is 1.93 g/ml. The terpolymer is a highly ductile material that can be deformed to more than 700 % in uniaxial tensile tests. The introduction of TFE units improves the overall crystalline nature of the polymer. Because of this, THV221AZ displays a low melting point at 115 ^{o}C and is commonly melt-processed in industrial applications.

The TG-DTA curve for THV221AZ is shown in Figure 4.29. The samples were heated at a rate of 5 ^{o}C/min to 500 ^{o}C in Nitrogen gas (50 ml/min flow rate). THV221AZ displayed an onset decomposition temperature of 403.9 ^{o}C. Complete decomposition into gaseous products was observed with a complete mass lost by 446.4 ^{o}C. In general, the decomposition of fluoropolymer generates fluoroalkenes, hydrogen fluoride, carbonyl fluoride and low molecular weight fluoropolymer particulates.

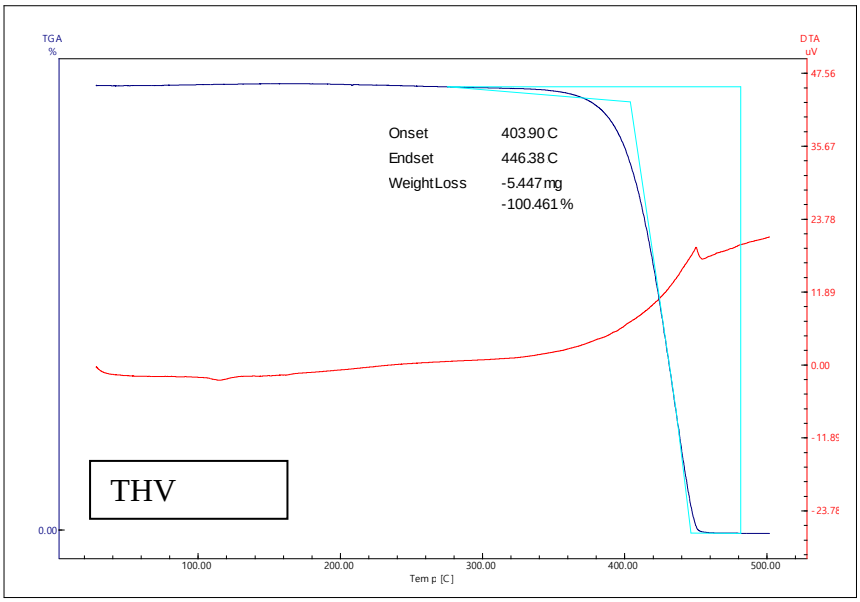

Figure 4.29: TG-DTA signal of THV heated at 10 °C/min in flowing N_2

4.5.2 Thermal and Pressure Characteristic of n-Al/n-NiO/THV

Al/NiO with optimized equivalence ratio of 1.2, yielding a calorimetric heat output of 3649 J/g was utilized throughout our study in varying percentage of THV (0 to 40 weight percent). The mixtures were subjected to a heating profile in a DSC and their respective thermal responses were analyzed. In an effort to understand the reaction mechanism of the nano-thermite reaction in the presence of the fluoropolymer, the reaction products were analyzed using powder XRD. The pressure-time analyses of these composites were studied using a dynamic pressure measurement system, by firing them inside a high strength Parr 1104B combustion vessel, containing 250 psi of argon.

The representative pressure-time profiles of Al/NiO nano-thermites (ER 1.2) with varying amount (0 – 40 wt%) of THV are shown in Figure 4.30. The dynamic pressure measurement for each sample was repeated 3 times using 0.25 ± 0.02 g of powder sample. Their weight normalized maximum pressure and average pressurization rate were plotted as shown in Figure 4.31. The average pressurization rate of each sample was taken from the 10^{th} to 90^{th} percentile of the maximum pressure value in each pressure-time profile.

The Al/NiO nano-thermite without any THV showed the highest pressurization rate but there is no linear relationship between the pressurization rate and amount of THV.

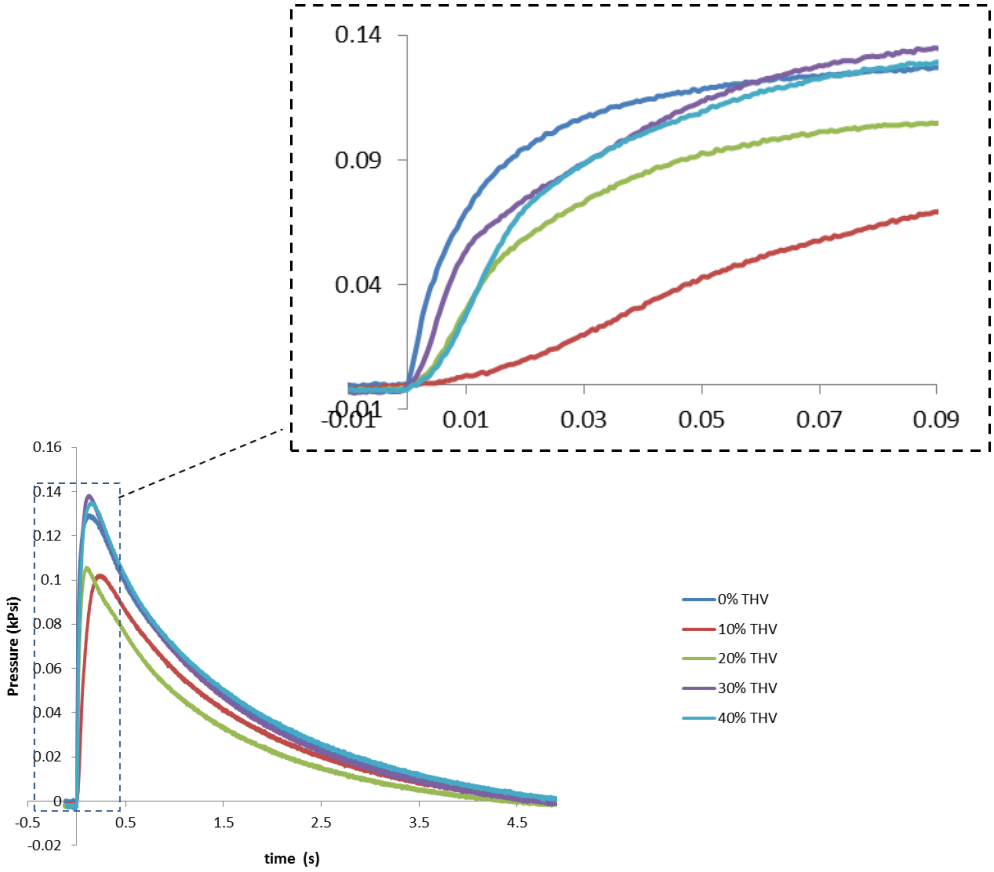

Figure 4.30: Pressure-time profiles of Al/NiO nano-thermites with varying amount (0 – 40 wt%) of THV.

Using Al/NiO nano-thermite as a control, compositions containing low THV content (10-20%) displayed a much reduced maximum pressure (-7.8 to -17.6% change) and pressurization rate (-22.6 to -66.4%). Composition containing 30 wt% THV content displayed a small increase in the maximum pressure (+9.8% change) with an almost similar pressurization rate (-0.4% change). Composition containing high THV content (40 wt %) showed an almost similar maximum pressure (-3.9% change) with a diminished pressurization rate (-40.2% change).

We conclude that the addition of organic fluoropolymer in the range of 10 to 40 wt% did not drastically increase the maximum pressure output of the n-Al/n-NiO system. A less than 10% increase in maximum pressure was observed for a 30 wt% THV addition to the

nano-thermite composition. Addition of either too little (≤ 20 wt%) or too much (≥ 40 wt%) THV could result in a decrease in both maximum pressure and pressurization rate. Although the organic species resulting from the decomposition of THV fluoropolymer is expected to increase the maximum pressure output of a n-Al/n-NiO system, it is not generally observed in our results. We believed that a lowered adiabatic combustion temperature from the addition of a fluoropolymer to the nano-thermite system has brought down the overall pressure produced from the system. The resulting reaction rates, as deduced from their pressurization rates, of all n-Al/n-NiO containing THV were also reduced.

(a)

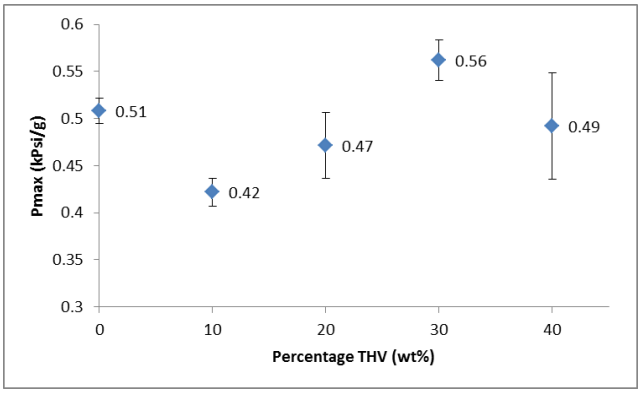

(b)

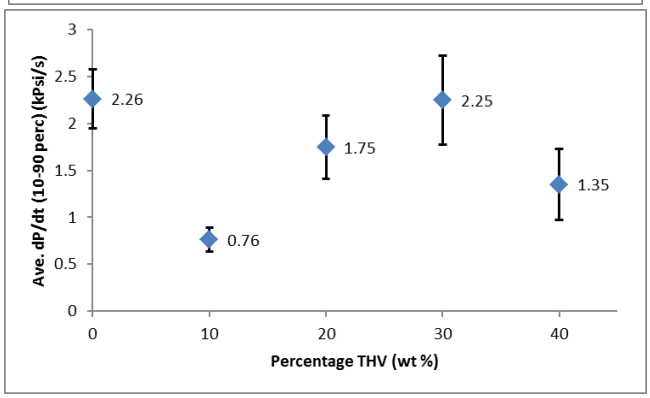

Figure 4.31: (a) Weight normalized maximum pressure and (b) average pressurization rate (10^{th}-90^{th} percentile) with varying amount (0 – 40 wt%) of THV.

Thermochemical calculations were performed using EXPLO5 program to predict the adiabatic combustion temperature as well as the amount of gaseous products from the reaction of Al/NiO/THV in varying compositions. The calculations were performed using isochoric combustion. The results are plotted against the amount of THV as shown in Figure 4.32 (Refer to Appendix A for full calculation data). The adiabatic combustion temperature was predicted to decrease with increasing amount of THV (Figure 4.32 a).

The amount of gaseous products was predicted to increase with increasing amount of THV from 0 to 40 wt% and decreased with further increase to 50 wt% of THV. This trend suggests that the amount of gaseous products do not increase indefinitely with increasing amount of organic binder. Amount of gaseous products start to decrease when too much THV is present due to the continuous lowering of combustion temperature with increasing amount of THV.

(a)

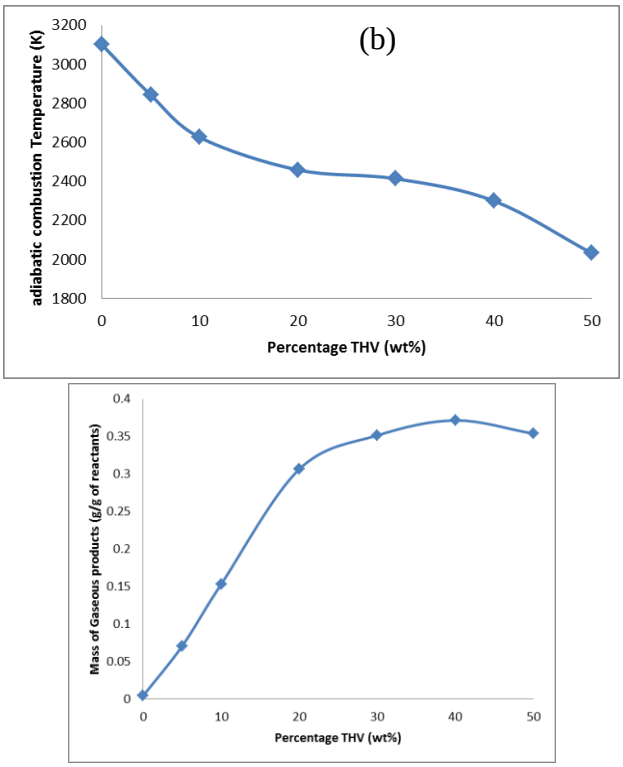

Figure 4.32: (a) Adiabatic combustion temperature and (b) mass of gaseous products of Al/NiO with varying weight percentage of THV using thermochemical calculations performed using EXPLO5 program.

A change in the species and proportion of the gaseous products from combusting the varying Al/NiO/THV compositions was observed (Table 4.7). From the calculations, we observed that the main gaseous products from combusting Al/NiO comes from Ni, Al and Al_2O all of which occurs in small molar percentage of 0.1 to 0.4 mol%. This accounted for its theoretically low pressure generation characteristic. All the THV containing compositions had CO, H_2, AlF_2O, AlF_3, HF and varying hydrocarbon species (i.e. CH_4, C_2H_4, C_2H_6) as the main gaseous products. We also noted that only Al/NiO compositions containing less amount of THV (10-30 wt%) still contain gaseous Ni, Al

and Al_2O, while none of these are found in high THV content (50 wt%) composition. Gaseous Al and Al_2O are also not found in Al/NiO with 40 wt% THV. The lowered combustion temperature in compositions with higher THV content is responsible for this phenomenon.

While our observed trend in the pressure studies was not fully replicated in the prediction using EXPLO5, the calculations gave us an insight to the plausible contributing factors of its actual pressure performance.

Table 4.7: Predicted gaseous product species from isochoric combustion of Al/NiO having 0 to 50 wt% THV. Calculations performed using EXPLO5.

Composition	Main gaseous products	Sub gaseous products (< 0.1 mol%)
Al/NiO	Al_2O, Ni, Al	AlO, Al_2, Al_2O_2
Al/NiO + 10% THV	CO, H_2, AlF_2O, AlF_3, HF	C_2H_4, H, H_2O, CO_2, Ni, Al_2O, AlOH, Al, AlH, CH_4
Al/NiO + 20% THV	CO, H_2, AlF_2O, AlF_3, HF, CH_4	C_2H_4, H, H_2O, CO_2, Ni, Al_2O, AlOH, Al, AlH, C_2H_6
Al/NiO + 30% THV	CO, H_2, AlF_2O, AlF_3, HF, CH_4	C_2H_4, H, H_2O, CO_2, Ni, Al_2O, AlOH, Al, AlH, C_2H_6
Al/NiO + 40% THV	CO, H_2, AlF_2O, AlF_3, HF, CH_4	C_2H_4, H, H_2O, CO_2, Ni, AlOH, C_2H_6
Al/NiO + 50% THV	CO, H_2, AlF_2O, AlF_3, HF, CH_4, C_2H_4	H, H_2O, CO_2, C_2H_6

The samples were also studied under a very different condition using a DSC to observe their heat flow profiles. Samples were heated under flowing Argon (50 ml/min) at a slow heating rate of 5 ^oC/min and their heat flow against temperature profiles were plotted as shown in Figure 4.33. XRD compositional analyses were done on the reaction products collected from both the dynamic pressure studies and DSC (Figure 4.34, Figure 4.35 and Table 4.8).

A delayed reaction exotherm was observed for the Al/NiO reaction at around 600 ^oC for samples containing THV, where the original reaction exotherm occurred at 539 ^oC for pure n-Al/n-NiO sample. The heat of reaction of this Al/NiO reaction exotherm was heavily diminished in the sample containing high amount of THV (40 wt%). All samples containing THV showed a mild exotherm at around 420 ^oC due to the decomposition of THV. Samples containing higher amount of THV (30 and 40 wt%) showed an additional

reaction exotherm at around 500 °C. This is attributed to the reaction of NiO with F contained in the THV, as evident from the detection of NiF_3 in their reaction products (Figure 4.34b and Table 4.8). This reaction is not encouraged in a scenario with too little THV (10 and 20 wt%) and thus explaining the absent of reaction exotherm at 500 °C and Ni F_3 in their reaction products.

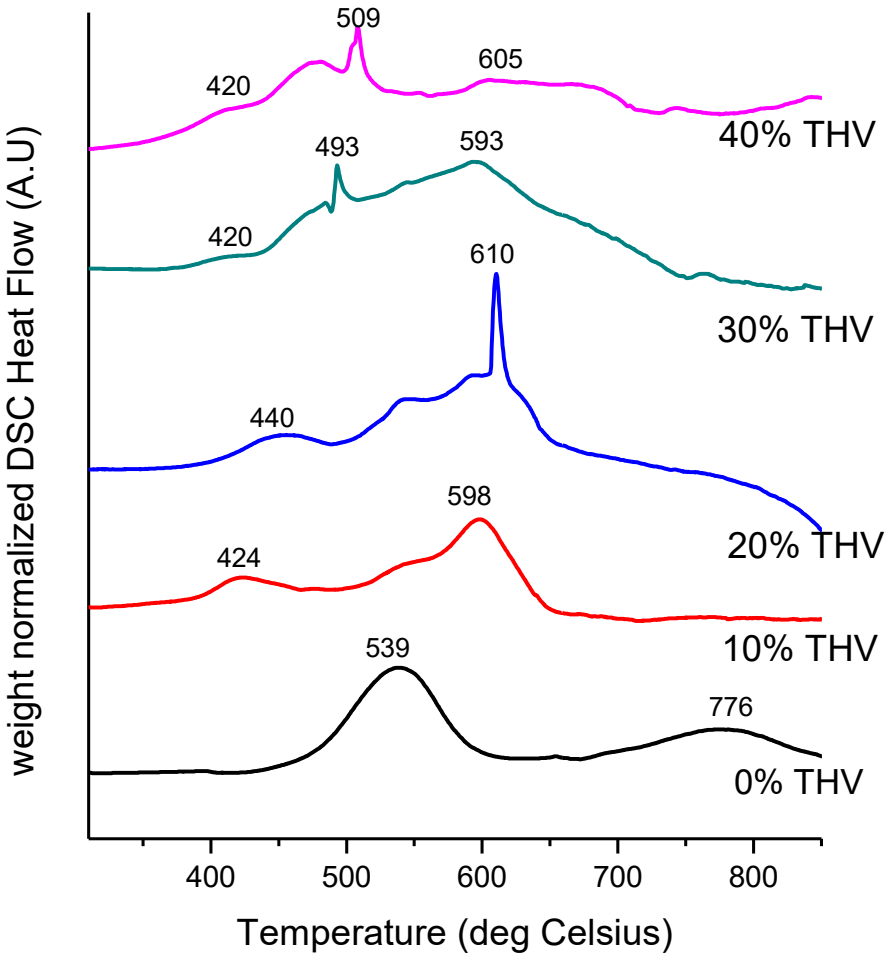

Figure 4.33: Weight normalized Heat Flow against temperature of n-Al/n-NiO with varying amount of THV (0-40 wt%) measured at 5 °C/min in argon using a DSC

We observed that the reaction products obtained from each sample differs when they were reacted under the different conditions set in an enclosed high-pressure constant volume vessel and within a DSC. The samples were instantaneously ignited using a nichrome wire (Nichrome melting point 1400 °C) within an enclosed argon environment under high pressure (250 psi) when they are reacted in a high-pressure vessel. On the

other hand, the samples were heated very slowly at 5 ^{o}C/min in a continuous flow of argon gas within a DSC. The gaseous decomposition products of THV (decomposition onset temperature is 404 ^{o}C) may not completely react with the other solid reactants such as NiO and Al. Thus, AlF_3 if not detected in the products of all DSC samples while NiF_3 is only detected for samples with higher THV content.

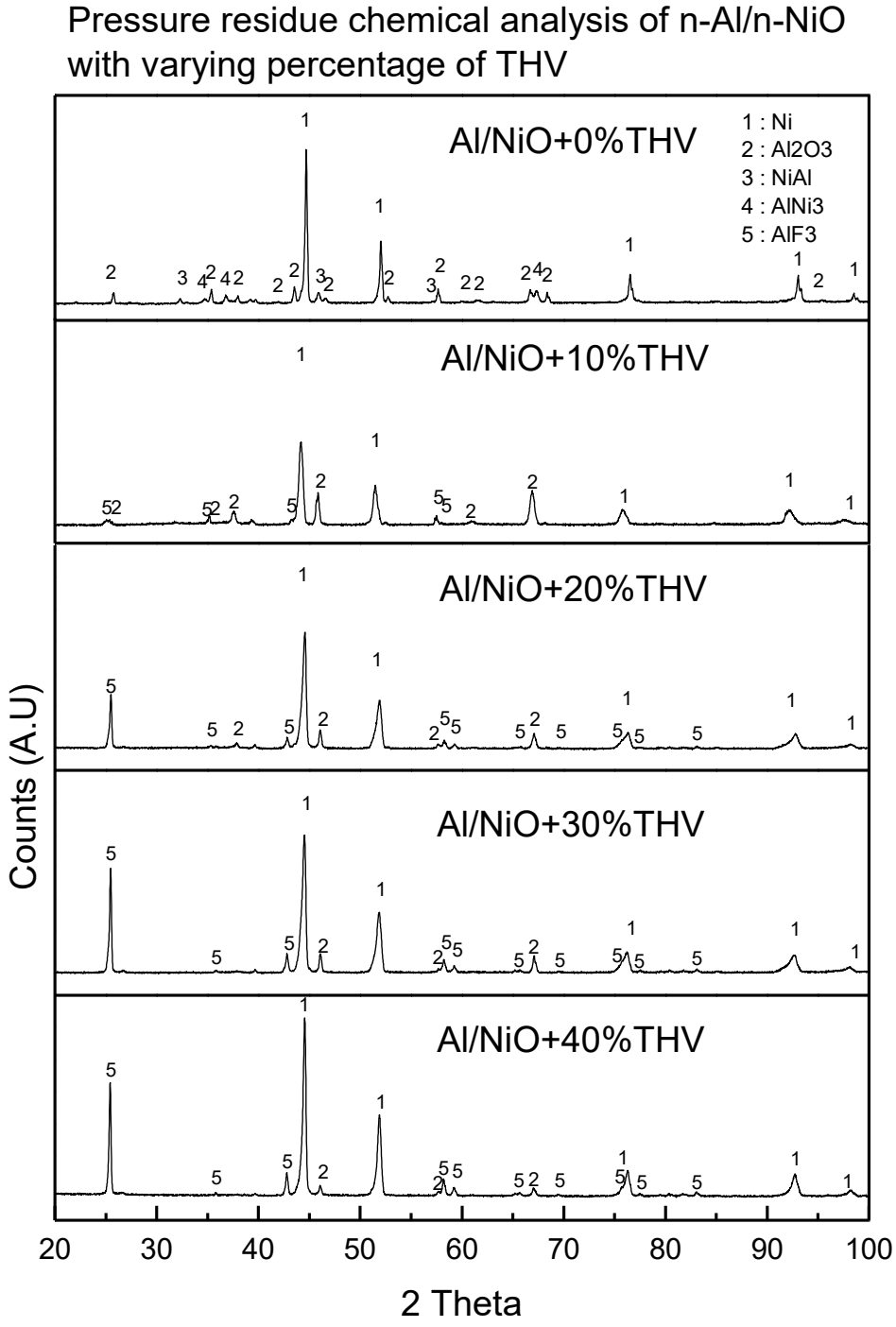

Figure 4.34: XRD spectra of reaction products from Al/NiO with varying amount of THV (0 to 40 wt% THV) reacted within an enclosed constant volume high pressure vessel with 250 psi Argon.

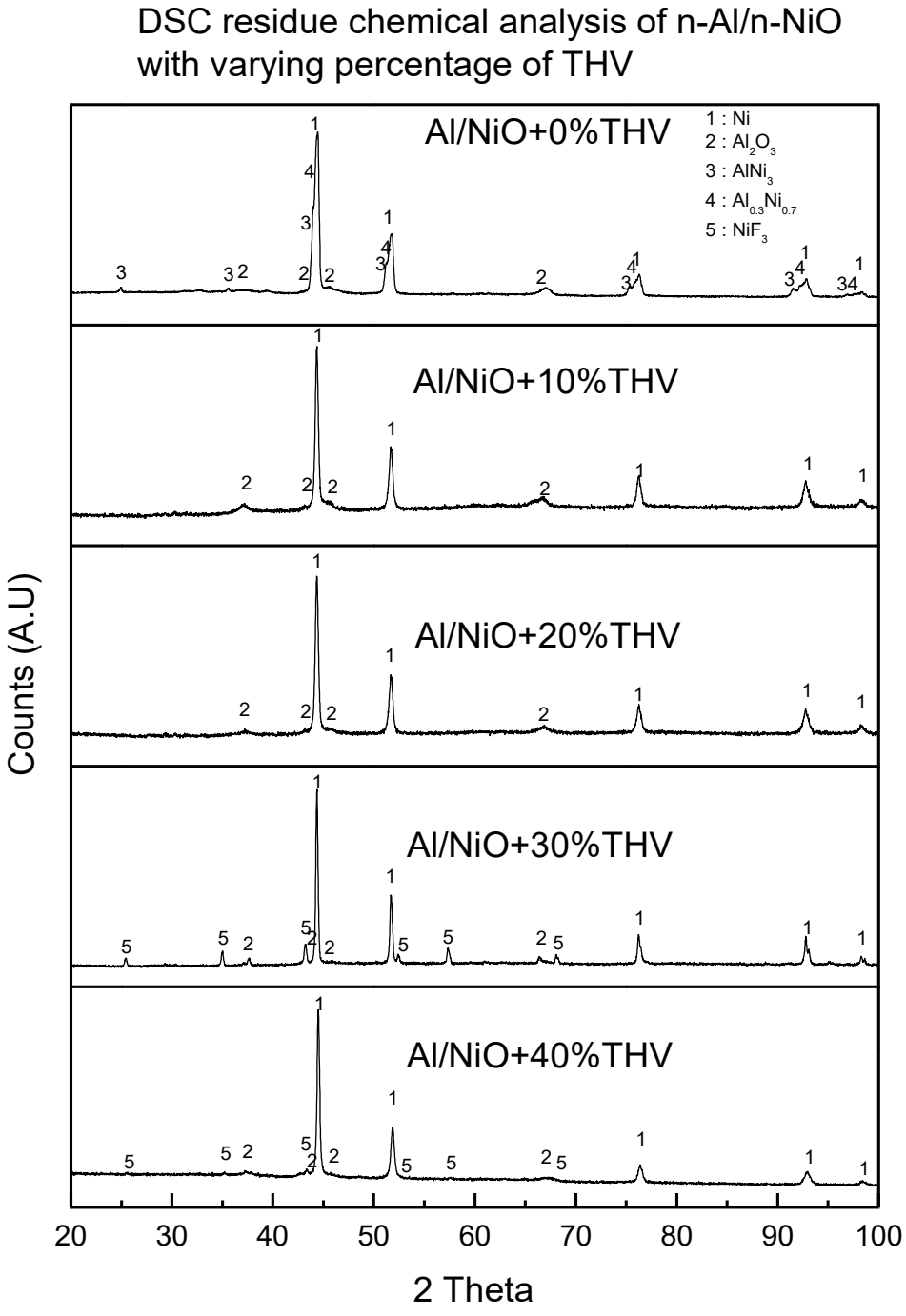

Figure 4.35: XRD spectra of reaction products from Al/NiO with varying amount of THV (0 to 40 wt% THV) reacted at slow heating rate of 5 ^{o}C/min under flowing Argon in a DSC.

Table 4.8: XRD composition analysis of reaction products collected from reaction of n-Al/n-NiO with varying percentage of THV (0 to 40 wt%), conducted (a) in an enclosed constant volume high pressure vessel (250 psi argon) and (b) in a DSC pan undergoing slow heating rate of 5 ^{o}C/min with 50 ml/min of flowing Argon.

% THV	0	10	20	30	40
(a) XRD composition of product (reaction in Enclosed Pressure Vessel)	Ni Al_2O_3 $NiAl_3$ NiAl	Ni Al_2O_3 AlF_3	Ni Al_2O_3 AlF_3	Ni Al_2O_3 AlF_3	Ni Al_2O_3 AlF_3
(b) XRD composition of product (reaction in DSC	Ni Al2O3 $Ni_{0.879}Al_{0.121}$ Ni_3Al	Ni Al_2O_3	Ni Al_2O_3	Ni Al_2O_3 NiF_3	Ni Al_2O_3 NiF_3

4.6 Sensitivity to Stimuli Studies

Nano-thermites are inherently sensitive to ignition via ESD and friction. Safety evaluation through sensitivity measurement of Al/NiO nano-thermite with respect to friction, impact and ESD was carried out to understand their risk of accidental ignition by these external stimuli. It is not well understood if surface functionalization and self-assembly would change the materials' sensitivity to these stimuli. This study serves to evaluate the sensitivity of the surface-functionalized nano-thermites to these external stimuli and also help us understand if surface functionalization and polymer coating can be an alternative technique to improve the safety in handling of these materials.

n-Al/n-NiO nano-thermites were shown to be very sensitive to friction (< 54 N), sensitive to ESD (MIE < 0.086 mJ) and insensitive to impact (Table 4.9). According to the United Nations (UN) guidelines for the transport of dangerous or hazardous goods, a material that is having friction sensitivity of 10-80 N is classified as very sensitive, a ESD

sensitivity of < 100 mJ is classed as sensitive, while an impact sensitivity if > 40 J is classed as insensitive [8]. A human body can discharge up to 8.33 mJ [9], making the safe handling of nano-thermites very challenging.

Table 4.9: Sensitivity to Friction, Impact and ESD of physically mixed n-Al/n-NiO, self-assembled n-Al-APTMS/n-NiO-GPTMS and n-Al/n-NiO with 30wt% THV fluoropolymer

Sensitivity Data			
Samples	**Friction**	**Impact**	**ESD**
n-Al/ n-NiO physically mixed (ER1.2)	< 54 N	> 50 J	MIE: < 0.086 mJ
n-Al-APTMS/ n-NiO-GPTMS self-assembled (ER1.2)	< 30 N	> 50 J	MIE: 23.81 mJ
n-Al/ n-NiO physically mixed (ER1.2) + THV (70:30)	> 360N	< 50 J	MIE: 5.82 mJ

Values in red: actual value is below measurable limit of machine
Values in green: actual value is above measurable limit of machine

The results suggest that sensitivity to electrostatic discharge is affected by the surface grafting and physical coatings of the nano-thermites. The surface grafting with organosilanes as well as polymer coating could effectively reduce the high ESD sensitivity of these n-Al/n-NiO nano-thermite materials. The electrostatic minimum ignition energy (MIE) was observed to increase by at least 277 times in organosilane-grafted n-Al/n-NiO while a 68 times increase was observed for 30wt% THV polymer coated n-Al/n-NiO. The organosilane grafting introduced on the n-Al-APTMS/n-NiO-GPTMS has a much increased ESD MIE of 23.81 mJ, which is much higher than what the human body is capable of discharging (up to 8.33 mJ). This is a very good improvement in the normal safe handling of n-Al/n-NiO nano-thermites.

The 30 wt% THV polymer coating could effectively render the friction-sensitive n-Al/n-NiO completely insensitive to friction as displayed in the tremendous increase in friction sensitivity from < 54N to > 360N. However, the organosilanes-grafted self-assembled n-Al/n-NiO displayed higher sensitivity to friction. The increased friction sensitivity was attributed to the increased homogeneity of mixing in the self-assembled binary system.

All the n-Al/n-NiO measured were insensitive to impact, which is in line with what is commonly observed for nano-thermites, No significant change in impact sensitivity of n-Al/n-NiO from surface functionalization and coating was observed.

The sensitivity data of n-Al/n-CuO and their similar addition of organosilane modifiers and THV fluoropolymer can be found in Appendix B. In comparison to n-Al/n-CuO, n-Al/n-NiO had significantly lower sensitivity to Friction and Impact and are consequently safer to handle. Similar improvement in the ESD sensitivity from surface functionalization and fluoropolymer addition were also observed in the n-Al/n-CuO system. Improvement in Friction sensitivity was also observed for n-Al/n-CuO with THV fluoropolymer.

References

1. Dreizin, E. L., Metal-based reactive nanomaterials. *Progress in Energy and Combustion Science* **2009,** *35* (2), 141-167.
2. Fischer, S. H.; Grubelich, M. *Theoretical energy release of thermites, intermetallics, and combustible metals*; Sandia National Labs., Albuquerque, NM (US): 1998.
3. Zhang, Y.; Jiang, H.; Zhao, X.; Yan, Y.; Zhang, W.; Li, Y., Characteristics of the Energetic Micro-initiator Through Integrating Al/Ni Nano-multilayers with Cu Film Bridge. *Nanoscale Research Letters* **2017,** *12* (1), 38.
4. Pettit, F. S.; Randklev, E. H.; Felten, E. J., Formation of NiAl2O4 by Solid State Reaction. *Journal of the American Ceramic Society* **1966,** *49* (4), 199-203.
5. Puszynski, J. A.; Bulian, C. J.; Swiatkiewicz, J. J., Processing and Ignition Characteristics of Aluminum-Bismuth Trioxide Nanothermite System. *Journal of Propulsion and Power* **2007,** *23* (4), 698-706.
6. Udhayabanu, V.; Singh, N.; Murty, B. S., Mechanical activation of aluminothermic reduction of NiO by high energy ball milling. *Journal of Alloys and Compounds* **2010,** *497* (1), 142-146.
7. Sun, J.; Pantoya, M. L.; Simon, S. L., Dependence of size and size distribution on reactivity of aluminum nanoparticles in reactions with oxygen and MoO3. *Thermochimica Acta* **2006,** *444* (2), 117-127.
8. Klapötke, T. M., *Chemistry of high-energy materials*. Walter de Gruyter GmbH & Co KG: 2017.
9. Greason, W. D., Electrostatic discharge characteristics for the human body and circuit packs. *Journal of Electrostatics* **2003,** *59* (3), 285-300.

Chapter 5

Conclusion, Impact and Recommendation

Conclusions are discussed on the work performed in this report. The effect of surface functionalization, self-assembly as well as fluoropolymer addition on the materials pressurization rate as well as sensitivity are discussed. The implications and impact on the current thermite research are elaborated. This work has explored the less discussed n-Al/n-NiO system found in the literature and characterized their pressure generation, energy and sensitivity to unwanted stimuli. The surface functionalization and fluoropolymer introduced could successfully reduce the sensitivity of such hazardous material. The reaction rate of n-Al/n-NiO could also be preserved when the right amount of fluoropolymer is introduced into the system. Recommended future work is also discussed in this section. It contains two main suggested areas of work for future research in this material. The first involves surface functionalization and self-assembly of Al and NiO nanoparticles with energetic linkers and studying their effect on energy release rate. The second area focused on studying n-Al/n-NiO in actual applications where high-heat producing and low gas-generating compositions are desired. Potential applications range from primer composition in detonators to door breaching or metal cutting.

5.1 Conclusion

Self-assembled n-Al/n-NiO via grafting of the nanoparticles with organosilanes having complementary functional end groups were prepared. The self-assembled nano-thermites were proven to show better homogeneity in their intermixing, apparent from the elemental mapping in their SEM imaging. It display complete redox reaction at the nanoscale level, taking place before aluminum melting, as observed from its DSC profile. This is not the case for physically mixed nano-thermites where reaction exotherms, both before and after aluminum melting, were observed. Heat release rate appeared to be higher as observed from the sharper exotherm in the DSC profile of the self-assembled n-Al/n-NiO.

In terms of pressure generation characteristics, the normalized peak pressure was indifferent for n-Al/n-NiO nano-thermites regardless of grafting or mixing homogeneity. Self-assembled n-Al-APTMS/ n-NiO-GPTMS showed faster pressure generation rate in comparison to a physically mixed n-Al-APTMS/ n-NiO-GPTMS. Pressure generation rate is a direct reflection of the materials reaction rate. Thus, a higher reactivity from the self-assembly process can be concluded. However, it should be noted that the inclusion of organosilane grafting still impedes the reaction rate of the nano-thermites as n-Al/ n-NiO had an overall better pressurization rate in comparison to n-Al-APTMS/n-NiO-GPTMS. The organosilane grafting were also proven to increase the activation energy barrier of the nano-thermite, from the calculations made by both Kissinger and Ozawa-Flynn-Wall techniques.

The activation energy barriers of n-Al/n-NiO and grafted n-Al-APTMS/n-NiO-GPTMS were estimated to be 203 and 240 kJ/mol, respectively, using the model-free technique described by Kissinger. An increase in activation energy barrier in organosilane-grafted n-Al and n-NiO was indicated. We conclude that while the organosilane grafting could improve the intermixing of the reactants, the additional diffusion barrier imposed from the surface grafting on these nanoparticles could not effectively increase the reaction rates of n-Al and n-NiO.

THV, a fluoropolymer, was added to n-Al/n-NiO to produce a composite powder. The polymer could act as a binder and is required if a 3-Dimensional matrix of n-Al/n-NiO is

desired. The composite powder has the potential to be compressed into pellets to create 3-Dimensional structures. The pressure generation characteristics of n-Al/n-NiO/THV were evaluated. It was observed that the pressurization rate could be preserved only when the right amount of THV is introduced. In the studies conducted, 30 wt% of THV with n-Al/n-NiO of ER 1.2 gave the optimized result. It should be noted that other amount of THV could provide optimized results when a different ER of n-Al/n-NiO was used. This is a result of the active reaction of Al with F when they were ignited in an enclosed isochoric vessel. It did not significantly alter the maximum pressure produced by n-Al/n-NiO, thus preserving the low gas generation characteristic of Al/NiO reactions.

It was also observed that F could either react with Al or NiO, depending on the reaction conditions. Reaction conditions refer to the rate of thermal ignition, reaction environment and whether the reaction was conducted in an enclosed environment or a dynamic environment.

The addition of THV to n-Al/n-NiO could successfully reduce both the ESD and friction sensitivity of this nano-thermite. It rendered the material completely insensitive to friction and while it is still considered sensitive to ESD, the minimum ignition energy has increased tremendously by at least 68 times.

5.2 Implication and Impact

Nano-thermites had been heavily researched on in the past few decades. While they are many available combinations of Al with different metal oxides, not all of them have been explored extensively. The ones that received most attention were mostly highly gaseous system with fast combustion rates, which had potential applications as actuators or igniters. There were not many research data available on n-Al/n-NiO nano-thermite system. While the system is theoretically low in gas production, there were no pressure characterizations performed on this system. Neither can sensitivity data be found on this particular nano-thermite system. The lack of sensitivity data made it difficult to understand the safety in handling this material.

The work produced in this report serves to develop an understanding of the sensitivity and hence the associated safety in handling such hazardous material. The effect on

sensitivity to ESD, friction and impact by introducing surface modifiers and fluoropolymer to the nano-thermite system were also evaluated. Surface grafting and introduction of fluoropolymer were both effective in reducing the high sensitivity of such materials to ESD and friction, thus making them safer for handling.

While there were other similar research on the addition of polymeric coating or binder to nano-thermite systems, they typically result in a large reduction in the reaction rates of nano-thermites. The use of inert binders could sometimes result in the loss of ignitability of such reactive materials. The overall reaction rate was nearly preserved when the right amount of THV fluoropolymer was included in the system. THV presents itself as a potential polymeric binder that could both reduce the high sensitivity of n-Al/n-NiO nano-thermite as well as preserving its reactivity and ignitability, if the optimized amount is added.

5.3 Recommendation for Future Work

5.3.1 Surface Functionalization and Self-Assembly using energetic linkers

In the work presented in this report, we demonstrated the effectiveness of self-assembly but fail to improve the overall reactivity due to the addition of dead weight introduced in the surface functionalization. An alternative technique for surface functionalization and self-assembly using energetic linkers could be attempted to overcome this problem. Triazole and tetrazole organic linkers can form via click chemistry 4 using either azide-alkyne or azide-nitrile cycloaddition, respectively. Triazoles and Tetrazoles are high-nitrogen compounds, which is a class of green energetic compounds that possess a high energetic density. However their high energy content is also accompanied with instability making them rather difficult to handle safely. It can be explored if such high energy materials can be used in very small quantity as a surface linker that could both link the fuel to the oxidizer by acting as a self-assembly driver as well as increase the energetic property of the system without impairing the sensitivity.

Using the affinity of either organosilanes or carboxylic acids to common metal oxide surfaces, these organic grafters with either azide, alkyne or nitrile functional ends can be

used to surface functionalize the nanoparticles with complimentary groups to bring about the nanoparticle self-assembly.

5.3.2 Research for Actual Application

n-Al/n-NiO is a thermite composition with inherently low gas production. Current research platform on thermites placed too much focus on thermite system with high heat and gas generating compositions including n-Al/n-CuO, n-Al/n-Fe2O3, n-Al/n-MoO3 and n-Al/n-Bi2O3. While heat and gas had been common performance factors for many pyrotechnic and propellant compositions, gas generation may not be a desirable property in some applications. In applications within confined spaces, too much gas generated can be detrimental to the original structure in place.

One possible application of n-Al/n-NiO thermite is its use as a primer composition within a detonator. A detonator typically contains an ignition source, followed by a pyrotechnic primer composition, a primary explosive and finally an output secondary explosive. Such primer composition should produce sufficient heat to initiate the primary explosive but not produce too much gas, which could destroy the encapsulation before DDT (Deflagration to Detonation Transition) is achieved by the secondary explosive.

The use of nano-thermites as pyrotechnic composition can potentially replace the use of primary explosives (either fully or partially) such as lead azide and lead styphanate, which are both toxic due to their lead content and very dangerous to handle due to their high sensitivity[1]. Nano-thermite (n-Al/n-CuO) had been used in conjunction with secondary explosive in miniature devices for the initiation of High Explosives, eliminating the use of primary explosives completely. [2].

The large amount of heat and little amount of gas also makes n-Al/n-NiO potentially useful in metal cutting or door breaching applications. Kim et al had adopted n-Al/n-CuO, which were placed on miniaturized chip igniters to produce large amount of heat, capable of breaching doors [3]. n-Al/n-NiO would potentially be a better candidate as the amount of gas produced is significantly less, rendering the door breaching process much safer.

Research work can be conducted on n-Al/n-NiO compositions to realize their practical usage as a primer composition within detonators, as potential replacement of lead containing primary explosive, as well as safer metal cutting or door breaching process.

5.4 Reflection on the Hypothesis

At the beginning of this work, a hypothesis was made. It was hypothesized that by introducing complimentary functional groups on both the fuel and oxidizer particles, such surface modification can lead to better intermixing and the increased area of contact between them in a nano-thermite system can improve their energy release rate. The incorporation of energetic polymer was hypothesized to reduce their sensitivity to external stimuli and improve the safety of handling these materials while potentially preserving the reaction rate of n-Al/ n-NiO.

The use of organosilane surface functionalization, to improve the mixing homogeneity, in hope of improving the reaction rate of n-Al/n-NiO was not completely successful. While the improved mixing brought about by the introduction of organosilane surface modifiers proved to be successful, the inert nature of the organosilane and the additional barrier created at the reaction interface between Al and NiO increased the activation energy barrier for the Al-NiO reaction. An overall improvement in reaction rate was not achieved from the surface functionalization and self-assembly. The improved reaction rate from better homogeneity was accompanied with a reduction caused by the additional diffusion barrier created at the reaction interface. However, as a side note, the organosilane surface grafting was able to reduce the high ESD sensitivity of n-Al/n-NiO by increasing the minimum ignition energy above 8.33 mJ, which is the maximum value that a human body is capable of discharging. This is a significant improvement in the safety of handling this material.

Fluoropolymer (THV) addition could successfully reduce both the ESD and friction sensitivity of n-Al/n-NiO. It rendered the material completely insensitive to friction. The pressurization rate, which was used as a reflection of the material's reaction rate, was preserved only when the right amount of THV is introduced into the nano-thermite system. 30 wt% of THV with n-Al/n-NiO of ER 1.2 gave the optimized result in the

studies conducted. It was observed that unlike other inert polymeric binder, the active involvement of F (from THV) in the reaction with Al made it an active participant in the inter-reaction with Al and NiO. Thus, the composition could be tuned to produce optimized reaction rate.

References

1. Ilyushin, M. A.; Tselinsky, I. V.; Shugalei, I. V., Environmentally Friendly Energetic Materials for Initiation Devices. *Central European Journal of Energetic Materials* **2012,** *9* (4), 293-327.
2. Ludovic, G.; Andrea, N.; Fabien, J.; Bernard, M.; Jeremy, B.; Laurent, R.; Carole, R., Nanothermite/RDX-Based Miniature Device for Impact Ignition of High Explosives. *Propellants, Explosives, Pyrotechnics* **2017,** *42* (3), 308-317.
3. Kim, K. J.; Jung, H.; Kim, J. H.; Jang, N. S.; Kim, J. M.; Kim, S. H., Nanoenergetic material-on-multiwalled carbon nanotubes paper chip as compact and flexible igniter. *Carbon* **2017,** *114*, 217-223.

Appendix A

```
                          alniothv-er1.2-90to10-virial.txt
                                                EXPLO5_V6.04
                                                27-Feb-18
                                                2:43:28 PM
                                                ==========


RESULTS OF THERMOCHEMICAL CALCULATION:
--------------------------------------

  Job title : Al/NiO (ER 1.2) +10%THV
  Comment   :

Combustion condition:
---------------------
     Isochoric combustion (V=const.)
     Loading density   = 0.200  g/cm3
     EOS :  Virial


Reactant information:
-----------------------
     1.  Aluminium (Al),  18.409   %
     2.  Aluminium oxide (Al2O3),  7.889   %
     3.  Nickel (II) oxide (NiO),  63.702   %
     4.  Polytetrafluoroethylene (PTFE),  3.538   %
     5.  Hexfluoropropene-Vinylidene fluorid polymer (PVDF-HFP),  6.462   %

      C(0.146) H(0.073) O(0.652) Al(0.503) F(0.220) Ni(0.512)

       Molecular weight             = 60.05
       Oxygen balance               = -22.20391  %
       Enthalpy of formation        = -4107.88  kJ/kg
       Internal energy of formation = -4088.40  kJ/kg


Combustion parameters :
-----------------------
     - Heat of isochoric combustion             =  -2269.39  kJ/kg
     - Adiabatic combustion temperature         =  2625.2 K
     - Pressure in closed vessel                =  19.201  MPa
     - Force or 'specific energy'(F = nRT)      =  0.08881  MJ/kg
     - Covolume of gaseous products             =  0.208  cm3/g
     - Compressibility factor                   =  1.045
     - Total mol number of gaseous products     =  4.069  mol/kg explosive
     - Volume of gaseous products (at SATP)     =  100.86  L/kg explosive
     - Mass of gaseous products                 =  153.1  g/kg explosive
     - Mass of condensed products               =  847.0  g/kg explosive
     - Mean molecular mass of gaseous prod.     =  37.616  g
     - Mean molecular mass of all products      =  90.565  g
     - Specific gas constant                    =  33.829  J/kg K
     - Specific heat capacity at p=const. (Cp)  =  69.22  J/kg K
     - Specific heat capacity at V=const. (Cv)  =  67.19  J/mol K
     - Specific heat ratio (Cp/Cv)              =  1.0303


Composition of combustion products:
-------------------------------------------------------------------
   Product             mol/mol           mol/kg             mol%
-------------------------------------------------------------------
      Al2O3(l) =       1.583742 E-01     2.637251 E00      23.8840
      CO =             1.460294 E-01     2.431684 E00      22.0223
      AlNi3(s) =       1.258582 E-01     2.095793 E00      18.9803
                                  Page 1
```

alniothv-er1.2-90to10-virial.txt

Ni(l) =	1.013036 E-01	1.686910 E00	15.2773
H2 =	3.402556 E-02	5.665944 E-01	5.1313
NiF2(s) =	3.321476 E-02	5.530928 E-01	5.0090
AlF2O =	3.018907 E-02	5.027091 E-01	4.5527
AlF3 =	2.978483 E-02	4.959777 E-01	4.4918
HF =	3.638777 E-03	6.059300 E-02	0.5488
H =	2.932050 E-04	4.882456 E-03	0.0442
CH4 =	9.596469 E-05	1.598006 E-03	0.0145
H2O =	8.182092 E-05	1.362484 E-03	0.0123
Ni =	7.448553 E-05	1.240335 E-03	0.0112
CO2 =	5.030058 E-05	8.376063 E-04	0.0076
Al2O =	3.327498 E-05	5.540957 E-04	0.0050
Al =	1.792901 E-05	2.985543 E-04	0.0027
C2H4 =	1.273878 E-05	2.121265 E-04	0.0019
AlH =	1.039172 E-05	1.730431 E-04	0.0016
AlOH =	9.121302 E-06	1.518881 E-04	0.0014
OH =	1.525714 E-07	2.540623 E-06	0.0000
AlO =	1.433303 E-07	2.386739 E-06	0.0000
C2H6 =	3.437939 E-08	5.724863 E-07	0.0000
Al2O2 =	1.467122 E-08	2.443055 E-07	0.0000
Ni(s) =	1.005227 E-08	1.673906 E-07	0.0000
CFO =	7.731882 E-09	1.287515 E-07	0.0000
Al2 =	6.645752 E-09	1.106652 E-07	0.0000
CF =	4.155767 E-09	6.920192 E-08	0.0000
CH3OH =	2.505500 E-09	4.172163 E-08	0.0000
NiO =	1.933590 E-09	3.219818 E-08	0.0000
O =	7.866705 E-10	1.309965 E-08	0.0000
CF2O =	4.590947 E-10	7.644855 E-09	0.0000
CF2 =	3.578046 E-10	5.958171 E-09	0.0000
Al2O3(s) =	1.122214 E-10	1.868714 E-09	0.0000
CH2F2 =	1.028908 E-10	1.713339 E-09	0.0000
C(gr) =	5.642160 E-11	9.395338 E-10	0.0000
AlNi(s) =	4.680823 E-11	7.794516 E-10	0.0000
Al(l) =	4.084097 E-12	6.800847 E-11	0.0000
Ni(CO)4 =	3.752524 E-12	6.248711 E-11	0.0000
Al(s) =	2.479117 E-12	4.128231 E-11	0.0000
Al3Ni2(s) =	2.183334 E-12	3.635692 E-11	0.0000
O2 =	7.111056 E-13	1.184135 E-11	0.0000
AlF3(s) =	6.378783 E-13	1.062196 E-11	0.0000
AlF3(l) =	3.279917 E-13	5.461725 E-12	0.0000
HFO =	6.225017 E-14	1.036591 E-12	0.0000
Al3Ni(s) =	3.542882 E-14	5.899615 E-13	0.0000
NiAl2O4(s) =	1.803220 E-14	3.002726 E-13	0.0000
NiO(l) =	6.441539 E-15	1.072646 E-13	0.0000
NiO(s) =	2.896635 E-15	4.823482 E-14	0.0000
F2 =	2.782308 E-15	4.633106 E-14	0.0000
FO =	1.598593 E-15	2.661980 E-14	0.0000
CF4 =	3.763694 E-16	6.267311 E-15	0.0000
Ni(CO)4(l) =	3.720034 E-20	6.194609 E-19	0.0000

Notes:
- DataBase: D:\EXPLO5_V6.04\New DB-15feb2018.xlsx
- Activity : Model 1: Condensed products form pure phase (Default)

Page 2

```
                          alniothv-er1.2-80to20-virial.txt
                                                  EXPLO5_V6.04
                                                  27-Feb-18
                                                  2:53:35 PM
                                                  ==============

RESULTS OF THERMOCHEMICAL CALCULATION:
--------------------------------------

  Job title : Al/NiO (ER 1.2) +20%THV
  Comment   :

Combustion condition:
---------------------
     Isochoric combustion (V=const.)
     Loading density   = 0.200  g/cm3
     EOS :  Virial


Reactant information:
-----------------------
     1.  Aluminium (Al),  16.363   %
     2.  Aluminium oxide (Al2O3),  7.013   %
     3.  Nickel (II) oxide (NiO),  56.624   %
     4.  Polytetrafluoroethylene (PTFE),  7.076   %
     5.  Hexfluoropropene-Vinylidene fluorid polymer (PVDF-HFP),  12.924   %

      C(0.316) H(0.157) O(0.627) Al(0.484) F(0.476) Ni(0.493)

       Molecular weight             = 64.99
       Oxygen balance               = -26.21325  %
       Enthalpy of formation        = -4503.75  kJ/kg
       Internal energy of formation = -4479.73  kJ/kg


Combustion parameters :
-----------------------
     - Heat of isochoric combustion             =  -2023.20  kJ/kg
     - Adiabatic combustion temperature         =  2458.4 K
     - Pressure in closed vessel                =  33.222  MPa
     - Force or 'specific energy'(F = nRT)      =  0.14878  MJ/kg
     - Covolume of gaseous products             =  0.390  cm3/g
     - Compressibility factor                   =  1.087
     - Total mol number of gaseous products     =  7.279  mol/kg explosive
     - Volume of gaseous products (at SATP)     =  180.44  L/kg explosive
     - Mass of gaseous products                 =  306.4  g/kg explosive
     - Mass of condensed products               =  693.7  g/kg explosive
     - Mean molecular mass of gaseous prod.     =  42.086  g
     - Mean molecular mass of all products      =  68.016  g
     - Specific gas constant                    =  60.519  J/kg K
     - Specific heat capacity at p=const. (Cp)  =  72.90  J/kg K
     - Specific heat capacity at V=const. (Cv)  =  68.95  J/mol K
     - Specific heat ratio (Cp/Cv)              =  1.0573


Composition of combustion products:
-------------------------------------------------------------------
   Product             mol/mol           mol/kg             mol%
-------------------------------------------------------------------
      CO =             2.366088 E-01     3.640599 E00      24.7617
      Ni(l) =          1.658216 E-01     2.551426 E00      17.3536
      Al2O3(l) =       1.134445 E-01     1.745522 E00      11.8722
                                  Page 1
```

alniothv-er1.2-80to20-virial.txt

AlF3 =	1.064634 E-01	1.638108 E00	11.1417
AlNi3(s) =	1.005909 E-01	1.547750 E00	10.5271
C(gr) =	7.751744 E-02	1.192728 E00	8.1124
H2 =	7.110324 E-02	1.094035 E00	7.4411
AlF2O =	4.960814 E-02	7.632995 E-01	5.1916
NiF2(s) =	2.508306 E-02	3.859425 E-01	2.6250
HF =	6.983560 E-03	1.074531 E-01	0.7308
CH4 =	1.474843 E-03	2.269279 E-02	0.1543
C2H4 =	3.896205 E-04	5.994925 E-03	0.0408
H =	2.202302 E-04	3.388589 E-03	0.0230
H2O =	1.253350 E-04	1.928477 E-03	0.0131
CO2 =	6.421893 E-05	9.881095 E-04	0.0067
Ni =	2.479143 E-05	3.814552 E-04	0.0026
Al2O =	5.170645 E-06	7.955852 E-05	0.0005
AlOH =	4.304013 E-06	6.622403 E-05	0.0005
Al =	3.713239 E-06	5.713404 E-05	0.0004
AlH =	3.692822 E-06	5.681988 E-05	0.0004
C2H6 =	3.005546 E-06	4.624507 E-05	0.0003
AlO =	2.220182 E-08	3.416100 E-07	0.0000
CH3OH =	1.873052 E-08	2.881986 E-07	0.0000
Al2O3(s) =	1.741045 E-08	2.678873 E-07	0.0000
CFO =	7.971478 E-09	1.226538 E-07	0.0000
CF =	3.384593 E-09	5.207730 E-08	0.0000
Al2O2 =	1.626621 E-09	2.502813 E-08	0.0000
CF2O =	1.046810 E-09	1.610683 E-08	0.0000
CH2F2 =	7.098538 E-10	1.092222 E-08	0.0000
CF2 =	6.011054 E-10	9.248954 E-09	0.0000
Al2 =	4.376846 E-10	6.734468 E-09	0.0000
NiO =	3.145680 E-10	4.840124 E-09	0.0000
Ni(s) =	2.458563 E-10	3.782887 E-09	0.0000
AlNi(s) =	3.397690 E-11	5.227881 E-10	0.0000
Ni(CO)4 =	2.770598 E-11	4.263002 E-10	0.0000
AlF3(s) =	4.539786 E-12	6.985176 E-11	0.0000
Al(l) =	1.861771 E-12	2.864629 E-11	0.0000
AlF3(l) =	1.676433 E-12	2.579456 E-11	0.0000
Al(s) =	9.883693 E-13	1.520762 E-11	0.0000
Al3Ni2(s) =	7.578308 E-13	1.166042 E-11	0.0000
HFO =	2.329221 E-14	3.583873 E-13	0.0000
NiAl2O4(s) =	1.846040 E-14	2.840423 E-13	0.0000
Al3Ni(s) =	7.297108 E-15	1.122775 E-13	0.0000
NiO(l) =	3.335022 E-15	5.131457 E-14	0.0000
NiO(s) =	2.054038 E-15	3.160461 E-14	0.0000
CF4 =	1.733108 E-15	2.666659 E-14	0.0000
F2 =	8.709971 E-16	1.340166 E-14	0.0000
FO =	2.246140 E-16	3.456041 E-15	0.0000
Ni(CO)4(l) =	1.608444 E-19	2.474845 E-18	0.0000

Notes:
- DataBase: D:\EXPLO5_V6.04\New DB-15feb2018.xlsx
- Activity : Model 1: Condensed products form pure phase (Default)

alniothv-er1.2-70to30-virial.txt
EXPLO5_V6.04
27-Feb-18
2:34:40 PM

RESULTS OF THERMOCHEMICAL CALCULATION:

Job title : Al/NiO (ER 1.2) +30%THV
Comment :

Combustion condition:

Isochoric combustion (V=const.)
Loading density = 0.200 g/cm3
EOS : Virial

Reactant information:

1. Aluminium (Al), 14.318 %
2. Aluminium oxide (Al2O3), 6.136 %
3. Nickel (II) oxide (NiO), 49.546 %
4. Polytetrafluoroethylene (PTFE), 10.614 %
5. Hexfluoropropene-Vinylidene fluorid polymer (PVDF-HFP), 19.386 %

C(0.517) H(0.257) O(0.598) Al(0.461) F(0.778) Ni(0.470)

Molecular weight = 70.81
Oxygen balance = -30.22349 %
Enthalpy of formation = -4899.45 kJ/kg
Internal energy of formation = -4870.89 kJ/kg

Combustion parameters :

- Heat of isochoric combustion = -2295.55 kJ/kg
- Adiabatic combustion temperature = 2413.4 K
- Pressure in closed vessel = 36.092 MPa
- Force or 'specific energy'(F = nRT) = 0.15989 MJ/kg
- Covolume of gaseous products = 0.435 cm3/g
- Compressibility factor = 1.098
- Total mol number of gaseous products = 7.969 mol/kg explosive
- Volume of gaseous products (at SATP) = 197.54 L/kg explosive
- Mass of gaseous products = 351.4 g/kg explosive
- Mass of condensed products = 648.6 g/kg explosive
- Mean molecular mass of gaseous prod. = 44.092 g
- Mean molecular mass of all products = 51.067 g
- Specific gas constant = 66.253 J/kg K
- Specific heat capacity at p=const. (Cp) = 90.47 J/kg K
- Specific heat capacity at V=const. (Cv) = 85.75 J/mol K
- Specific heat ratio (Cp/Cv) = 1.0550

Composition of combustion products:

Product	mol/mol	mol/kg	mol%
Ni(l) =	3.097531 E-01	4.374149 E00	22.3372
C(gr) =	2.965069 E-01	4.187094 E00	21.3820
CO =	2.149873 E-01	3.035922 E00	15.5034

alniothv-er1.2-70to30-virial.txt

AlF3 =	1.605210 E-01	2.266782 E00	11.5757
H2 =	1.137193 E-01	1.605876 E00	8.2006
Al2O3(l) =	1.074279 E-01	1.517033 E00	7.7470
NiF2(s) =	8.307547 E-02	1.173142 E00	5.9908
AlF2O =	6.000873 E-02	8.474076 E-01	4.3274
AlNi3(s) =	2.563046 E-02	3.619380 E-01	1.8483
HF =	9.839299 E-03	1.389447 E-01	0.7095
CH4 =	3.807300 E-03	5.376442 E-02	0.2746
C2H4 =	9.119741 E-04	1.287835 E-02	0.0658
H =	2.369367 E-04	3.345878 E-03	0.0171
H2O =	1.834202 E-04	2.590151 E-03	0.0132
CO2 =	5.456934 E-05	7.705957 E-04	0.0039
Ni =	1.906556 E-05	2.692324 E-04	0.0014
C2H6 =	1.161851 E-05	1.640697 E-04	0.0008
Al2O3(s) =	4.281029 E-06	6.045414 E-05	0.0003
AlOH =	4.014830 E-06	5.669504 E-05	0.0003
AlH =	3.160992 E-06	4.463765 E-05	0.0002
Al2O =	3.134436 E-06	4.426264 E-05	0.0002
Al =	2.463519 E-06	3.478834 E-05	0.0002
CH3OH =	3.925092 E-08	5.542782 E-07	0.0000
AlO =	1.356746 E-08	1.915917 E-07	0.0000
CFO =	6.309436 E-09	8.909810 E-08	0.0000
CF =	2.493304 E-09	3.520896 E-08	0.0000
CH2F2 =	1.182154 E-09	1.669367 E-08	0.0000
CF2O =	1.041034 E-09	1.470086 E-08	0.0000
Al2O2 =	8.953740 E-10	1.264394 E-08	0.0000
CF2 =	5.448614 E-10	7.694208 E-09	0.0000
Ni(s) =	2.629925 E-10	3.713823 E-09	0.0000
Al2 =	2.056344 E-10	2.903847 E-09	0.0000
NiO =	1.965501 E-10	2.775564 E-09	0.0000
AlNi(s) =	3.077482 E-11	4.345837 E-10	0.0000
Ni(CO)4 =	1.611580 E-11	2.275777 E-10	0.0000
AlF3(s) =	8.089822 E-12	1.142397 E-10	0.0000
AlF3(l) =	2.668285 E-12	3.767993 E-11	0.0000
Al(l) =	1.471088 E-12	2.077383 E-11	0.0000
Al(s) =	7.550585 E-13	1.066249 E-11	0.0000
Al3Ni2(s) =	5.441862 E-13	7.684674 E-12	0.0000
HFO =	2.035538 E-14	2.874466 E-13	0.0000
NiAl2O4(s) =	1.858475 E-14	2.624428 E-13	0.0000
Al3Ni(s) =	4.487125 E-15	6.336451 E-14	0.0000
NiO(l) =	2.767156 E-15	3.907613 E-14	0.0000
CF4 =	2.092027 E-15	2.954236 E-14	0.0000
NiO(s) =	1.865554 E-15	2.634425 E-14	0.0000
F2 =	6.509868 E-16	9.192848 E-15	0.0000
FO =	1.337295 E-16	1.888448 E-15	0.0000
Ni(CO)4(l) =	7.611799 E-20	1.074893 E-18	0.0000

Notes:
- DataBase: D:\EXPLO5_V6.04\New DB-15feb2018.xlsx
- Activity : Model 1: Condensed products form pure phase (Default)

Page 2

alniothv-er1.2-60to40-virial.txt
EXPLO5_V6.04
27-Feb-18
2:20:40 PM

RESULTS OF THERMOCHEMICAL CALCULATION:

Job title : Al/NiO (ER 1.2) +40%THV
Comment :

Combustion condition:

Isochoric combustion (V=const.)
Loading density = 0.200 g/cm3
EOS : Virial

Reactant information:

1. Aluminium (Al), 12.272 %
2. Aluminium oxide (Al2O3), 5.2596 %
3. Nickel (II) oxide (NiO), 42.468 %
4. Polytetrafluoroethylene (PTFE), 14.152 %
5. Hexfluoropropene-Vinylidene fluorid polymer (PVDF-HFP), 25.848 %

C(0.757) H(0.376) O(0.563) Al(0.434) F(1.139) Ni(0.442)

Molecular weight = 77.78
Oxygen balance = -34.23283 %
Enthalpy of formation = -5295.26 kJ/kg
Internal energy of formation = -5262.15 kJ/kg

Combustion parameters :

- Heat of isochoric combustion = -2489.26 kJ/kg
- Adiabatic combustion temperature = 2300.0 K
- Pressure in closed vessel = 37.925 MPa
- Force or 'specific energy'(F = nRT) = 0.16671 MJ/kg
- Covolume of gaseous products = 0.465 cm3/g
- Compressibility factor = 1.106
- Total mol number of gaseous products = 8.718 mol/kg explosive
- Volume of gaseous products (at SATP) = 216.11 L/kg explosive
- Mass of gaseous products = 371.4 g/kg explosive
- Mass of condensed products = 628.6 g/kg explosive
- Mean molecular mass of gaseous prod. = 42.607 g
- Mean molecular mass of all products = 45.245 g
- Specific gas constant = 72.480 J/kg K
- Specific heat capacity at p=const. (Cp) = 109.09 J/kg K
- Specific heat capacity at V=const. (Cv) = 103.41 J/mol K
- Specific heat ratio (Cp/Cv) = 1.0550

Composition of combustion products:

Product	mol/mol	mol/kg	mol%
C(gr) =	5.110645 E-01	6.570231 E00	29.7271
Ni(l) =	2.356768 E-01	3.029855 E00	13.7086
CO =	2.343958 E-01	3.013386 E00	13.6341

Page 1

alniothv-er1.2-60to40-virial.txt

NiF2(s) =	2.065687 E-01	2.655642 E00	12.0155
AlF3 =	1.940406 E-01	2.494581 E00	11.2868
H2 =	1.597579 E-01	2.053843 E00	9.2926
Al2O3(s) =	8.659261 E-02	1.113232 E00	5.0368
AlF2O =	6.452070 E-02	8.294763 E-01	3.7530
HF =	1.451025 E-02	1.865434 E-01	0.8440
CH4 =	8.676740 E-03	1.115479 E-01	0.5047
C2H4 =	1.598354 E-03	2.054840 E-02	0.0930
Al2O3(l) =	1.156102 E-03	1.486281 E-02	0.0672
H2O =	3.221490 E-04	4.141538 E-03	0.0187
H =	1.714814 E-04	2.204560 E-03	0.0100
CO2 =	7.897538 E-05	1.015305 E-03	0.0046
C2H6 =	3.513725 E-05	4.517235 E-04	0.0020
Ni(s) =	1.134984 E-05	1.459133 E-04	0.0007
Ni =	8.335870 E-06	1.071657 E-04	0.0005
AlOH =	1.470061 E-06	1.889906 E-05	0.0001
AlH =	5.781611 E-07	7.432823 E-06	0.0000
Al =	3.396454 E-07	4.366472 E-06	0.0000
Al2O =	2.519232 E-07	3.238718 E-06	0.0000
CH3OH =	8.115010 E-08	1.043263 E-06	0.0000
CFO =	4.685949 E-09	6.024242 E-08	0.0000
AlO =	2.384140 E-09	3.065044 E-08	0.0000
CH2F2 =	1.807496 E-09	2.323712 E-08	0.0000
CF2O =	1.412215 E-09	1.815540 E-08	0.0000
CF =	9.611074 E-10	1.235597 E-08	0.0000
CF2 =	3.623178 E-10	4.657947 E-09	0.0000
Al2O2 =	8.818682 E-11	1.133727 E-09	0.0000
AlNi3(s) =	8.503324 E-11	1.093185 E-09	0.0000
NiO =	7.805925 E-11	1.003527 E-09	0.0000
Ni(CO)4 =	2.124543 E-11	2.731307 E-10	0.0000
AlF3(s) =	1.719469 E-11	2.210544 E-10	0.0000
AlNi(s) =	9.887594 E-12	1.271146 E-10	0.0000
Al2 =	5.239953 E-12	6.736468 E-11	0.0000
AlF3(l) =	4.180366 E-12	5.374267 E-11	0.0000
Al(l) =	3.656353 E-13	4.700598 E-12	0.0000
Al(s) =	1.735967 E-13	2.231754 E-12	0.0000
NiAl2O4(s) =	2.661712 E-14	3.421890 E-13	0.0000
Al3Ni2(s) =	2.287912 E-14	2.941333 E-13	0.0000
HFO =	1.318976 E-14	1.695672 E-13	0.0000
CF4 =	2.936422 E-15	3.775056 E-14	0.0000
NiO(l) =	2.673326 E-15	3.436820 E-14	0.0000
NiO(s) =	2.289189 E-15	2.942975 E-14	0.0000
F2 =	2.576448 E-16	3.312274 E-15	0.0000
Al3Ni(s) =	1.245760 E-16	1.601546 E-15	0.0000
FO =	4.617551 E-17	5.936311 E-16	0.0000
Ni(CO)4(l) =	6.623674 E-20	8.515376 E-19	0.0000

Notes:
- DataBase: D:\EXPLO5_V6.04\New DB-15feb2018.xlsx
- Activity : Model 1: Condensed products form pure phase (Default)

Page 2

```
                          alniothv-er1.2-50to50-virial.txt
                                                  EXPLO5_V6.04
                                                  27-Feb-18
                                                  2:57:47 PM
                                                  ==============

RESULTS OF THERMOCHEMICAL CALCULATION:
--------------------------------------

  Job title : Al/NiO (ER 1.2) +50%THV
  Comment   :

Combustion condition:
---------------------
     Isochoric combustion (V=const.)
     Loading density   = 0.200  g/cm3
     EOS :  Virial


Reactant information:
-----------------------
     1.  Aluminium (Al),  10.227   %
     2.  Aluminium oxide (Al2O3),  4.383   %
     3.  Nickel (II) oxide (NiO),  35.39   %
     4.  Polytetrafluoroethylene (PTFE),  17.69   %
     5.  Hexfluoropropene-Vinylidene fluorid polymer (PVDF-HFP),  32.31   %

      C(1.050) H(0.522) O(0.520) Al(0.401) F(1.579) Ni(0.409)

       Molecular weight             = 86.28
       Oxygen balance               = -38.24307  %
       Enthalpy of formation        = -5691.03  kJ/kg
       Internal energy of formation = -5653.38  kJ/kg


Combustion parameters :
-----------------------
     - Heat of isochoric combustion             =  -2639.50  kJ/kg
     - Adiabatic combustion temperature         =  2032.1 K
     - Pressure in closed vessel                =  34.46  MPa
     - Force or 'specific energy'(F = nRT)      =  0.15094  MJ/kg
     - Covolume of gaseous products             =  0.456  cm3/g
     - Compressibility factor                   =  1.104
     - Total mol number of gaseous products     =  8.934  mol/kg explosive
     - Volume of gaseous products (at SATP)     =  221.46  L/kg explosive
     - Mass of gaseous products                 =  353.8  g/kg explosive
     - Mass of condensed products               =  646.2  g/kg explosive
     - Mean molecular mass of gaseous prod.     =  39.600  g
     - Mean molecular mass of all products      =  42.860  g
     - Specific gas constant                    =  74.275  J/kg K
     - Specific heat capacity at p=const. (Cp)  =  142.42  J/kg K
     - Specific heat capacity at V=const. (Cv)  =  135.93  J/mol K
     - Specific heat ratio (Cp/Cv)              =  1.0478


Composition of combustion products:
-------------------------------------------------------------------
   Product             mol/mol           mol/kg             mol%
-------------------------------------------------------------------
      C(gr) =          7.640064 E-01     8.855435 E00      37.9545
      NiF2(s) =        4.081206 E-01     4.730439 E00      20.2747
      CO =             2.588702 E-01     3.000510 E00      12.8602
                                  Page 1
```

alniothv-er1.2-50to50-virial.txt

AlF3 =	2.105695 E-01	2.440666 E00	10.4607
H2 =	1.962437 E-01	2.274619 E00	9.7490
Al2O3(s) =	6.939472 E-02	8.043395 E-01	3.4474
AlF2O =	5.184481 E-02	6.009222 E-01	2.5756
HF =	2.723327 E-02	3.156550 E-01	1.3529
CH4 =	2.287626 E-02	2.651539 E-01	1.1365
C2H4 =	2.014117 E-03	2.334520 E-02	0.1001
H2O =	7.538225 E-04	8.737396 E-03	0.0374
Ni(l) =	6.624567 E-04	7.678394 E-03	0.0329
CO2 =	1.982485 E-04	2.297856 E-03	0.0098
C2H6 =	1.138805 E-04	1.319964 E-03	0.0057
H =	4.431495 E-05	5.136452 E-04	0.0022
AlF3(s) =	7.982916 E-06	9.252828 E-05	0.0004
Ni =	6.050124 E-07	7.012570 E-06	0.0000
CH3OH =	1.673671 E-07	1.939916 E-06	0.0000
Ni(s) =	5.190750 E-08	6.016488 E-07	0.0000
AlOH =	4.307886 E-08	4.993178 E-07	0.0000
CF2O =	2.862464 E-09	3.317821 E-08	0.0000
CH2F2 =	2.783462 E-09	3.226252 E-08	0.0000
AlH =	2.363702 E-09	2.739717 E-08	0.0000
CFO =	1.752148 E-09	2.030878 E-08	0.0000
Al =	8.463574 E-10	9.809948 E-09	0.0000
Al2O =	1.064905 E-10	1.234309 E-09	0.0000
CF2 =	9.669374 E-11	1.120757 E-09	0.0000
Al2O3(l) =	8.111334 E-11	9.401674 E-10	0.0000
CF =	5.589596 E-11	6.478781 E-10	0.0000
Ni(CO)4 =	3.710749 E-11	4.301050 E-10	0.0000
AlO =	1.206672 E-11	1.398628 E-10	0.0000
AlF3(l) =	1.187480 E-11	1.376383 E-10	0.0000
NiO =	4.414877 E-12	5.117190 E-11	0.0000
AlNi3(s) =	2.710124 E-12	3.141247 E-11	0.0000
AlNi(s) =	4.022229 E-13	4.662080 E-12	0.0000
Al2O2 =	6.743829 E-14	7.816629 E-13	0.0000
NiAl2O4(s) =	4.240969 E-14	4.915617 E-13	0.0000
CF4 =	6.372414 E-15	7.386129 E-14	0.0000
Al(l) =	5.788892 E-15	6.709781 E-14	0.0000
NiO(s) =	3.680143 E-15	4.265575 E-14	0.0000
HFO =	2.514258 E-15	2.914223 E-14	0.0000
Al(s) =	2.346208 E-15	2.719439 E-14	0.0000
NiO(l) =	2.260940 E-15	2.620607 E-14	0.0000
Al2 =	8.614307 E-17	9.984660 E-16	0.0000
F2 =	1.616372 E-17	1.873503 E-16	0.0000
FO =	2.030430 E-18	2.353428 E-17	0.0000
Al3Ni2(s) =	1.063553 E-18	1.232741 E-17	0.0000
Ni(CO)4(l) =	4.848626 E-20	5.619939 E-19	0.0000
Al3Ni(s) =	2.065580 E-21	2.394170 E-20	0.0000

Notes:
- DataBase: D:\EXPLO5_V6.04\New DB-15feb2018.xlsx
- Activity : Model 1: Condensed products form pure phase (Default)

Page 2

Appendix B

The sensitivity to ESD, Friction and Impact of n-Al/n-CuO was conducted in a separate work not discussed in detail within this report. Similar to the work on n-Al/n-NiO discussed here, self-assembly through the surface functionalization of n-Al and n-CuO with APTMS and GPTMS, respectively, were performed. 20 wt% of THV was added to the n-Al/n-CuO in a similar technique described in this report for n-Al/n-NiO. The sensitivity of n-Al/n-CuO serve as a benchmark to understand the sensitivity of n-Al/n-NiO when compared to another more well-known nano-thermite system.

Table A.1: Sensitivity to Friction, Impact and ESD of physically mixed n-Al/n-CuO, self-assembled n-Al-APTMS/n-CuO-GPTMS and n-Al/n-CuO with 30 wt% THV fluoropolymer

Sensitivity Data			
Material	**Friction (N)**	**Impact (J)**	**ESD (mJ)**
Al CuO physically mixed (ER1.25)	< 5 N	< 2.50 J	MIE: < 0.042 mJ
Al CuO self-assembled (ER1.25)	< 5 N	> 50 J	MIE: < 0.046 mJ
Al CuO physically mixed (ER1.25) + THV (80:20)	< 120 N	< 50 J	MIE: 4.67 mJ
Al CuO self-assembled (ER1.25) + THV (80:20)	< 96 N	> 50 J	MIE: 2.23 mJ

Values in red: actual value is below measurable limit of machine

Values in green: actual value is above measurable limit of machine